

MODEL UPDATING OF A HELICOPTER STRUCTURE USING A NEWLY
DEVELOPED CORRELATION IMPROVEMENT TECHNIQUE

A THESIS SUBMITTED TO
THE GRADUATE SCHOOL OF NATURAL AND APPLIED SCIENCES
OF
MIDDLE EAST TECHNICAL UNIVERSITY

BY

FATİH ALTUNEL

IN PARTIAL FULFILLMENT OF THE REQUIREMENTS
FOR
THE DEGREE OF MASTER OF SCIENCE
IN
MECHANICAL ENGINEERING

DECEMBER 2009

Approval of the thesis:

**MODEL UPDATING OF A HELICOPTER STRUCTURE USING A
NEWLY DEVELOPED CORRELATION IMPROVEMENT
TECHNIQUE**

submitted by **FATİH ALTUNEL** in partial fulfillment of the requirements for
the degree of **Master of Science in Mechanical Engineering Department,**
Middle East Technical University by,

Prof. Dr. Canan Özgen
Dean, Graduate School of **Natural and Applied Sciences** _____

Prof. Dr. Süha Oral
Head of Department, **Mechanical Engineering** _____

Prof. Dr. Mehmet Çalışkan
Supervisor, **Mechanical Engineering Dept., METU** _____

Assoc. Prof. Dr. Mehmet Çelik
Co. Supervisor, **Mechanical Design Dept., ASELSAN** _____

Examining Committee Members

Asst. Prof. Dr. Yiğit Yazıcıoğlu
Mechanical Engineering Dept., METU _____

Prof. Dr. Mehmet Çalışkan
Mechanical Engineering Dept., METU _____

Prof. Dr. Yavuz Yaman
Aerospace Engineering Dept., METU _____

Assoc. Prof. Dr. Mehmet Çelik
Mechanical Design Dept., ASELSAN _____

Asst. Prof. Dr. Gökhan O. Özgen
Mechanical Engineering Dept., METU _____

Date: 07/12/2009

I hereby declare that all information in this document has been obtained and presented in accordance with academic rules and ethical conduct. I also declare that, as required by these rules and conduct, I have fully cited and referenced all material and results that are not original to this work.

Name, Last Name: Fatih ALTUNEL

Signature:

ABSTRACT

MODEL UPDATING OF A HELICOPTER STRUCTURE USING A NEWLY DEVELOPED CORRELATION IMPROVEMENT TECHNIQUE

ALTUNEL, Fatih

M.S., Department of Mechanical Engineering

Supervisor: Prof. Dr. Mehmet Çalışkan

Co. Supervisor: Assoc. Prof. Dr. Mehmet Çelik

December 2009, 181 Pages

Numerical model usage has substantially increased in many industries. It is the aerospace industry that numerical models play possibly the most important role for development of optimum design. However, numerical models need experimental verification. This experimental verification is used not only for validation, but also updating numerical model parameters. Verified and updated models are used to analyze a vast amount of cases that structure is anticipated to face in real life.

In this thesis, structural finite element model updating of a utility helicopter fuselage was performed as a case study. Initially, experimental modal analyses were performed using modal shakers. Modal analysis of test results was carried out using LMS Test.lab software. At the same time, finite element analysis of the helicopter fuselage was performed by MSC.Patran & Nastran software.

Initial updating was processed first for the whole helicopter fuselage then, tail of the helicopter was tried to be updated.

Furthermore, a new method was proposed for the optimum node removal location for getting better Modal Assurance Criterion (MAC) matrix. This routine was tried on the helicopter case study and it showed better performance than the Coordinate Modal Assurance Criterion (coMAC) that is often used in such analyses.

Keywords: Model Updating, Experimental Modal Analysis, Helicopter FEM Analysis, Modal Assurance Criterion

ÖZ

YENİ GELİŞTİRİLMİŞ KORELASYON İYİLEŞTİRME TEKNİĞİ İLE BİR HELİKOPTER YAPISAL MODELİNİN GÜNCELLENMESİ

ALTUNEL, Fatih

Yüksek Lisans, Makine Mühendisliği Anabilim Dalı

Tez Yöneticisi: Prof. Dr. Mehmet Çalışkan

Yrd. Tez Yöneticisi: Doç. Dr. Mehmet Çelik

Aralık 2009, 181 Sayfa

Sayısal model kullanımı birçok endüstride giderek artmaktadır. Fakat, havacılık endüstrisinde en iyi tasarımın elde edilmesi için sayısal modelleme belki de en büyük öneme sahiptir. Ancak, sayısal hesaplamaların deneysel olarak doğrulanmasına ihtiyaç vardır. Deneysel sadece doğrulama imkânı tanımamakta, sayısal modellerin güncellenmesine de imkân tanımaktadır. Bu sayede, doğrulanmış ve güncellenmiş analitik modeller, her türlü durumun analizinde kolaylıkla kullanılabilir.

Bu tezde, bir genel maksat helikopterin yapısal sonlu elemanlar model güncellemesi gerçekleştirilmeye çalışılmıştır. İlk aşama olarak helikopterin deneysel modal analizleri sarsıcı kullanılarak gerçekleştirilmiştir. Elde edilen test sonuçları ise LMS Test.Lab yazılımı kullanılarak analiz edilmiştir. Ayrıca, helikopterin sonlu elemanlar analizleri MSC.Patran & Nastran yazılımlarında

yapılmıştır. Güncelleme çalışmaları öncelikle tüm helikopter gövdesi için uygulanmıştır. Ardından, kuyruk kısmının güncellenmesine çalışılmıştır.

Ayrıca, modelden çıkarılması gereken en uygun konumu hesaplayarak daha iyi MAC matrisi elde edilmesine olanak sağlayan yeni bir metot önerilmiştir. Önerilen metot, helikopter modeli için denenmiş ve coMAC metodundan daha iyi çalıştığı görülmüştür.

Anahtar Kelimeler: Model Güncelleme, Deneysel Modal Analiz, Helikopter Sonlu Elemanlar Analizi, Modal Güvence Kriteri

To my father, for his unbelievable support in my life

ACKNOWLEDGEMENTS

I would like to express my gratitude to my supervisor Prof. Dr. Mehmet Çalışkan and co-supervisor Assoc. Prof. Dr. Mehmet Çelik for their guidance, criticism and insight throughout this work.

I would also like to thank Murat and Serap Aykan for their support, suggestions, comments and patience throughout my works.

I am grateful to my friends Mustafa Murat Karasan, İsmail Güler and Murat Öztürk in Aselsan Inc.

Lastly, I want to thank Bias Inc. and DTA Inc. for their help and support.

TABLE OF CONTENTS

ABSTRACT.....	iv
ÖZ.....	vi
ACKNOWLEDGEMENTS.....	ix
TABLE OF CONTENTS.....	x
LIST OF TABLES.....	xii
LIST OF FIGURES.....	xv
NOMENCLATURE.....	xx
ABBREVIATIONS.....	xxi
CHAPTERS	
1. INTRODUCTION.....	1
1.1 Motivation for the Research.....	1
1.2 Objectives of the Thesis.....	5
1.3 Outline of the Thesis.....	5
2. MODEL UPDATING TECHNOLOGY.....	7
2.1 Background.....	7
2.2 Model Updating Techniques.....	11
2.2.1 Updating Through Numerical Techniques.....	12
2.2.2 Updating Through Input Data.....	14
3. PROCEDURES REQUIRED FOR MODEL UPATING.....	17
3.1 Finite Element Method.....	18
3.2 Modal Test and Analysis.....	22
3.2.1 Modal Test Techniques.....	23
3.2.2 Modal Analysis of Test Results.....	31

3.3 Reduction and Expansion Methods	35
3.3.1 Finite Element Model Reduction	36
3.3.2 Experimental Modal Data Expansion	39
3.4 Correlation Techniques	39
3.4.1 Modal Assurance Criterion (MAC)	40
3.4.2 Coordinate Modal Assurance Criterion (coMAC).....	41
3.4.3 Frequency Response Assurance Criterion (FRAC)	41
3.4.4 Orthogonality (OR).....	42
3.5 Sensitivity Analysis	42
3.6 Model Updating (Optimization)	45
4. A NEW DIAGNOSTIC TOOL FOR IMPROVED MAC.....	48
5. CASE STUDIES ON A MILITARY HELICOPTER	53
5.1 Modal Test and Analysis	54
5.1.1 Pretest Configuration	55
5.1.2 Modal Tests.....	58
5.1.3 Modal Analysis	63
5.2 Finite Element Analysis.....	71
5.3 Model Updating	82
5.3.1 Model Updating of the Complete Helicopter Fuselage	83
5.3.2 Model Updating of the Tail.....	105
6. DISCUSSION AND CONCLUSIONS	144
REFERENCES	150
APPENDIX A.....	154
APPENDIX B	158
APPENDIX C	160
APPENDIX D.....	167
APPENDIX E	177

LIST OF TABLES

TABLES

Table 2.1 Comparison of different procedures [5].....	8
Table 5.1 Stabilized natural frequencies of the tail.....	65
Table 5.2 Stabilized natural frequencies of the complete helicopter fuselage..	68
Table 5.3 Tail and complete fuselage finite element model properties	77
Table 5.4 First 10 natural frequencies of the tail finite element model	77
Table 5.5 First 10 natural frequencies of the complete helicopter finite element model.....	79
Table 5.6 Initial MAC and frequency difference values of complete helicopter fuselage	83
Table 5.7 Design variables for sensitivity analysis of complete helicopter fuselage model	84
Table 5.8 Sensitivities of paired mode shapes on beam cross section areas.....	86
Table 5.9 Sensitivities of paired mode shapes on beam first moment of areas	87
Table 5.10 Sensitivities of paired mode shapes on beam second moment of areas	88
Table 5.11 Sensitivities of paired mode shapes on beam torsional stiffness....	89
Table 5.12 Sensitivities of paired mode shapes on material properties and shell thicknesses	90
Table 5.13 Summed sensitivities of paired mode shapes on design variables..	91
Table 5.14 MAC updating results with objective functions of increasing all MAC and decreasing all frequency differences.....	94
Table 5.15 Frequency difference updating results with objective functions of increasing all MAC and decreasing all frequency differences	94
Table 5.16 MAC updating results with objective functions of increasing all MAC	100

Table 5.17	Frequency difference updating results with objective functions of decreasing all frequency differences.....	101
Table 5.18	Updating results for objective function of decreasing frequency difference 2	102
Table 5.19	Updating results for objective function of increasing only MAC_1	103
Table 5.20	Initial MAC and frequency difference values of the tail model ...	105
Table 5.21	Design variables of the tail model	105
Table 5.22	Sensitivities of paired mode shapes on beam cross section areas.	107
Table 5.23	Sensitivities of paired mode shapes on beam first moment of areas	108
Table 5.24	Sensitivities of paired mode shapes on beam second moment of areas	108
Table 5.25	Sensitivities of paired mode shapes on beam torsional stiffness..	109
Table 5.26	Sensitivities of paired mode shapes on material properties and shell thicknesses	110
Table 5.27	Summed sensitivities of paired mode shapes on design variables	113
Table 5.28	MAC updating results with objective functions of increasing all MAC and decreasing all frequency differences.....	116
Table 5.29	Frequency difference updating results with objective functions of increasing all MAC and decreasing all frequency differences	116
Table 5.30	Changes of design variables for the first optimization	118
Table 5.31	MAC updating results with objective functions of increasing all MAC	124
Table 5.32	Frequency difference updating results with objective functions of decreasing all frequency differences.....	126
Table 5.33	Frequency difference 1 and 2 updating results for objective functions of decreasing Freq_Diff_1 and 2	127
Table 5.34	Updating results for objective function of increasing only MAC_4	129
Table 5.35	coMAC node removals and related MAC values	130

Table 5.36 nrMAC node removals and related MAC values with weights 0,25;0,25;0,25;0,25	131
Table 5.37 nrMAC node removals and related MAC values with weights 0,1;0,4;0,4;0,1	133
Table 5.38 Updating of MAC values under removal of 10 nodes according to coMAC.....	136
Table 5.39 Updating of MAC values under removal of 20 nodes according to coMAC.....	137
Table 5.40 Updating of MAC values under removal of 10 nodes according to nrMAC with weights 0,25;0,25;0,25;0,25	139
Table 5.41 Updating of MAC values under removal of 10 nodes according to nrMAC with weights 0,1;0,4;0,4;0,1	140
Table 5.42 Updating of MAC values under removal of 20 nodes according to nrMAC with weights 0,25;0,25;0,25;0,25	142
Table 6.1 MAC change summary for tail model updating	146
Table 6.2 Total MAC change summary for tail model updating.....	147

LIST OF FIGURES

FIGURES

Figure 1.1 Design to manufacturing diagram for industries in recent years.....	4
Figure 3.1 Diagram of model updating procedures	17
Figure 3.2 Coarse mesh, single quadrature element	19
Figure 3.3 Fine mesh with loading and boundary conditions.....	20
Figure 3.4 Electro-dynamic shaker with stinger attachment	24
Figure 3.5 a) Force Transducer, b) Impact Hammer with different tips.....	25
Figure 3.6 Basic items of a measurement system.....	26
Figure 3.7 Driving point hammer test on sponge	28
Figure 3.8 Roving hammer test.....	29
Figure 3.9 A typical shaker test	30
Figure 3.10 A typical shaker test where accelerometer location is changed	31
Figure 3.11 Measured and curve-fitted FRF curves with correlation and error percentage	35
Figure 3.12 Schematic of Reduction/Expansion Process	36
Figure 4.1 MAC matrix diagram	50
Figure 4.2 MAC matrix diagonal numbering	51
Figure 4.3 Statistical tabulation of each MAC value (M).....	51
Figure 5.1 Utility Helicopter.....	53
Figure 5.2 Model updating procedure followed for updating.....	54
Figure 5.3 Foams that are used for free-free boundary condition.....	55
Figure 5.4 The part that connect stinger to the helicopter	56
Figure 5.5 Steel part to which shaker is connected.....	56
Figure 5.6 Force transducer (Line circle) and driving point accelerometer (Dashed circle).....	58
Figure 5.7 Accelerometer locations at tail end	59

Figure 5.8 Accelerometer locations at tail front	59
Figure 5.9 Accelerometer locations at main body	59
Figure 5.10 Accelerometer locations at main body front	60
Figure 5.11 Shaker, controller, and amplifier system.....	61
Figure 5.12 IOtech data acquisition system.....	61
Figure 5.13 Stinger directions, vertical and transverse respectively	62
Figure 5.14 Graphs that are checked during modal tests.....	63
Figure 5.15 Modal analysis model of the tail	64
Figure 5.16 First lateral bending mode (Second stabilized mode) of the tail (3.5 Hz).....	66
Figure 5.17 First vertical bending mode (Fourth stabilized mode) of the tail (7.2 Hz).....	66
Figure 5.18 Second vertical bending mode (Sixth stabilized mode) of the tail (9.6 Hz).....	67
Figure 5.19 Second lateral bending mode (Twenty-fifth stabilized mode) of the	67
Figure 5.20 Modal analysis model of the complete helicopter fuselage.....	68
Figure 5.21 First lateral bending mode (Eighth stabilized mode shape) of the complete helicopter fuselage (10.7 Hz)	69
Figure 5.22 First vertical bending mode (Nineth stabilized mode shape) of the complete helicopter fuselage (13.3 Hz)	70
Figure 5.23 Second lateral bending mode (Fourteenth stabilized mode shape) of the complete helicopter fuselage (20.9 Hz)	70
Figure 5.24 Lateral rigid body mode of the complete helicopter fuselage (4.7 Hz).....	71
Figure 5.25 Surface model of the helicopter structure.....	72
Figure 5.26 Finite element model of the complete helicopter fuselage.....	73
Figure 5.27 Finite element model of the tail.....	73
Figure 5.28 Beam elements (green in color) on the helicopter structure.....	74
Figure 5.29 Refined finite element model of the tail	75
Figure 5.30 Refined finite element model of the whole helicopter	75
Figure 5.31 Boundary condition of the tail in all six DOF	76

Figure 5.32 First lateral bending mode of the tail finite element model (11.4 Hz).....	78
Figure 5.33 First vertical bending mode of the tail finite element model (14.5 Hz).....	78
Figure 5.34 First torsion mode of the tail finite element model (35.6 Hz).....	79
Figure 5.35 First lateral bending mode of the complete helicopter fuselage finite element model (17.6 Hz).....	80
Figure 5.36 First vertical bending mode of the complete helicopter fuselage finite element model (22.8 Hz).....	81
Figure 5.37 First torsion mode of the complete helicopter fuselage finite element.....	81
Figure 5.38 An example to a local mode (4 th mode, 40.1 Hz).....	82
Figure 5.39 Surface element property variables in different colors.....	85
Figure 5.40 Beam element property variables in different colors	85
Figure 5.41 Summed sensitivities of paired mode shapes on design variables	92
Figure 5.42 Change of MAC's for sensitivity based optimization	93
Figure 5.43 Change of frequency differences for sensitivity based optimization	93
Figure 5.44 MAC updating results with objective functions of increasing all MAC and decreasing all frequency differences.....	95
Figure 5.45 Frequency difference results with objective functions of increasing all MAC and decreasing all frequency differences.....	96
Figure 5.46 Change of beam cross-section areas for first optimization	96
Figure 5.47 Change of beam first moment of areas for first optimization	97
Figure 5.48 Change of beam second moment of areas for first optimization...	97
Figure 5.49 Change of shell thicknesses for first optimization	98
Figure 5.50 Change of beam torsional stiffnesses for first optimization.....	98
Figure 5.51 Change of material elastic modulus for first optimization	99
Figure 5.52 Change of material density for first optimization.....	99
Figure 5.53 MAC updating results with objective functions of increasing all MAC	101

Figure 5.54 Frequency difference updating results with objective functions of decreasing all frequency differences.....	102
Figure 5.55 Updating results for objective function of decreasing frequency difference 2	103
Figure 5.56 Updating results for objective function of increasing only MAC_1	104
Figure 5.57 Surface element property variables in different colors.....	106
Figure 5.58 Beam element property variables in different colors	107
Figure 5.59 Sensitivities of paired mode shapes on beam cross section areas	111
Figure 5.60 Sensitivities of paired mode shapes on beam first moment of area	111
Figure 5.61 Sensitivities of paired mode shapes on beam second moment of area.....	112
Figure 5.62 Sensitivities of paired mode shapes on beam torsional stiffness.	112
Figure 5.63 Sensitivities of paired mode shapes on material properties and shell thicknesses	113
Figure 5.64 Summed sensitivities of paired mode shapes on design variables	114
Figure 5.65 Change of MAC's for gradient sensitivity based optimization...	115
Figure 5.66 Change of frequency differences for gradient sensitivity based optimization	115
Figure 5.67 MAC updating results with objective functions of increasing all MAC and decreasing all frequency differences.....	117
Figure 5.68 Frequency difference updating results with objective functions of increasing all MAC and decreasing all frequency differences	118
Figure 5.69 Change of beam cross-section areas for the first optimization....	121
Figure 5.70 Change of beam first moment of areas for the first optimization	121
Figure 5.71 Change of beam second moment of areas for the first optimization	122
Figure 5.72 Change of shell thicknesses for the first optimization.....	122
Figure 5.73 Change of beam torsional stiffnesses for the first optimization..	123

Figure 5.74 Change of material elastic modulus for the first optimization (N/m ²).....	123
Figure 5.75 Change of material density for the first optimization (kg/m ³)..	124
Figure 5.76 MAC updating results with objective functions of increasing all MAC	125
Figure 5.77 Frequency difference updating results with objective functions of decreasing all frequency differences.....	126
Figure 5.78 Frequency difference 1 and 2 updating results for objective functions of decreasing Freq_Diff_1 and 2	128
Figure 5.79 Updating results for objective function of increasing only MAC_4	129
Figure 5.80 Changes of MAC values according to node removals by coMAC	131
Figure 5.81 Changes of MAC values according to node removals by nrMAC with weights 0,25;0,25;0,25;0,25.....	133
Figure 5.82 Changes of MAC values according to node removals by nrMAC with weights 0,1;0,4;0,4;0,1.....	134
Figure 5.83 Different motion of 33rd accelerometer location from global mode	135
Figure 5.84 Different motions of 102nd and 103rd accelerometer locations from global mode.....	135
Figure 5.85 Updating of MAC values under removal of 10 nodes according to coMAC.....	137
Figure 5.86 Updating of MAC values under removal of 20 nodes according to coMAC.....	138
Figure 5.87 Updating of MAC values under removal of 10 nodes according to nrMAC with weights 0,25;0,25;0,25;0,25	140
Figure 5.88 Updating of MAC values under removal of 10 nodes according to nrMAC with weights 0,1;0,4;0,4;0,1	141
Figure 5.89 Updating of MAC values under removal of 20 nodes according to nrMAC with weights 0,25;0,25;0,25;0,25	142

Figure 5.90 Change of material elastic modulus without and with node removal
..... 143

NOMENCLATURE

t	Time
x	Displacement
\dot{x}	Velocity
\ddot{x}	Acceleration
ω	Excitation Frequency
ω_r	Undamped Natural Frequency
λ_r	Eigenvalue
$X(\omega)$	System Response
$F(\omega)$	Forcing Function
$H(\omega)$	Frequency Response Function
$[M]$	Mass Matrix
$[K]$	Stiffness Matrix
$[Z]$	Dynamic Stiffness Matrix
m	Mass
k	Stiffness
c	Damping
n_r	Damping Loss Factor
$\alpha(\omega)$	Receptance
$Y(\omega)$	Mobility
$A(\omega)$	Accelerance
m_r	Modal Mass
k_r	Modal Stiffness
$[U_r]$	Eigenvector
$[\phi_r]$	Mass Normalized Eigenvector

ABBREVIATIONS

FRF	Frequency Response Function
DOF	Degree of Freedom
FEM	Finite Element Method
MAC	Modal Assurance Criterion
nrMAC	Node Removal Modal Assurance Criterion Method
coMAC	Coordinate Modal Assurance Criterion
FEA	Finite element Analysis
SDOF	Single Degree of Freedom
MDOF	Multi Degree of Freedom
BCSA	Beam Cross-Section Area
BFAMI	Beam First Moment of Area
BSAMI	Beam Second Moment of Area
BTS	Beam Torsional Stiffness
MD	Material Density
MEM	Material Elastic Modulus
ST	Shell Thickness

CHAPTER 1

INTRODUCTION

1.1 Motivation for the Research

Computer technology has made great advances for the past ten years. Besides its unbelievable advance, computers assisted in the development of new innovations, providing increased computational processing capability. Moreover, the increased accessibility of computers and their partnership with numerical methods has had a significant impact on the engineering problem-solving.

Exact solutions to many engineering problems are hard and time consuming to find. Therefore, approximate solution algorithms are designed and implemented. Numerical analysis is the discipline of methods and algorithms used to obtain approximate, but reasonably accurate solutions to mathematical problems. The proposed numerical method should be questioned and analyzed carefully, since the method gives an approximate solution. If it is proved that the approximation is sufficiently accurate, it can be used to solve the actual engineering problems.

Model updating is the procedure of modifying a numerical model according to its experimentally acquired counterpart. In this procedure, numerical model, generally finite element model, is the numerical model that gives approximate solutions to engineering problems. On the other hand, experimental model (Structural), which is acquired in accordance with experiments on actual structure, is believed to be the accurate model for updating.

Finite element method (FEM), sometimes called finite element analysis, is used to find approximate solutions to problems arising in physics and engineering. Now, FEM is used in many field of engineering to simulate the actual structures. Along with advances in computer technology, simulations of structures under different environmental conditions increased their importance in industries aerospace, defense, automotive, etc. In these industries, FEM is found to be an effective and efficient tool to reach the goals of better systems while saving for time and money. Today, there are many commercial software, like Ansys, Nastran, Abaqus etc., that are used for these goals. By using this method, structural analyses below are performed with ease:

- Static analysis to see the effects of different loads and boundary conditions on the structure,
- Modal analysis in order to get natural frequencies and mode shapes of the systems,
- Transient analysis to see the effects of time varying loads,
- Fatigue analysis in order to get fatigue performance of the system and to predict its fatigue life.

In addition to the improvements in computer technology, data acquisition and sensor technologies made great progress through years. With these advances, structures are tested with sophisticated systems in many aspects. Some of the principal advantages that came with this technology development are:

- New sensor innovations with more sensitivity and capacity,
- Improved data acquisition systems that can acquire more data with increased speed,

Although there are a lot of developments in testing equipments, experiments still take more time and money than simulations. That is why; model updating is the popular trend for the past 10 years. There are many commercial software

such as LMS Virtual.Lab which updates finite element models according to experimental data straightforwardly.

In recent years, the general trend of industries for products design to manufacturing process is shown in Figure 1.1.

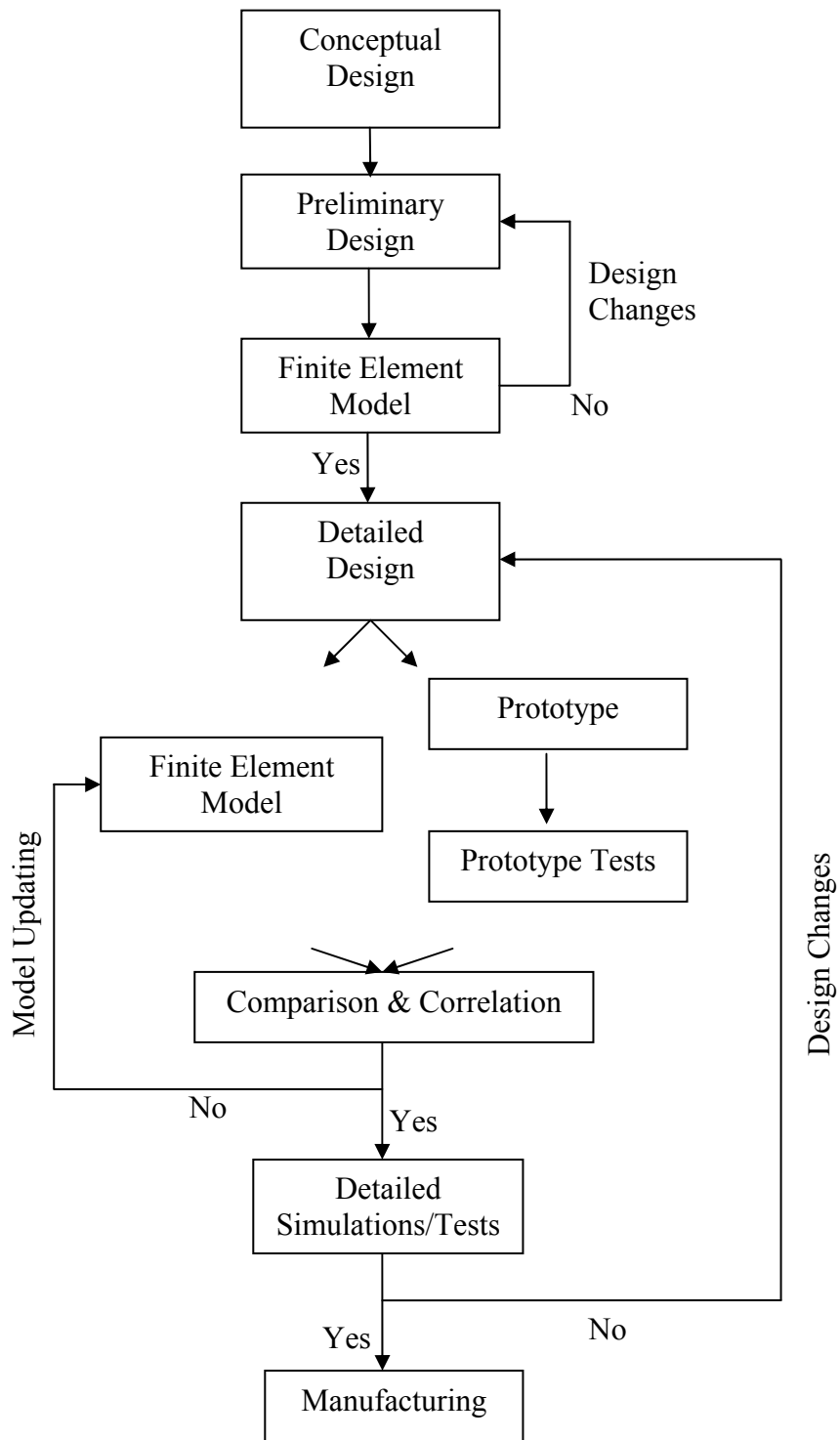


Figure 1.1 Design to manufacturing diagram for industries in recent years

1.2 Objectives of the Thesis

The objectives can be summarized as:

- Analyzing model updating performance by using commercial software LMS Virtual.Lab on an aerospace platform.
- Organizing difficulties in real world updating problems and solutions to them.
- Propose a new technique to find the optimum node removal in order to improve the MAC matrix.
- Validate the proposed method by using a real structure and experimental data.

1.3 Outline of the Thesis

The outline of the thesis is as follows:

Chapter 2 focuses on model updating techniques and the background information coming from the literature. Updating through numerical techniques and input data is summarized in detail.

Chapter 3 gives detailed information about the techniques required to be handled before model updating. It includes the techniques of reduction of numerical models and expansion of experimental models. Moreover, experimental modal analysis methods are summarized. Additionally, introductory information about sensitivity analysis and optimization techniques is given.

In chapter 4, the new method to find the optimum node removal location for better MAC matrix diagonal is introduced. The theory behind the proposed method is also introduced.

Chapter 5 includes the model updating case studies performed both on the helicopter tail and complete fuselage. The application and performance of proposed method is examined and compared with the Coordinate Modal Assurance Criterion.

Finally, in chapter 6, the results of case studies are discussed and concluding explanations are presented. Also, difficulties that are faced in updating of whole helicopter fuselage are summarized with solutions to them.

CHAPTER 2

MODEL UPDATING TECHNOLOGY

2.1 Background

Numerical analysis techniques found application in many industries with the progress of computer technology. One of the popular and widely used techniques is the Finite Element Method (FEM). This method evolved through years and is used in many fields of engineering like aerospace, automotive, ship building and civil engineering. With its proven flexibility, approximate solutions could be obtained for difficult problems. In order to make these approximations more close to real structure properties, finite element model results are revised directly according to experimental results. This revision process is called model updating.

Literature on model updating is nearly 30 years old. Many model updating methods have been proposed through years. Some of the methods found progress in years, but some lost usage.

In early model updating studies, Baruch [1] studied on updating through indirect method to correct the stiffness and flexibility matrices. Berman and Nagy [2] proposed an indirect method to correct the mass and stiffness matrices.

Lin and Zhu [3] further developed frequency response function (FRF) method to identify damping matrices of structural systems, as well as mass and stiffness matrices. Complex updating formulations have been established for both case of

proportional and non-proportional damping. They succeeded in complex FRF updating method by deriving accurate updated mass and stiffness modeling errors and system damping matrices.

Uhl et al. [4] correlated helicopter finite element model to ground test model by using Modal Assurance Criterion (MAC) and investigated the increasing/decreasing effects of test nodes on MAC matrix by contribution analysis (MACCo) which was performed in LMS CAE Gateway software. According to the research, excluding a measurement point can result in a significantly improved MAC matrix.

Göge and Link [5] compared two different computational model updating methods that make use of the inverse sensitivity approach. First method uses eigenvalue and mode shape differences as residuals, while second method uses eigenvalue and frequency response errors. Both methods have the ability to update physical mass, stiffness and geometrical parameters. Because second method use resonance and frequency response data at resonance peaks, it has the ability to update viscous damping parameters additionally. According to general results, using eigenvalue and mode shape residuals gave physically meaningful results for the worked application. However, both methods were successful to reproduce the measured data. Rating of the two updating procedure is shown below:

Table 2.1 Comparison of different procedures [5]

Mode Shape Residuals vs. Response Residuals		
Category	Procedure 1	Procedure 2
Improvement of average frequency deviations (active freq. range, unmod. structure)	1	0

Table 2.1 continued

Improvement of average frequency deviations (passive active freq. range, unmod. structure)	1	0
Improvement of average mode/FRF correlation (active freq. range, unmod. structure)	1	0
Improvement of average frequency deviations (mod.1)	1	0
Improvement of average mode/FRF correlation (mode.1)	0	1
Visual improvement of resonances of FRFs (unmod.)	0	1
Visual improvement of antiresonances of FRFs (unmod.)	0	1
Visual improvement of resonances of FRFs (mod.1)	1	0
Visual improvement of antiresonances of FRFs (mod.1)	1	1
Robustness of CMU procedures	1	0
Time exposure for complete model validation	1	1
Inaccuracies concerning the experimental data	0	1
Total Points	8	6

Göge [6] used inverse sensitivity approach to update and validate the finite element model of a civil four-engine aircraft according to Ground Vibration Test results. Residuals containing the differences between numerical and measured eigenfrequencies and mode shapes are minimized. With the sensitivity study of 18 parameters, the procedure has proven to be quite

effective not only for active but also for passive frequency range. MAC values are greatly increased and frequency deviations are decreased significantly.

Brown et al. [7] examined the difficulties in the updating of finite element models for industrial applications. He tried to overcome the below mentioned difficulties by using Sensitivity Base Element by Element Updating Method.

a) The possibility of structural removal as a result of minimization of residuals through the reduction of mass and stiffness, rather than through the localization and correction of modeling errors.

b) The difficulty of localizing errors in different substructures for large structural models.

c) With real data, inconsistent mode normalization can prevent the localization of errors and make the evaluation of convergence difficult.

d) The evaluation of the quality of the update can be difficult using few measurement points.

Kozak et al. [8] presents a new error localization technique which computes the so-called Miscorrelation Index (MCI) for each coordinate as a function of frequency. A new model updating routine which minimizes this index is introduced. This new routine does not require numerical FRF data but needs experimental FRF results. Nevertheless, the method is capable of handling cases with incomplete measured data by using expanded modal data for the rest of the points.

Jesus Lopez-Diez et al. [9] worked on error localization of finite element models for direct model updating. Other than Modal Assurance Criterion (MAC), Modal Effective Mass (MEM) was suggested additionally in order to correlate analytical and experimental modes. MEM seemed to be very useful to identify the sources of discrepancies between test and analysis when updating for error location.

Göge and Link [10] applied the classical inverse sensitivity approach to update user selected stiffness, mass and geometric parameters in order to minimize the deviations between analytical and measured natural frequencies and mode shapes. Updating parameters were selected according to sensitivity analysis and excellent results were achieved.

Kozak [11] in his master thesis investigated the model updating techniques and divided them into two categories as Direct and Indirect (Iterative) methods. According to this classification, direct model updating methods extract mass, stiffness and damping parameters from the measured data and implement those in the original mathematical model. On the other hand, iterative model updating methods make adjustments on individual elements by the calculated updating factors.

Köksal et al. [12] compared three structural reanalysis methods which uses FRF data for correlation. Computational efficiency of the methods was the base for the comparison.

2.2 Model Updating Techniques

There are several different model updating techniques proposed through years. Categorization of these techniques can be made in two ways:

- Updating through numerical techniques
 - Direct methods
 - Iterative (Indirect) methods
- Updating through input data
 - Modal data based methods
 - Response function based methods

These categories are summarized in the following sections.

2.2.1 Updating Through Numerical Techniques

2.2.1.1 Direct methods

Direct model updating methods use the experimental modal data in order to update the finite element model (whole system matrices) directly. Therefore, updated mathematical model and the experimental model match exactly in numerical base. Although direct methods have lower processing time and no convergence problem, they have the disadvantages summarized below [13]:

- High quality modal test and analysis results are needed.
- In order to have the degree of freedom compatibility, experimental mode shapes must be expanded from which there will be errors coming
 - The methods generally loose the connectivity to the structure and updated matrices are usually populated
 - There is no guarantee for the positive definiteness of the updated mass and stiffness matrices.

Direct model updating methods are divided mainly into 3 groups [14] as shown below:

- I. Methods using Lagrange Multipliers,
- II. Matrix mixing methods,
- III. Error matrix methods

Methods using Lagrange multipliers work as an optimization tool and try to minimize an objective function along with additional constraints. There are

proposed algorithms that correct the system stiffness or mass matrices. Since connectivity pattern is destroyed, applicability of these methods is limited.

On the other hand, matrix mixing methods construct the inverses of the global mass and stiffness matrices according to measurements for which all modes are assumed to be measured at all DOFs.

Finally, error matrix methods directly estimate the errors in the mass and stiffness matrices assuming the error is small.

2.2.1.2 Iterative methods

Iterative (indirect) methods mainly try to improve the correlation between the experimental and numerical models via a penalty function. Although penalty function is usually non-linear, the problem has to be linearized and optimized iteratively. In this optimization process, individual elements are updated by design parameters such as its geometry of material properties. Compared to direct methods, parameterization provides physically more meaningful results. System of equations as shown below is solved for the design parameter changes and the FE model is updated [14].

$$[S]\{\Delta\phi\} = \{\varepsilon\} \quad (2.1)$$

where $[S]$ is the sensitivity matrix, $\{\Delta\phi\}$ the changes in updating parameters and $\{\varepsilon\}$ the residual, the difference between the measured and predicted dynamic properties.

Iterative methods have the advantages of updating parameter variety and weighting opportunity of measured and numerical data. However, three major problems with the use of iterative methods are [15]:

- Necessity of the correlation of experimental and numerical modes but there is no guarantee that all modes will be correlated.
- Because of mass distribution difference between numerical model and the actual structure, there can be scale problem. By using modal scale factor (MSF), problem can be solved.
- Theoretical model probably may not include the damping although experimental model does.

2.2.2 Updating Through Input Data

Model updating techniques can be categorized according to the input data that is used for model updating. The use of modal parameters, namely eigenvalues and eigenvectors, for model updating is called “Modal data based model updating”. On the other hand, if frequency response functions (FRF) are used for updating, it is called “FRF based model updating” or “Response Function Method (RFM).

2.2.2.1 Modal Data Based Model Updating

As stated in the preceding section, modal data based methods update the numerical model according to modal parameters. These modal parameters are extracted from measured data. This extraction process introduces errors in addition to inaccuracies present in the measured data. There are many methods using this procedure. Kozak [11] and Rad [13] have investigated and compared different methods in their theses.

2.2.2.2 Response Function Based Model Updating

The history and background of FRF based model updating is not long compared to modal data based updating. However, for the past ten years, there have been many researches about RFM by Lin and Zhu [3], Rad [13], Grafe [14].

RFM updating uses the measured quantities directly. Therefore, there are no errors due to parameter extraction as modal data based updating methods. Another advantage of RFM is that it is not limited to eigenvalue and eigenvector parameters because many frequency points coming from available test data can be used for updating calculations.

Modak et al. [16] compared the inverse eigensensitivity (IESM) and the response function method (RFM) of the categories modal data based and FRF based updating, respectively. The results are concluded as:

- Both methods predicted the errors with a good accuracy in the case of complete and incomplete data.
- For the worked study which includes incomplete experimental data, the RFM performed better than the IESM.
- In the presence of noise, IESM predicted the discrepancies more accurately.
- The selection of frequency points in terms of their location and number in the case of RFM seemed very important for its convergence.

The calculation of frequency response function, which is the main input for RFM, is shown below.

For a single degree of freedom system [17]

$$m\ddot{x}(t) + c\dot{x}(t) + kx(t) = f(t) \quad (2.2)$$

Where m , c , k are mass, damping and stiffness constants respectively. The Fourier or frequency (ω) domain equivalent of the equation (2.2) is:

$$\left[-m\omega^2 + jc\omega + k\right]X(\omega) = F(\omega) \quad (2.3)$$

Restating the above equation,

$$X(\omega) = H(\omega)F(\omega) \quad (2.4)$$

Where

$$H(\omega) = \frac{1}{-m\omega^2 + jc\omega + k} \quad (2.5)$$

Equation (2.4) states that the system response $X(\omega)$ is directly related to the system forcing function $F(\omega)$ through the quantity $H(\omega)$. If the system forcing functions $F(\omega)$ and its response $X(\omega)$, are known, $H(\omega)$ can be calculated. That is,

$$H(\omega) = \frac{X(\omega)}{F(\omega)} \quad (2.6)$$

The quantity $H(\omega)$ is known as the Frequency Response Function (FRF) of the system.

If the ratio is displacement to force, then equation (2.6) is called the receptance and shown with $\alpha(\omega)$. There are other forms of frequency response function according to the response type. Taking first derivative of displacement, one gets the mobility, $[Y] = j\omega\alpha(\omega)$. If second derivative is taken, one gets the accelerance (or inertance), $[A] = -\omega^2\alpha(\omega)$.

CHAPTER 3

PROCEDURES REQUIRED FOR MODEL UPDATING

Model Updating methods referenced in this thesis consist of some numerical approximations and processes. The processes are shown in Figure 3.1.

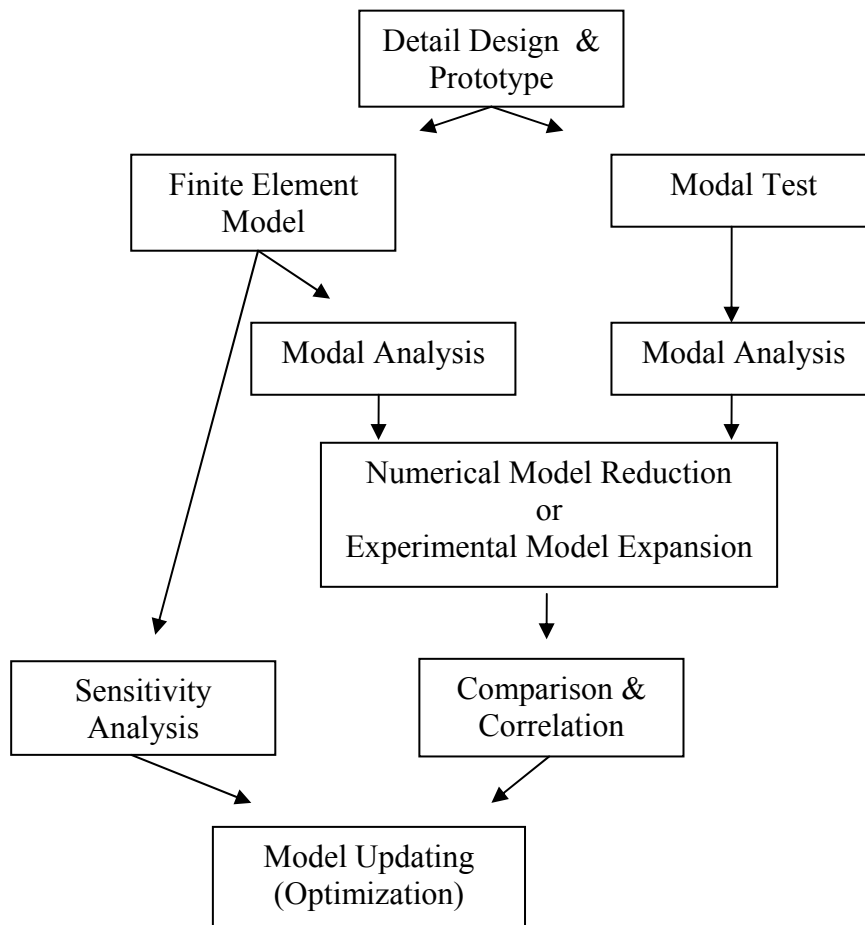


Figure 3.1 Diagram of model updating procedures

This section is devoted to the processes that are used through model updating procedure. As seen from the diagram, there are mainly two flows. The first flow is related to FEM and it can be referred to as the verification model/process. Second flow is associated with the test model and can be referred to as the reference model/process.

In the verification process, finite element model of the structure is developed. Using this model, modal analysis is performed in order to get natural frequency and mode shapes. Additionally, sensitivity analysis is carried out to see the sensitivity of the dynamic properties of the model according to design parameters.

In the reference process, first of all, modal test of the actual structure is completed. Test results are analyzed to get natural frequency and mode shapes of the actual system. At this point, in order to have a compatible degree of freedom (DOF) for the verification and reference model, either verification model DOF is reduced or reference model DOF is expanded.

After this process, the two models are compared and correlated according to methods like Modal Assurance Criterion (MAC), Frequency Response Assurance Criterion (FRAC). Finally, model updating is completed by finding the optimum design parameters. The detailed information about these methods is summarized in the following sections.

3.1 Finite Element Method

Through years, engineers and academicians tried to obtain the closed-form numerical solutions for most of the engineering problems. However, the problems in the form of differential equations are generally difficult to obtain an exact solution. Moreover, problems became more and more complex through

years. Therefore, numerical methods are adopted to solve these differential equations by approximations. Because of its flexibility, practical efficiency and generality, Finite Element Method (FEM) is the mostly used approximate numerical solution technique in the industry. Google search engine yielded over 4 million results in 2009 for the phrase “finite element”.

The degree of approximation is closely related with the accuracy of the result of finite element analysis (FEA). If approximation degree is increased, solution time and cost are increased together with accuracy.

The basic idea of FEM is to divide the actual body into finite elements which are called “elements”. Each element forms a simple unit whose behavior can be analyzed without difficulty. Elements are connected to each other by points that are called “nodes”. The whole model that consists of these nodes and elements is called “mesh” and the process of making the mesh is called the mesh generation. In order to obtain a reasonably accurate solution, the number of nodes should be in the order of ten thousands.

The quality of the mesh (coarse, medium or fine) is one of the important factors for accurate approximations. Coarse mesh (Figure 3.2) increases discretization errors but is solved quickly. However, fine mesh (Figure 3.3) gives reasonably accurate results but the computer time, and hence the cost, also increases.

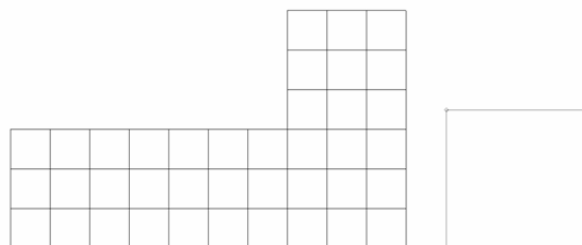


Figure 3.2 Coarse mesh, single quadrature element

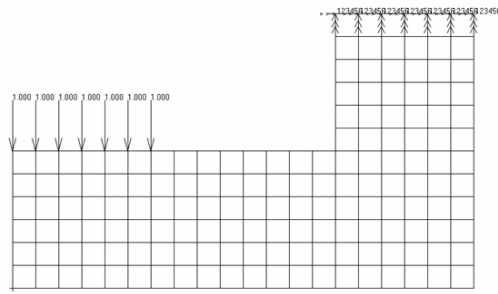


Figure 3.3 Fine mesh with loading and boundary conditions

FEM analyzes the mathematical model, rather than the actual physical problem whatever the analysis method is. Therefore, there are modeling, discretization and numerical errors related to numerical solution of the actual structure [18]. An example for modeling error is the elementary beam theory where a beam is represented by a line which ignores deformations associated with transverse shear. Discretization error exists because the physical structure has infinitely many DOF while the FEM has a finite number of DOF. For two analyses with different mesh quality, coarse meshed FE model will have more discretization error and represent the actual geometry not as good as refined FE model. Numerical error is introduced by the computer which rounds and truncates the numbers as it forms and solves the matrices. Although generally numerical error is small, it may increase depending on modeling problems.

There are mainly three types of engineering problems;

- Equilibrium Problems
- Eigenvalue Problems
- Propagation Problems

Eigenvalue problem is the main interest in this thesis study and starts with solving the equation of motion for free, time-invariant and undamped system:

$$[M]\{\ddot{x}(t)\} + [K]\{x(t)\} = 0 \quad (3.1)$$

Where $[M]$, $[K]$ are the mass and stiffness matrices of the system respectively. Assuming steady-state harmonic solution of the form:

$$\{x\} = \{U\} e^{i\omega t} \quad (3.2)$$

Differentiating twice one gets

$$\{\ddot{x}\} = -\omega^2 \{U\} e^{i\omega t} \quad (3.3)$$

Substituting equations (3.2) and (3.3) into equation (3.1) and simplification, the following equation is obtained:

$$([K] - \omega^2 [M])\{U\} = 0 \quad (3.4)$$

There are two possible solutions to this eigenvalue problem

1. If $\det([K] - \omega^2 [M]) \neq 0$, then the only possibility is $\{\phi\} = 0$ which is a trivial solution and is not interesting from a physical point of view.
2. If $\det([K] - \omega^2 [M]) = 0$, then there is a nontrivial solution to the eigenvalue problem. The eigenvalue problem is reduced to

$$\det([K] - \lambda [M]) = 0 \quad (3.5)$$

Where $\lambda = \omega^2$ is called the eigenvalue. If the structure has N dynamic degrees of freedom, then there are N numbers of eigenvalues. ω stands for the natural frequencies (also known as normal frequencies, fundamental frequencies or

resonant frequencies) of the structure. The eigenvector $\{U_k\}$ associated with the natural frequency ω_k is called normal mode or mode shape. The normal mode corresponds to deflected shape patterns of the structure.

3.2 Modal Test and Analysis

As mentioned in the preceding sections, numerical solutions to numerical problems give approximate results for actual structures. The accuracy of these approximations should be proved by experiments on actual structures.

For example, dynamical properties calculated using numerical models are approximations to actual structures. Experimental modal tests (generally called Modal Test) give the engineers the opportunity to see the accuracy of these approximations. After modal tests, dynamical properties are extracted from measured data by using different mathematical methods. This extraction process is called the “Experimental Modal Analysis”. By modal properties, it is generally referred to:

- Natural frequencies,
- Mode shapes,
- Damping factors

Modal test and analysis process can be automated as a procedure which can be summarized as:

- I. Excitation of the structure by modal shaker or hammer with a low magnitude input,
- II. Responses are measured in the form of acceleration and force at different locations,

III. Frequency Response Functions (FRF) are calculated using measured data.

IV. Modal parameters are extracted from FRF's by modal analysis techniques.

Modal test and analysis methods are summarized in the following sections.

3.2.1 Modal Test Techniques

Modal test is the most popular method which is used to determine the dynamic behavior of structures by non-destructive and easily performed techniques. The responses from various locations are measured for known excitations. Excitation is measured generally in the form of force by using force transducers. On the other hand, responses are measured usually in the form of acceleration by using accelerometers. There are many books related to this subject. Ewins [19] focused directly on this subject and showed particular attention to three important aspects of the measurement process for high-quality modal testing.

- Boundary and excitation conditions of the structure;
- The quantities that are to be measured;
- Appropriate signal processing for the test type

Test structure should be prepared carefully before measurement. For this reason, boundary condition of the structure is the first thing to choose. There are mainly two type of boundary conditions; free or grounded.

For the free boundary condition, test object has no connection to the ground and suspended freely in space. Rigid body modes in six directions, three translations and three rotations, can be observed in this condition. These rigid modes can be determined easily since they do not exhibit any bending or twisting motion. In

reality it is impractical to provide a proper free boundary condition. For this reason, test object must be connected to ground in such a way that the actual boundary condition of the test structure closely approximates this condition. For this approximation, the popular methods are;

- Hanging the test object to the ceiling by using soft springs like bands,
- Supporting the test object on very soft springs like foams.

The other boundary condition, grounded, is accomplished by fixing the necessary points of the structure to the main platform or ground. In practice, grounding is not as easy as it seems. The ground or platform should be rigid enough to fix the test object.

Vibration tests require an external exciter to generate the necessary vibration input. For this purpose, there are several devices available for the excitation of the test object. They can be gathered in two types [19]; contacting and non-contacting. Shaker with connecting rod (stinger) as shown in Figure 3.4 is an example to contacting type excitation. By using shaker, test object is excited in continuous (random, sinusoidal etc.) or transient (pulse, chirp etc.) forms throughout the test. Hammer as shown in Figure 3.5 is a second type excitation device by which the test structure is hit impulsively for a short period of time.



Figure 3.4 Electro-dynamic shaker with stinger attachment



Figure 3.5 a) Force Transducer, b) Impact Hammer with different tips

In addition to the computer technology, sensor technology has also made great advances through years. Today, many sophisticated sensor types (Accelerometers, force transducers, velocity probes, etc.) are used in many test platforms. Among these sensor types, accelerometers (mainly piezoelectric type) are the most popular and widely used sensors in experimental modal tests.

The most important thing that the great care at modal tests should be given to is the positions of sensors. If a structure is excited at its one of the resonant modes, some of the locations remain stationary whereas some move. These stationary points are called as "Nodal Points". Nodal point locations are generally different for different resonant frequencies of the test object. In order not to miss necessary modes of the test object, accelerometer locations should be chosen such that they are not located on the nodal points.

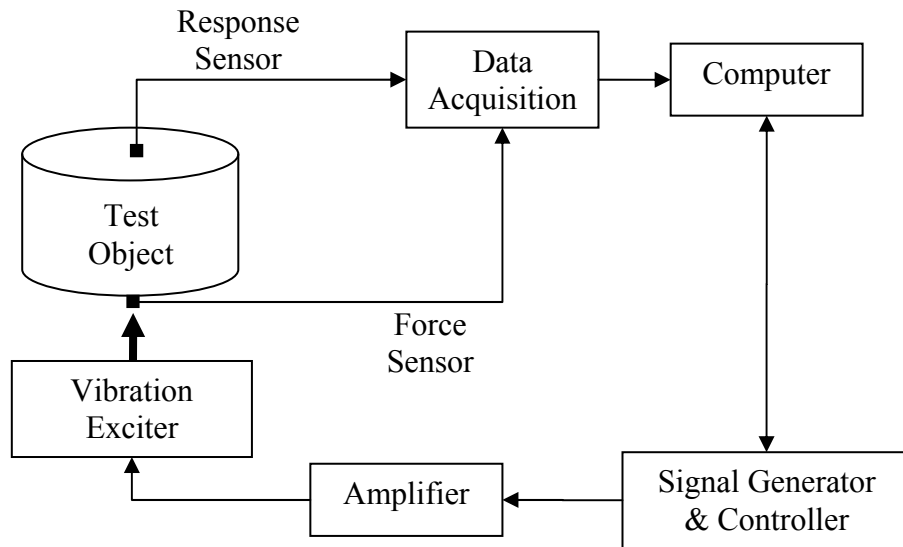


Figure 3.6 Basic items of a measurement system

A basic measurement system as shown in Figure 3.6 consists of many items like data acquisition, sensors, amplifier etc. In this system, signal is generated by a source which is called signal generator. Generally, signal generator devices also have controller modules to control the excitation signal applied to the test object. The generated signal's amplitude is low for the vibration exciter. For this reason, an amplifier is used to increase the amplitude of the signal. The amplified signal is used to drive the vibration exciter which excites the test object. There are generally two types of sensors; force and response, on the test object. Force sensor is used to monitor the excitation signal. Response sensors are used to sense the response of the test object to the excitation signal. There are different types of response sensors to sense acceleration, velocity, strain, etc. The response signals are recorded by a data acquisition system which process (signal conditioning, sampling etc.) the signals to obtain desired information. Acquired data are stored on a computer which also displays and analyzes the stored data.

Modal tests are carried out by using the devices shown and explained above. Excluding the response sensor types, vibration exciter is the changing part for different modal tests. Care has to be given to excitation selection. In the following section, detailed information for hammer and shaker tests is given.

3.2.1.1 Hammer Test

Experimental modal test by using hammer is a popular and relatively simple method to excite the system. However, greater attention has to be given to the analysis phase of hammer test. This type of test uses only a simple hammer with different tips and heads. Various tips at different hardness's and the mass of the hammer define the frequency limit of force spectrum. Giving an impulse, hard tip excites the system for a broader frequency range than the soft tip. Likewise, bigger hammer head is required in order to excite larger structures. In addition to these, a force transducer is generally attached to the tip in order to sense the force during impact.

Hammer test is advantageous since the testing system can be established easily with less equipment and cost. Moreover, engineer can be ready to test the system in a very little time. Although hammer test is easy to perform, if the structure is real big and heavy, then it is almost impossible to excite the structure with hammer. Other than that, hammer test is not as effective on nonlinear structures and has the risk of double impact occurrence. Additionally, excitation frequency is approximately limited to 400 Hz (changes with tip and hammer mass) for hammer tests.

Hammer tests can be performed in two configurations:

- Driving Point Test
- Roving Hammer Test

These are summarized in the following sections.

Driving Point Test

In this procedure, accelerometers are placed on the structure and driven by the hammer at only one location as shown in Figure 3.7. This location is generally one of the accelerometer locations and procedure is called “Driving Point”. With this method, only one column of the Frequency Response Function (FRF) matrix is obtained.

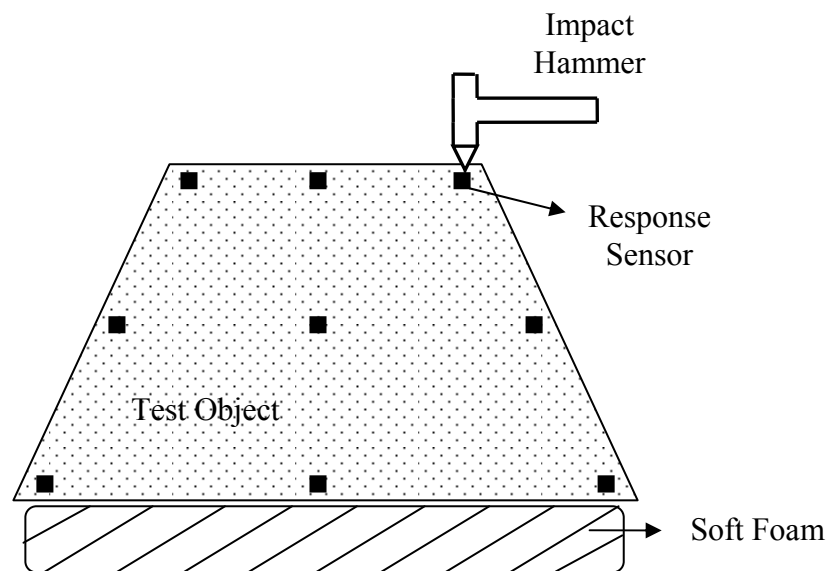


Figure 3.7 Driving point hammer test on sponge

Roving Hammer Test

In this procedure, accelerometers are placed on the structure and all accelerometer locations are driven by the hammer one by one as shown in Figure 3.8. This procedure is generally called “Roving Hammer”. Complete

Frequency Response Function (FRF) matrix of the system is obtained with this method.

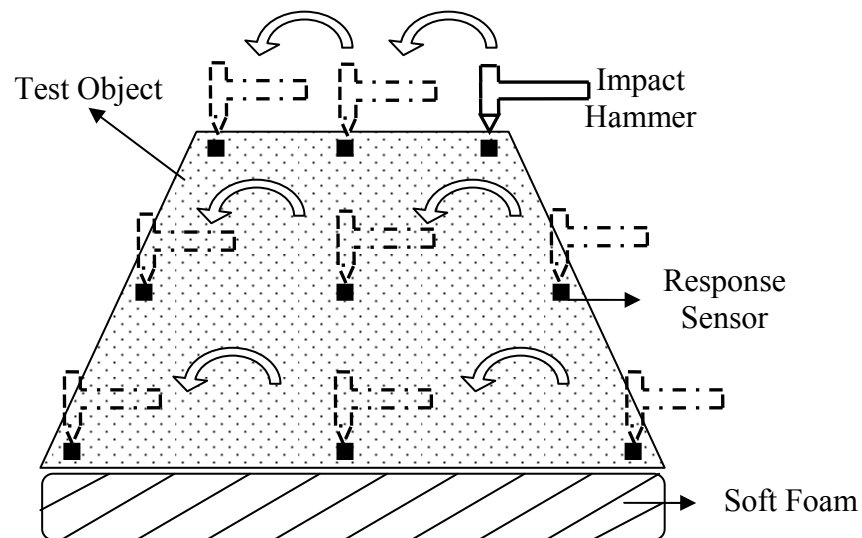


Figure 3.8 Roving hammer test

3.2.1.2 Shaker Test

Another popular method of experimental modal test is performed by using shaker. Excitation is given to the structure by a shaker through a connecting rod. Today there are types of mechanical, electromagnetic and electro hydraulic shakers which have differences in operation-capability. Frequency range of operation, stroke (maximum displacement), maximum acceleration, maximum force, maximum velocity are the main differences between shaker types. Therefore, appropriate shaker type should be selected for different applications.

Shakers have the opportunity to excite the structure in deterministic or non-deterministic (random) signals. Deterministic signals (sine, sine sweep, stepped sine, etc.) can be known at any instant in time and obey mathematical

relationships. However, non-deterministic signals (random, burst random, etc.) cannot be known at any instant in time, cannot be expressed by any explicit mathematical relationship.

Care has to be given to the connecting rod for this type of test. Wrong use and selection of rod can introduce unwanted excitations, modifications to the structure, etc. The connecting rod must be stiff enough in excitation direction while relatively flexible in other directions.

This method is generally divided into two categories. First one is performed by locating accelerometers and driving the shaker from one or multiple locations as shown in Figure 3.9. The number of columns of frequency response function (FRF) matrix is equal to number of shaker locations with this method.

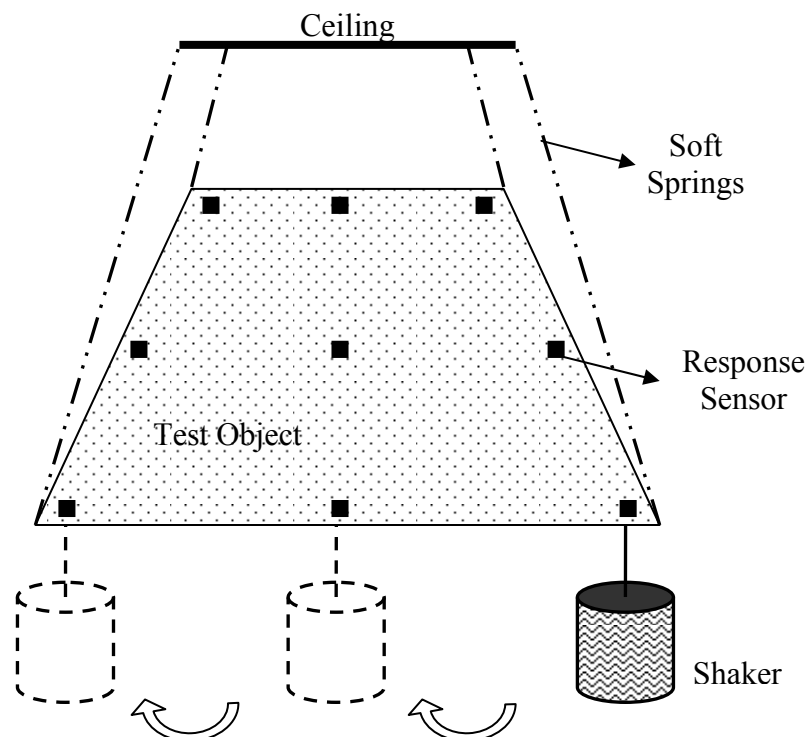


Figure 3.9 A typical shaker test

For the second category, only one shaker location is used but accelerometer locations are changed as shown in Figure 3.10. One column of Frequency Response Function (FRF) is obtained by this method.

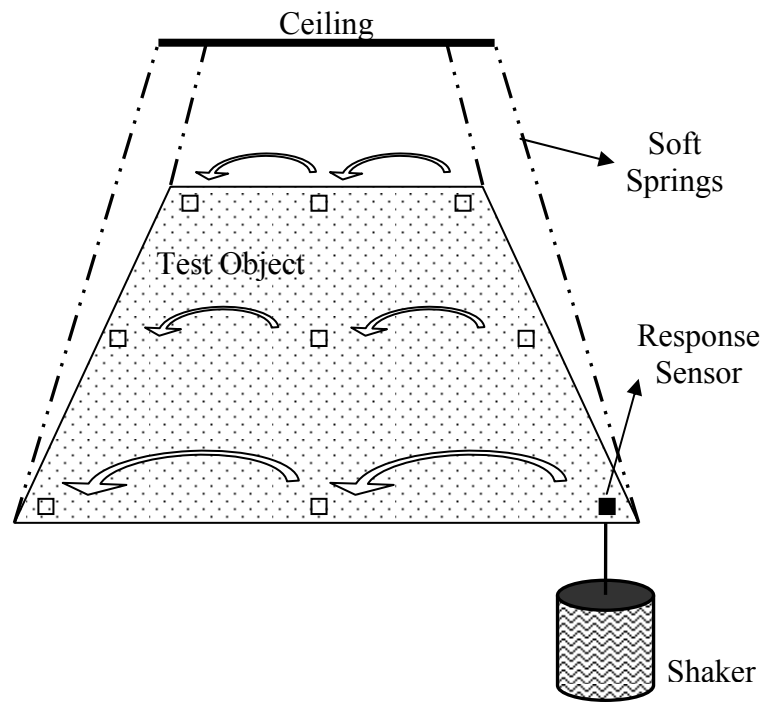


Figure 3.10 A typical shaker test where accelerometer location is changed

3.2.2 Modal Analysis of Test Results

After successful completion of the modal tests, modal analysis of measured data is performed. Modal analysis is mainly used to determine the modal characteristics of a system in terms of natural frequencies, mode shapes and damping (loss) factors.

There are four basic assumptions concerning any structure that are made in order to perform an experimental modal analysis [17]:

- The structure is assumed to be linear
- The structure is time-invariant, i.e., the parameters that are to be determined do not change in time.
- The structure obeys Maxwell's reciprocity, i.e., a force applied at DOF p causes a response at DOF q that is the same as the response at DOF p caused by the same force applied at DOF q.
- The structure is observable, i.e., the input-output measurements that are made contain enough information to generate an adequate behavioral model of the structure.

Before modal analysis, there are preliminary checks of FRF data as [19]:

- Visual Checks:
 - Low and high-frequency asymptotes
 - Incidence of anti-resonances
 - Overall shape of FRF skeleton
 - Nyquist plot inspection
- Assessment of Multiple-FRF data set using Singular Value Decomposition (SVD): These methods are appropriate for situations where several FRFs have been acquired. Generally used for elimination of singularity when inverse of a matrix is close to singularity.
- Mode Indicator Functions (MIFs): A more complex version of SVD. These methods are intended for sets of FRF data from multiple references. Such data are available from multiple-excitation measurements. Method shows visually whether a peak in the FRF is a natural frequency or not.

Modal analysis methods are categorized in many formats; Time Domain-Frequency Domain Methods, Direct-Indirect (Modal) Methods, Single Degree of Freedom (SDOF)-Multi Degree of Freedom (MDOF) analyses. Ewins [19]

stated that “The modal analyst must rely increasingly on the external provision of the most effective modal analysis software and can no longer expect to write his/her own routines, as was the case only a few years ago. The numerical and computation sophistication of state-of-the-art modal analysis procedures mean that practical implementation of these methods are beyond the means of the modal analyst.” Therefore, modal analyses in this thesis are performed by using LMS Test.Lab software.

Modal analysis tries to find the mathematical model of the actual structure by subjecting the measured data to some curve-fitting procedures. The base point is to obtain a mathematical model that behaves like the actual structure. Curve-fitting procedures are generally performed to measured frequency response functions. For proportionally damped multi degree-of-freedom systems, FRF formulation can be written in the form:

$$\alpha(\omega) = \frac{1}{K - \omega^2.M + j.\omega.C} \quad (3.6)$$

or equally:

$$\alpha_{ij}(\omega) = \sum_{r=1}^N \frac{U_{ir}.U_{jr}}{(k_r - \omega^2.m_r) + j.(\omega.c_r)} \quad (3.7)$$

where U_{ir} is the eigenvector, k_r is the modal stiffness, m_r is the modal mass.

Here natural frequencies are given as, $\omega_r = \sqrt{\frac{k_r}{m_r}}$

Modal mass (m_r) and modal stiffness (k_r) values are calculated by using

$$[U]^T[M][U] = [m_r] \quad (3.8)$$

$$[U]^T[K][U] = [k_r] \quad (3.9)$$

Moreover, mass normalization of the eigenvectors can be practiced as:

$$[\phi_r] = \frac{1}{\sqrt{m_r}} [U_r] \quad (3.10)$$

If equation (3.2) is normalized to m_r :

$$\alpha_{ij}(\omega) = \sum_{r=1}^N \frac{(\phi_{ir})(\phi_{jr})}{\omega_r^2 - \omega^2 + j\eta_r\omega_r^2}, \quad (3.11)$$

if modal constant is introduced:

$$\alpha_{ij}(\omega) = \sum_{r=1}^N \frac{{}_r A_{ij}}{\omega_r^2 - \omega^2 + j\eta_r\omega_r^2} \quad (3.12)$$

where ${}_r A_{ij}$ is the modal constant and equal to $(\phi_{ir})(\phi_{jr})$, η_r is the damping (loss) factor, ω_r is the natural frequency. Working on the natural frequency, modal constant and damping (loss) factors, the fitted curve is converged to the measured curve with minimum error. As an example, Figure 3.11 shows measured and curve-fitted plots of a frequency response function.

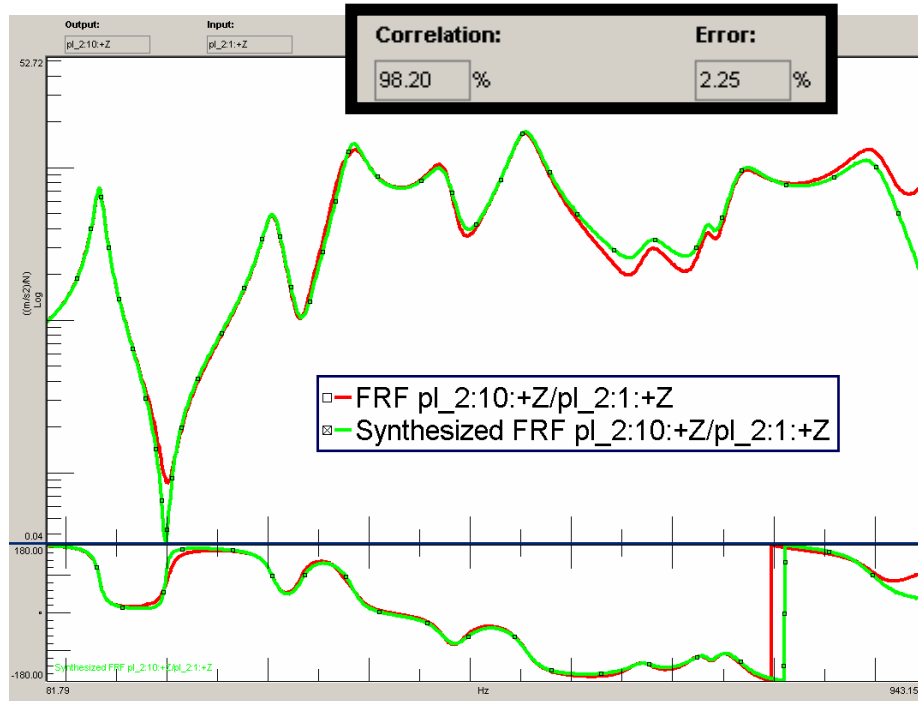


Figure 3.11 Measured and curve-fitted FRF curves with correlation and error percentage

Throughout this thesis, modal analyses of several case studies are carried out using LMS Test.Lab software. This is widely used software in industry that has different curve-fitting algorithms like Least Squares Complex Exponential, Polyreference Complex Exponential, etc. Detailed information about the procedures of modal analysis with LMS Test.Lab is presented in Appendix C.

3.3 Reduction and Expansion Methods

Reduction or expansion of model sizes is the important steps of the model updating studies. Care has to be given since accuracy of comparison/correlation of numerical and experimental model is dependent mainly on these methods.

Sizes of the numerical and experimental models have to be compatible in order to compare/correlate. Nevertheless, numerical models generally have sizes

(Degree of Freedom) of 1000-100000. However, experimental models are usually in the order of 2-200. With the advances in computer technology, the size difference is even more. In order to equalize the model sizes, either numerical model is reduced to experimental model size or experimental model is expanded to numerical model size.

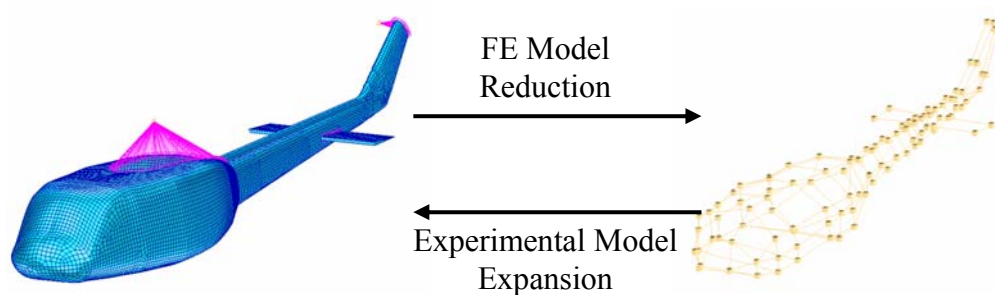


Figure 3.12 Schematic of Reduction/Expansion Process

Grafe [14], Kozak [11], Rad [13], Natke [15] etc. have examined the reduction and expansion methods in detail. These detailed examinations are given in the following sections.

3.3.1 Finite Element Model Reduction

The base and main purpose of this method is to reduce the size (DOF) of numerical model to the size of experimental model. Different methods were proposed for this purpose. The most popular ones are:

- Guyan Reduction
- Improved Reduction System
- System Equivalent Reduction Expansion Process

Guyan reduction has been used for reduction of large numerical models for years. LMS Virtual.Lab model updating module has both reduction and expansion capabilities. However, it uses Guyan reduction method during model updating [15].

Guyan reduction technique reduces the problem to a smaller one by relating certain degrees of freedom to certain others by means of constraint equations. The retained degrees of freedom are associated with large concentrations of mass and inertia.

All degrees of freedom must comply with the equation of motion,

$$[Z(\omega)].\{X_F\} = \{F_F\} \quad (3.13)$$

where $[Z(\omega)] = [K] - \omega^2.[M]$ is the dynamic stiffness matrix

The Guyan reduction method considers the static case where $\omega = 0$, when the dynamic stiffness matrix $[Z]$ can be replaced by the stiffness matrix $[K]$.

No external forces can be present at the deleted degrees of freedom, so partitioning results in:

$$\begin{bmatrix} K_{AA} & K_{AD} \\ K_{AD} & K_{DD} \end{bmatrix} \cdot \begin{Bmatrix} X_A \\ X_D \end{Bmatrix} = \begin{Bmatrix} F_A \\ 0 \end{Bmatrix} \quad (3.14)$$

where “A” is the active set and “D” is the deleted set of DOF. $[X_D]$ can be isolated from equation 3.14.

$$\{X_D\} = -[K_{DD}]^{-1} \cdot [K_{DA}] \cdot \{X_A\} \quad (3.15)$$

$[T_{static}]$ is given by:

$$[T_{static}] = -[K_{DD}]^{-1} \cdot [K_{DA}] \quad (3.16)$$

And if

$$[T_{Guyan}] = \begin{bmatrix} I \\ T_{static} \end{bmatrix} \quad (3.17)$$

The matrix reduction is achieved by:

$$\{X_F\} = [T_{Guyan}] \cdot \{X_A\} \quad (3.18)$$

This technique of matrix reduction is the easiest to use compared to other reduction techniques, but can be unreliable in the higher frequency ranges. Since this technique neglects inertia terms, it is also called “Static Condensation”. The omitted points’ selection should be made with care. Selection should be done on location of low mass regions.

Improved reduction system (IRS) method includes the inertial effects to the reduction procedure. In order to eliminate the reduction point selection problems in Guyan reduction, this method was developed [13]. Both methods give the same results for static problems. But for dynamic problems, where Guyan reduction does not take into account inertia effects, IRS gives accurate results.

System equivalent reduction expansion process (SEREP) method derives the rotational degrees of freedom from numerical model for the experimental model. Because of this opportunity, it gives better results in applications such as cross orthogonality checks between numerical and experimental modal vectors, linear and nonlinear forced response studies, etc [13].

3.3.2 Experimental Modal Data Expansion

Increasing the size (DOF) of experimental model to the size of numerical model is the main purpose of this method. By this method, unmeasured degrees of freedom are estimated. Some of the proposed expansion methods use the numerical model degrees of freedom for unmeasured locations. Additionally, some methods use measured degrees of freedom for unmeasured data directly by using fitting functions. There are also methods that use both measured and numerical degrees of freedom. The most popular methods are:

- Inverse Guyan Reduction (Kidder's Method)
- IRS Expansion
- SEREP Expansion

Since reduction techniques are used throughout this thesis, detailed information about expansion techniques can be found in [13], [14].

3.4 Correlation Techniques

Correlation of the numerical and experimental models for model updating has become increasingly important with the advances in updating algorithms. In order to compare these two models, correlation studies have to be performed.

Correlation can be divided into geometric and dynamic correlation. Geometric correlation makes the alignment between the two models by defining the transformation and scaling parameters. Before dynamic correlation, transformation and scaling parameters should be obtained by:

$$\{X_{Test}^{New}\} = \{T\}_{Translation} + [R]_{Rotation} \cdot S_{Scale} \cdot \{X_{Test}^{Old}\} \quad (3.19)$$

The correlation referenced in many sources in literature is the dynamic correlation and proposed in needs to [9]:

- Pair the experimental and numerical modes
- Measure the similarity between the two models.

For the last ten years, correlation algorithms have been also used to detect errors in the models [4], [20].

There are many dynamic correlation methods proposed to correlate numerical and experimental modes [21], [22]: Modal Scale Factor (MSF), Orthogonality (OR), Cross-Orthogonality (XOR), Modal Effective Mass (MEM), Modal Assurance Criterion (MAC), Frequency Response Assurance Criterion (FRAC), etc.

Detailed information about the most popular methods Orthogonality (OR), Modal Assurance Criterion (MAC), Frequency Response Assurance Criterion (FRAC) is given in the following sections.

3.4.1 Modal Assurance Criterion (MAC)

Similarities between two modal vectors are expressed by using modal assurance criterion. This criterion uses the formula given below [21]:

$$MAC(\{\phi\}_{Test}, \{\phi\}_{FE}) = \frac{\left| \{\phi\}_{Test}^{*t} \{\phi\}_{FE} \right|^2}{\left(\left| \{\phi\}_{Test}^{*t} \{\phi\}_{Test} \right| \right) \left(\left| \{\phi\}_{FE}^{*t} \{\phi\}_{FE} \right| \right)} \quad (3.20)$$

where * and t represents the complex conjugate and transpose of the vector respectively. MAC value can have values only between 0 and 1. The value of 0 means that two vectors are orthogonal and there is no correlation between them.

If the MAC value is 1, it means that vectors are fully correlated and equal to each other. The values below 0.3 are poorly correlated, whereas above 0.8 are well correlated. Between these values, model can be updated to get MAC values above 0.8.

3.4.2 Coordinate Modal Assurance Criterion (coMAC)

This criterion expresses mainly the similarities between nodes and uses the formula given as [21]:

$$coMAC(i) = \frac{\left(\sum_{j=1}^N |\phi_{FE}(i, j) \cdot \phi_{Test}^*(i, j)| \right)^2}{\left(\sum_{j=1}^N |\phi_{FE}(i, j)|^2 \right) \left(\sum_{j=1}^N |\phi_{Test}(i, j)|^2 \right)} \quad (3.21)$$

where * represents the complex conjugate of the vector. coMAC value can have values only between 0 and 1. The value of 0 means that experimental and numerical node locations have no correlation between them. If the coMAC value is 1, it means that nodes are fully correlated and equal to each other.

3.4.3 Frequency Response Assurance Criterion (FRAC)

Frequency response functions of numerical and experimental models are correlated by using frequency response assurance criterion (FRAC) which uses the formula given as [22]:

$$FRAC(i) = \frac{\left| \{H^{Test}(\omega)_i\}_j^{*t} \cdot \{H^{FE}(\omega)_i\}_j \right|^2}{\left(\{H^{Test}(\omega)_i\}_j^{*t} \cdot \{H^{Test}(\omega)_i\}_j \right) \cdot \left(\{H^{FE}(\omega)_i\}_j^{*t} \cdot \{H^{FE}(\omega)_i\}_j \right)} \quad (3.22)$$

FRAC computation gives results between 0 and 1. FRAC value of 0 stands for no correlation and 1 stands for full correlation.

3.4.4 Orthogonality (OR)

In this method matrix calculation is weighted with mass and stiffness matrices. The orthogonality matrix between numerical and experimental modes is calculated by using the formulas given as [13]:

$$OR_{Mass} = [\phi_{FE}]^T \cdot [M_{FE}] \cdot [\phi_{Test}] \quad (3.23)$$

$$OR_{Stiffness} = [\phi_{FE}]^T \cdot [K_{FE}] \cdot [\phi_{Test}] \quad (3.24)$$

In order to perform the orthogonality examination between vectors, one of the system matrices needs to be available.

3.5 Sensitivity Analysis

Optimization is a popular procedure used in many engineering problems in order to achieve a desired objective while satisfying specified design requirements. There are many application areas as [21]:

- Shape, sizing, topology optimization for structural design improvements,
- Model matching to produce similar structural responses,
- Maximizing the utility/profit for firms,
- Others that depend on designer's creativity.

Sensitivity analysis is the most important step for a better optimization. How the model behaves in response to changes in its inputs is of fundamental importance to ensure a correct and optimum use of the models. Many sensitivity analysis

methods were proposed in different fields. Frey [23] classified the methods into three main groups as:

- Mathematical Methods that obtain sensitivity of a model output to the range of variation of an input
- Statistical Methods that look for the effect of variance in inputs on the output distribution
- Graphical Methods that represent sensitivity in the form of graphs, charts, or surfaces.

Sensitivity analysis of numerical approximation problems are performed by mathematical models. Nominal Range Sensitivity Analysis (NRSA) methods and Differential Sensitivity Analysis (DSA) methods are mostly used ones for this class.

Nominal range sensitivity analysis varies individual model inputs across its complete range of possible values to obtain the effect on model output. During this evaluation, all other design variables remain fixed at their actual values. On the other hand, differential sensitivity analysis methods calculate the first-order partial derivatives of the outputs with respect to design variable changes.

For the model updating case, an updated FE model contains the optimum design parameters for best possible numerical and experimental model correlation. In order to find the optimum design parameter values, sensitivity analysis is performed at the beginning. FE design model parameters for which the target responses are more sensitive are natural candidates of design variables according to which sensitivity analysis will be performed.

Mottershead and Mares et al. [24] and Sinha et al. [25] updated the FEM by using eigenvalue sensitivities determined according to

$$\frac{\partial \lambda_i}{\partial \theta_j} = \varphi_i^T \left(\frac{\partial K}{\partial \theta_j} - \lambda_i \frac{\partial M}{\partial \theta_j} \right) \varphi_i \quad (3.25)$$

Where λ_i and φ_i represent the i th eigenvalue and eigenvector, respectively, and θ_j is an updating parameter.

For the aim of this thesis study, sensitivity analysis will be performed by using the MSC.Nastran software. This software has extensive capability for this purpose. Design sensitivity analysis in MSC.Nastran, in which the related solution technique is called Sol200, computes the rates of change of structural responses with respect to changes in design parameters. Shell thicknesses, beam dimensions, material variables, etc. are examples to design parameter selections.

MSC.Nastran computes the overall gradient matrix based on the partial derivatives of the design variables with respect to the targets through only one solver run. Full gradient matrix is obtained by only one solver run saving a lot of time [26].

Sol200 defines a design sensitivity coefficient as the rate of change of a particular response quantity i with respect to a change in a design variable x . For a vector of design variables X^0 :

$$\lambda_{ij} = \left. \frac{\partial r_j}{\partial x_i} \right|_{X^0} \quad (3.26)$$

where subscripts are for i -th design variable and the j -th response. Eigenvalue and eigenvector sensitivity analyses are based on equation (3.26). For this reason, only eigenvalue sensitivity analysis is detailed.

Starting with the eigenvalue problem [27]:

$$([K] - \lambda_n [M])\{U_n\} = 0 \quad (3.27)$$

where λ_n and U_n are the n -th eigenvalue and eigenvector, respectively. $[K]$ is the structural stiffness matrix, and $[M]$ is the structural mass matrix. Differentiating equation (3.27) with respect to the i -th design variable x_i to yield:

$$([K] - \lambda_n [M]) \frac{\partial \{U_n\}}{\partial x_i} + \left(\frac{\partial [K]}{\partial x_i} - \lambda_n \frac{\partial [M]}{\partial x_i} \right) \{U_n\} = \frac{\partial \lambda_n}{\partial x_i} [M] \{U_n\} \quad (3.28)$$

If equation (3.28) is pre-multiplied with $\{U_n\}^T$, the $\{U_n\}^T ([K] - \lambda_n [M])$ term then appears as the transpose of equation (3.27) and therefore zero. Then equation (3.28) can be solved as:

$$\frac{\partial \lambda_n}{\partial x_i} = \frac{\{U_n\}^T \left(\frac{\partial [K]}{\partial x_i} - \lambda_n \frac{\partial [M]}{\partial x_i} \right) \{U_n\}}{\{U_n\}^T [M] \{U_n\}} \quad (3.29)$$

3.6 Model Updating (Optimization)

Numerical models, which are built in order to simulate the dynamic characteristics of real structures, consist of many design variables. The correlation of numerical and experimental models relies on accuracy of design variables. In order to get an appropriate correlation, model updating is performed.

Model updating in this thesis is performed by optimization. Numerical model design variables are optimized for proper correlation of numerical and experimental models.

There are many optimization algorithms that are used in many engineering problems. Chapra and Canale [28] divided optimization problems into three main groups:

- One-Dimensional Unconstrained Optimization
- Multidimensional Unconstrained Optimization
- Constrained Optimization

Methods in one-dimensional unconstrained optimization are mainly used to find the minimum or maximum of a function of a single variable. Multidimensional unconstrained optimization methods find the minimum or maximum of a function of several variables. Methods in this group are divided again into two depending on whether there is need for derivative calculation [28]. Nongradient, or direct methods do not need derivative calculation. However, gradient methods need derivatives.

Constrained optimization methods are used for problems in which constraints are assigned. These methods are used mainly for optimization of many design variables in order to reach the objective functions without violating the constraints.

Throughout the case studies in this thesis, LMS Virtual.Lab optimization module is used. The module has different optimization methods that are used for different applications. Generalized Reduced Gradient (GRG) method, which is used within the Excel solver, is suggested for model updating applications. GRG method is a constrained optimization method. Under this method, there are two possibilities for gradient calculation. The first one is analytic which uses

the MAC sensitivity solutions for gradient features. The other one is the finite difference that has two methods for gradient calculation: forward or central difference. Forward difference method is represented as [28]:

$$f'(x_i) = \frac{f(x_{i+1}) - f(x_i)}{h} + O(h) \quad (3.30)$$

where h and O are called the step size and truncation error respectively.

On the other hand, central difference representation is as follows:

$$f'(x_i) = \frac{f(x_{i+1}) - f(x_{i-1}))}{2.h} + O(h^2) \quad (3.31)$$

CHAPTER 4

A NEW DIAGNOSTIC TOOL FOR IMPROVED MAC

In order to compare numerical and experimental models, there are some techniques for this process. MAC, coMAC, Orthogonality, FRAC are some of the proposed ones for which detailed information can be found in [9], [24] as mentioned in the previous chapter.

MAC is the mostly used correlation technique because of its ease of application and simplicity. As mentioned in section 3.4.1, this technique expresses the similarities between two modal vectors as a number ranging from zero (no correlation) to one (full correlation). Throughout this thesis, MAC is used for eigenvector correlation. Obtaining a better MAC matrix distribution is the main aim of model updating in this thesis.

Other than finding the degree of similarity or difference between two models, correlation techniques give also the opportunity of determining difference locations. Namely, they can be used for error localization.

For example, Coordinate Modal Assurance Criterion (coMAC) obtains the correlation between two nodes in terms of eigenvectors. Uncorrelated coordinates are expressed as error locations, assuming the experimental coordinate results are true. However, sometimes there might also be errors in the experimental data. There are several reasons for these errors. The input energy supplied by the shaker may not be enough for some locations. This results in lower signal to noise ratios at these locations or the signal can be even

lost in the noise resulting in a low quality FRF. In these measurements the system was assumed to be perfectly linear. However, literature [29] shows that aircraft structures also exhibit nonlinear characteristics. Such phenomena also results in low quality of correlation. For this reason, uncorrelated coordinates show the error locations from either numerical or experimental data.

Addition of these error locations to the MAC calculation decreases the possibility of finding true correlation of global models. In order to get rid of this problem, these error locations should be excluded from correlation calculations. For this purpose, a new diagnostic tool for improved MAC matrix is proposed in this section. This tool finds the optimized node locations that should be removed for better MAC values. This process takes into account the eigenvector weights which are entered by the user. The procedure of finding the best possible node location removal is given as follows:

- i. Modal Assurance Criterion (MAC) matrix is calculated.
- ii. Node location removal ordering is performed for each MAC diagonal value improvement.
- iii. Node removal ordering for total MAC diagonal enhancement is performed taking weights into account.
- iv. New MAC matrix is calculated.

Detailed information about the stages of this process is given below.

First of all, Modal Assurance Criterion (MAC) matrix is calculated according to the formula:

$$MAC(\{\phi\}_{Test}, \{\phi\}_{FE}) = \frac{\left| \{\phi\}_{Test}^{*t} \{\phi\}_{FE} \right|^2}{\left(\left| \{\phi\}_{Test}^{*t} \{\phi\}_{Test} \right| \right) \left(\left| \{\phi\}_{FE}^{*t} \{\phi\}_{FE} \right| \right)} \quad (4.1)$$

A MAC correlation matrix as shown in Figure 4.1 is calculated by using this computation. Diagonal of this figure should be more than 0.8 and off-diagonals should be less than 0.2 for better correlation.

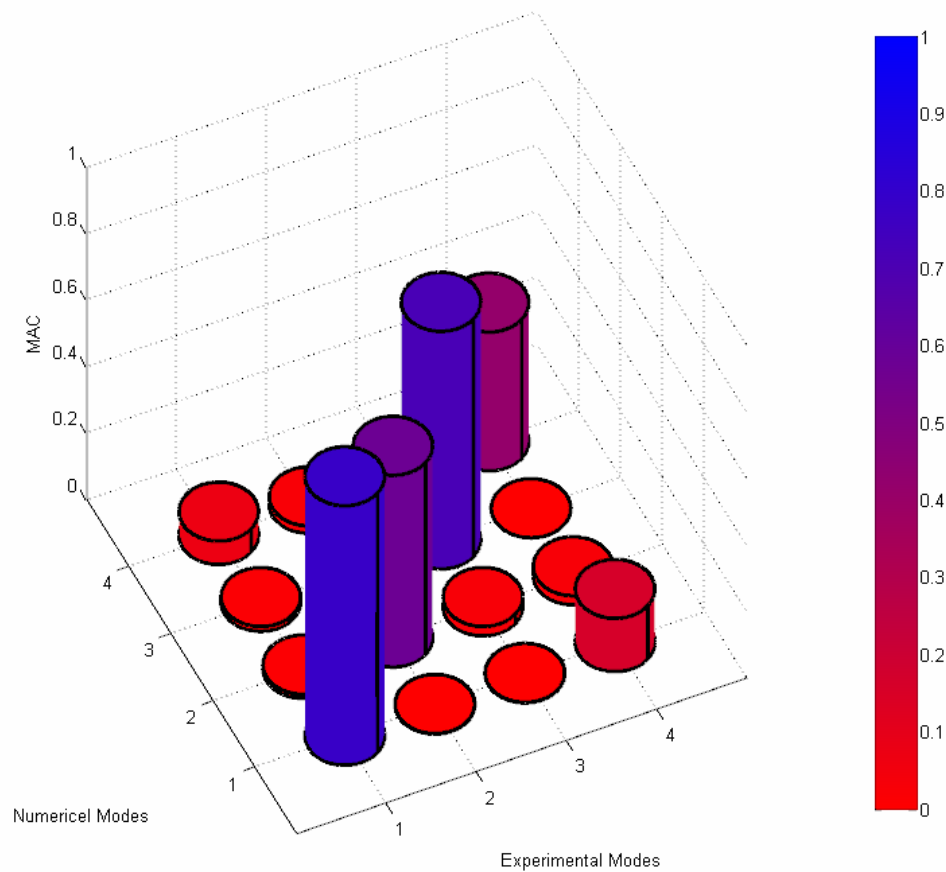


Figure 4.1 MAC matrix diagram

After MAC matrix calculation, the best possible node number elimination to improve each MAC diagonal value is found. For a 3x3 MAC matrix, these node numbers are found by using the algorithm:

$$\max\left(\frac{\partial M_1}{\partial N_1}, \frac{\partial M_1}{\partial N_2}, \dots, \frac{\partial M_1}{\partial N_n}\right)$$

$$\max\left(\frac{\partial M_2}{\partial N_1}, \frac{\partial M_2}{\partial N_2}, \dots, \frac{\partial M_2}{\partial N_n}\right)$$

$$\max\left(\frac{\partial M_3}{\partial N_1}, \frac{\partial M_3}{\partial N_2}, \dots, \frac{\partial M_3}{\partial N_n}\right) \quad (4.2)$$

where N for node number, n for total number of nodes, M for each MAC matrix diagonal. Numbering of a 3x3 MAC matrix diagonals is shown in Figure 4.2.

		M ₃
	M ₂	
M ₁		

Figure 4.2 MAC matrix diagonal numbering

This node elimination process is performed until a desired value of each MAC diagonal. Each node number is statistically tabulated on a table for each one of MAC value M. This statistical tabulation (S) is shown in Figure 4.3.

	N ₁	N ₂	N ₃	N ₄	N ₀
W ₁					
W ₂					
⋮	⋮		⋮	⋮	⋮
W _m					

Iteration Numbers

Figure 4.3 Statistical tabulation of each MAC value (M)

In this tabulation, W stands for weights of each MAC value. Weights of MAC values are entered as inverse of percentage of MAC values. If a MAC is more

important, then its MAC value is entered low. As an example, assume a 4x4 MAC matrix. If the order of importance of MAC values are $MAC_2 > MAC_1 > MAC_4 > MAC_3$, then MAC diagonals are $MAC_1=20$, $MAC_2=15$, $MAC_3=25$, $MAC_4=40$. Then weights of these values are transferred to the algorithm as $W_1=0,20$; $W_2=0,15$; $W_3=0,25$; $W_4=0,40$

After this statistical tabulation, correlations of nodes (C) are calculated by using the formula:

$$C(i) = \sum_{j=1}^m W_j * S_{j,i} \quad (4.3)$$

Small values of C's are eliminated from the MAC computation. The number of location elimination is strictly up to the user. This method is called nrMAC throughout the thesis for simplicity.

A Matlab code is written in order to compare and evaluate the performance of the proposed algorithm with coMAC. In this matlab code MAC, coMAC and proposed algorithm calculations are performed. The written code divides every location into x, y and z axis. After this division, it finds the best possible node axis removals for coMAC and the proposed algorithm. The code simply follows the procedure:

- i. Obtain natural frequencies and modes shapes from finite element analysis results of MSC.Nastran
- ii. Obtain natural frequencies and mode shapes from test results universal file
- iii. Compute MAC matrix
- iv. Compute coMAC and nrMAC
- v. Compute the optimum nodes for removal according to both coMAC and nrMAC.

CHAPTER 5

CASE STUDIES ON A MILITARY HELICOPTER

In these case studies, model updating of a military helicopter is performed using LMS Virtual.Lab software. The helicopter as shown in Figure 5.1 is a utility helicopter and it is mainly used for transportation of army personnel.

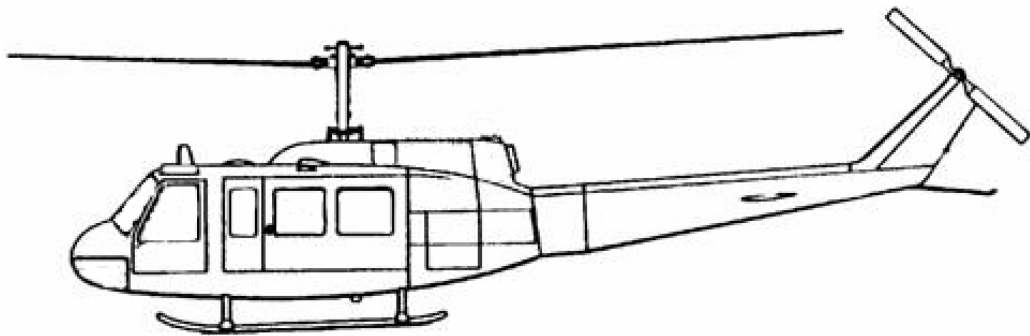


Figure 5.1 Utility Helicopter

The updating procedure is shown in Figure 5.2.

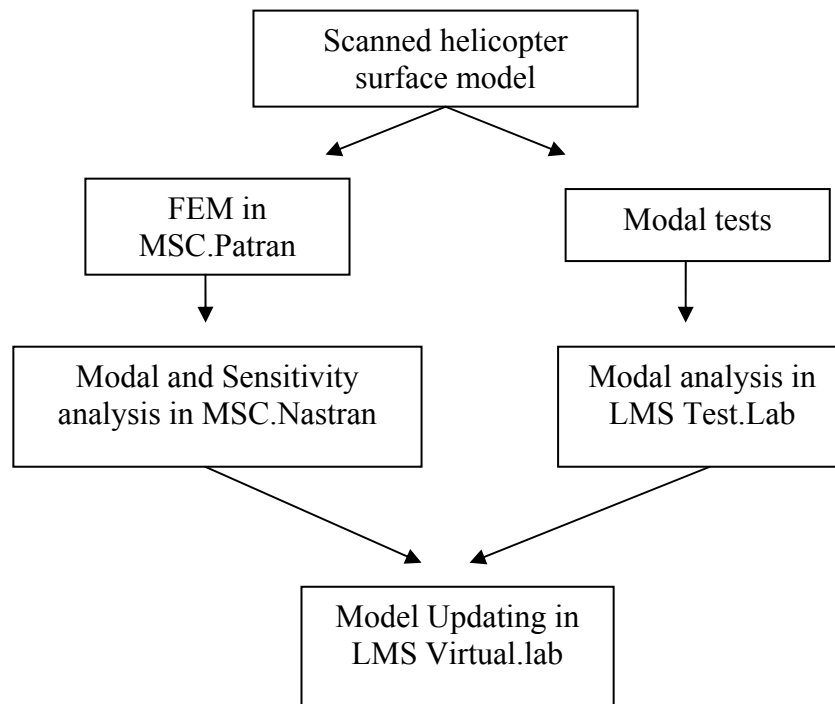


Figure 5.2 Model updating procedure followed for updating

5.1 Modal Test and Analysis

As mentioned in the previous sections, in order to calculate the modal properties of the helicopter, experimental data of either hammer or shaker test is required. For this case, shaker test is performed since;

- Structure is big enough that can not be excited with hammer,
- Accelerometers will be moved gradually, it is impossible to excite the whole structure at the same by using hammer, but it is easier to excite it with shaker.

5.1.1 Pretest Configuration

Some configurations and checks were performed prior to the modal tests. First of all, boundary conditions were studied. Dynamic properties of the helicopter should be investigated for a boundary condition where there is no connection between helicopter and the ground. In this condition, it can be simulated by hanging it from ceiling with weak springs or by placing the test object on air cushion or very soft foam. In this situation, it was more practical to place the helicopter on soft foam as shown in Figure 5.3. With this technique, free-free boundary condition was simulated and rigid body modes were checked.



Figure 5.3 Foams that are used for free-free boundary condition.

A connecting part as shown in Figure 5.4 was manufactured in order to connect the shaker stinger to the helicopter structure. It was manufactured from thick aluminum for appropriate rigidity and it was fixed to the tail with three bolts.

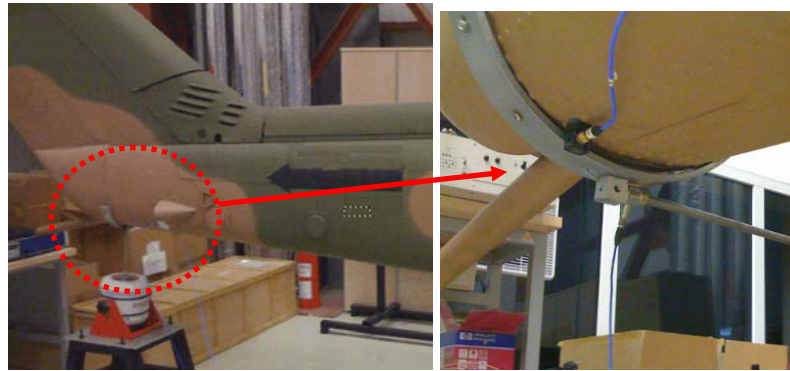


Figure 5.4 The part that connect stinger to the helicopter

In addition, a shaker is connected to a heavy cast iron metal table in order to prevent the shaker assembly to vibrate and move. This metal part with connecting sheet plate is shown in Figure 5.5.



Figure 5.5 Steel part to which shaker is connected

Moreover, the shaker and amplifier checks were carried out to see whether the existing hardware is enough to excite the whole structure. For this purpose, a sample excitation was given by Tira TV 51110 shaker with its amplifier and accelerometer signal at the nose of the helicopter was examined. It was observed that this shaking system was inappropriate because of low response levels for complete fuselage. For this reason, shaker is changed to Datapyhsics DP-V070 shaker system (Figure 5.5) together with Data Physics A-10C amplifier. This shaker performance was investigated and found to be sufficient for the tail section. However, the cabin and cockpit regions were still lightly excited. Therefore, due to hardware limitations, the tests were executed with this configuration.

The helicopter vibration is sensed by ICP type piezoelectric accelerometers because of their linearity, lightweight, small size and wide usage in aerospace applications. Eleven tri-axial piezoelectric accelerometers were used for the helicopter modal tests. One of the accelerometers was chosen as the driving point accelerometer and attached next to the stinger-helicopter connection point as shown in Figure 5.6 and its position is not changed for the whole test. Accelerometers were attached to the structure by using wax for proper dynamic characteristics and ease of the attachment.

In addition to accelerometers, one single-axis force transducer was used for force measurement and it is connected to the stringer as shown in Figure 5.6. This force data was used for FRF analysis.

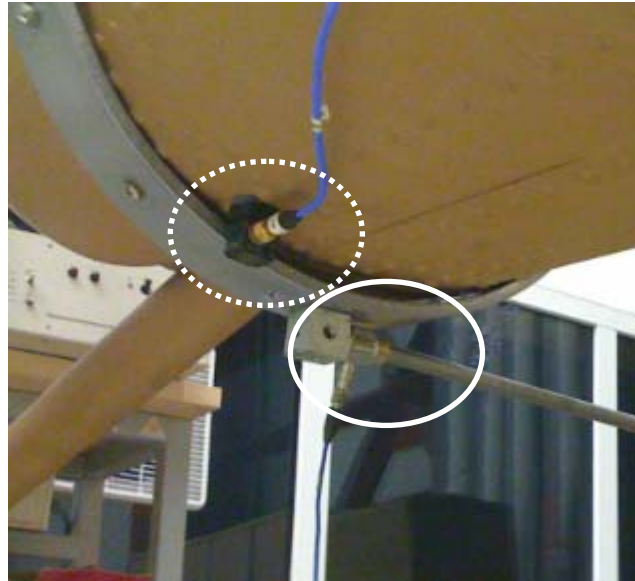


Figure 5.6 Force transducer (Line circle) and driving point accelerometer (Dashed circle)

Detailed information about test equipments can be found in Appendix A.

5.1.2 Modal Tests

After completion of pretest configuration and checks, modal tests were performed for 102 accelerometer locations. 10 accelerometers were rowed gradually on the helicopter. These accelerometer locations are shown in Figure 5.7 to Figure 5.10.



Figure 5.7 Accelerometer locations at tail end



Figure 5.8 Accelerometer locations at tail front



Figure 5.9 Accelerometer locations at main body



Figure 5.10 Accelerometer locations at main body front

In order to control and drive the shaker, portable Data Physics SignalCalc Ace data acquisition system was used. This system has capabilities of generating excitation signals of random noise, sine, chirp, burst-random, impulse, etc. Burst random profile was used for helicopter modal test because of its advantages like:

- Wide frequency range,
- Shorter testing time,
- No window requirement

The generated excitation signal was amplified by using Data Physics A-10C type amplifier. This shaker, controller and amplifier system is shown in Figure 5.11 and detailed information is given in Appendix A.



Figure 5.11 Shaker, controller, and amplifier system

The signal coming from the force transducer (single-axis) and ten accelerometers (2-axis) were measured and analyzed by IOtech data acquisition system as shown in Figure 5.12. The eZ-analyst software that is used with this system has the capabilities of real-time FFT, FRF analysis, windowing, etc.



Figure 5.12 IOtech data acquisition system

At the beginning of the tests, it was obvious that helicopter structure has mode shapes in different directions. In order to drive these different shapes, helicopter was excited in both vertical and transverse directions. For this reason, different

shaker directions were used as shown in Figure 5.13. Helicopter was not excited in longitudinal direction. It is mainly because the natural frequencies and related mode shapes in this direction would be very high. On the basis of this presumption, dynamic signals in longitudinal direction were not collected by accelerometers.

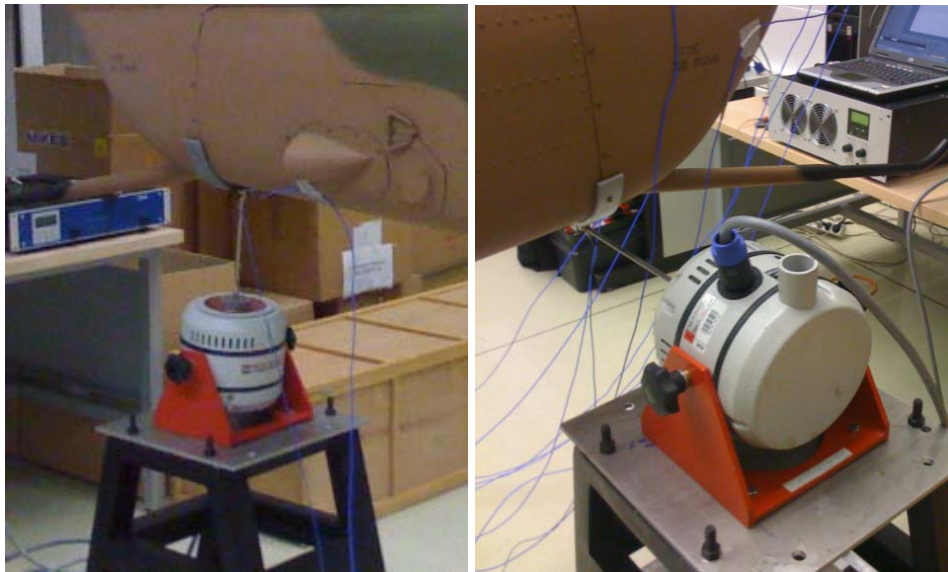


Figure 5.13 Stinger directions, vertical and transverse respectively

The graphs that visually checked during the modal tests are:

- Averaged FRF-magnitude estimates of the all accelerometer signals
- Averaged FRF-magnitude estimates of the excitation location accelerometer signal
- Averaged coherence estimates of different accelerometer signals
- Averaged spectral density function estimates of force transducer signal
- Time history of the force transducer signal

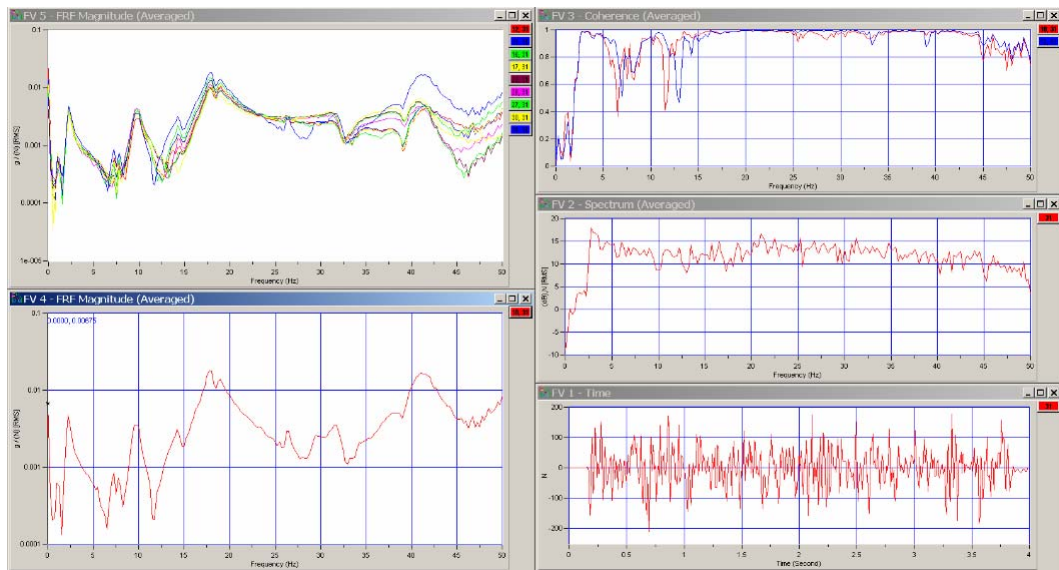


Figure 5.14 Graphs that are checked during modal tests

One of the checks that were made during modal tests is shown in Figure 5.14. In this figure, top left window shows averaged FRF-magnitude estimates of the ten accelerometer signals. Peaks and profiles are clear and compatible. The bottom left window shows averaged FRF-magnitude estimate of the excitation location accelerometer signal. The top right window shows averaged coherence estimates of different accelerometer signals. As it is seen, coherence is more than 0.8 for peak frequency locations. The middle right window shows averaged spectral density function estimate of force transducer signal. It is clear that energy of the executed signal remains nearly constant for the desired frequency range. The bottom right window shows time history of the force transducer signal.

5.1.3 Modal Analysis

After completion of the modal tests, modal analysis was carried out using LMS Test.Lab software. For modal analysis, software has many algorithms like Least Squares Complex Exponential, Polyreference Complex Exponential, etc. For

this case, Polymax algorithm is used. It is mainly because it can stabilize on more natural frequencies than other methods, and preferred especially in nonlinearity effected (backlash, joints, etc.) systems. One disadvantage of using this method is that it can stabilize on some frequencies which are not real modes. This disadvantage is eliminated by visual checks of the mode shapes.

Modal analysis of the helicopter is carried out for two different models. The first model includes only the tail of the helicopter as shown in Figure 5.15.

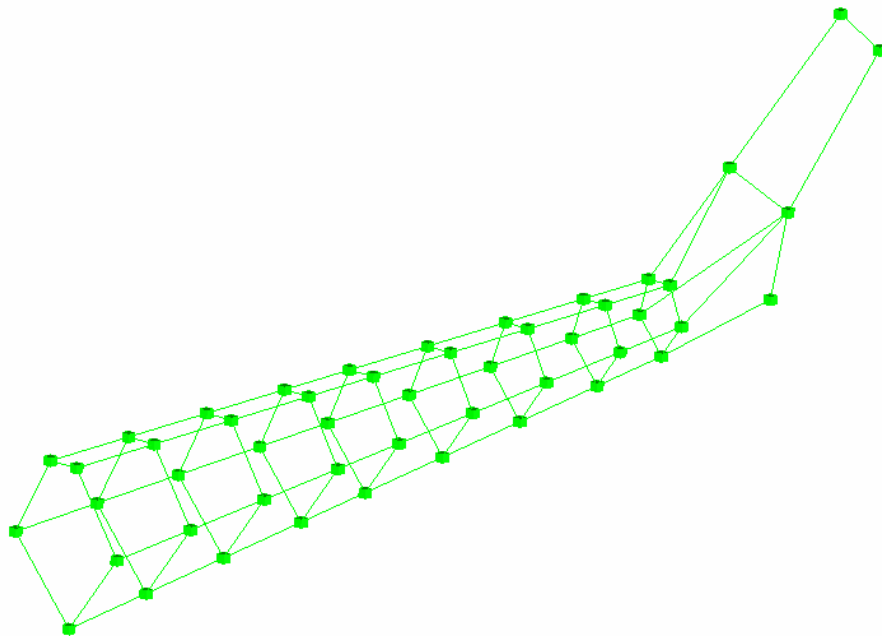


Figure 5.15 Modal analysis model of the tail

LMS Test.Lab polymax method stabilized on 30 natural frequencies for the tail. These natural frequencies are listed in Table 5.1.

Table 5.1 Stabilized natural frequencies of the tail

Mode #	Mode (Hz) with Damping Factor (%)	Mode #	Mode (Hz) with Damping Factor (%)	Mode #	Mode (Hz) with Damping Factor (%)
1	2,2-6,4	11	16,3-2,3	21	31,5-1,8
2	3,5-3,1	12	17,8-2,5	22	32,5-0,9
3	4,7-3,0	13	18,7-2,1	23	33,4-0,8
4	7,2-1,6	14	20,9-0,5	24	33,8-1,4
5	9,1-1,1	15	22,9-0,2	25	36,7-0,3
6	9,6-2,7	16	24,3-0,2	26	37,9-1,2
7	9,9-0,73	17	26,2-0,6	27	38,7-1,3
8	10,7-1,8	18	26,9-0,8	28	41,0-2,4
9	13,3-1,4	19	29,2-2,1	29	41,4-0,3
10	14,3-1,5	20	29,3-1,1	30	45,7-1,5

After visual checks, the reasonable mode shapes (flexible modes) were found. 2nd, 4th, 6th and 25th mode shapes are shown in Figure 5.16, Figure 5.17, Figure 5.18 and Figure 5.19 respectively.

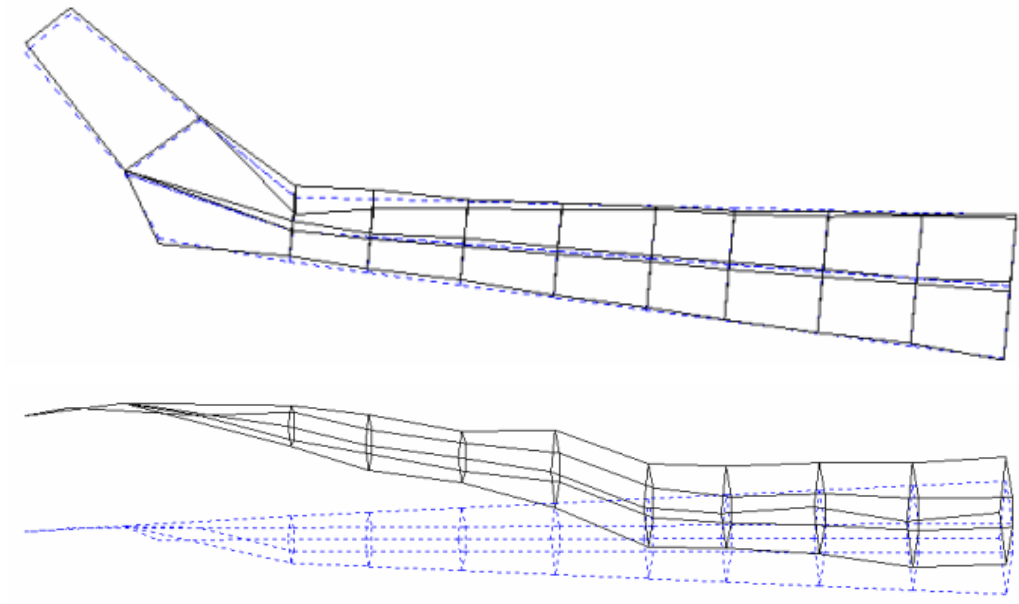


Figure 5.16 First lateral bending mode (Second stabilized mode) of the tail (3.5 Hz)

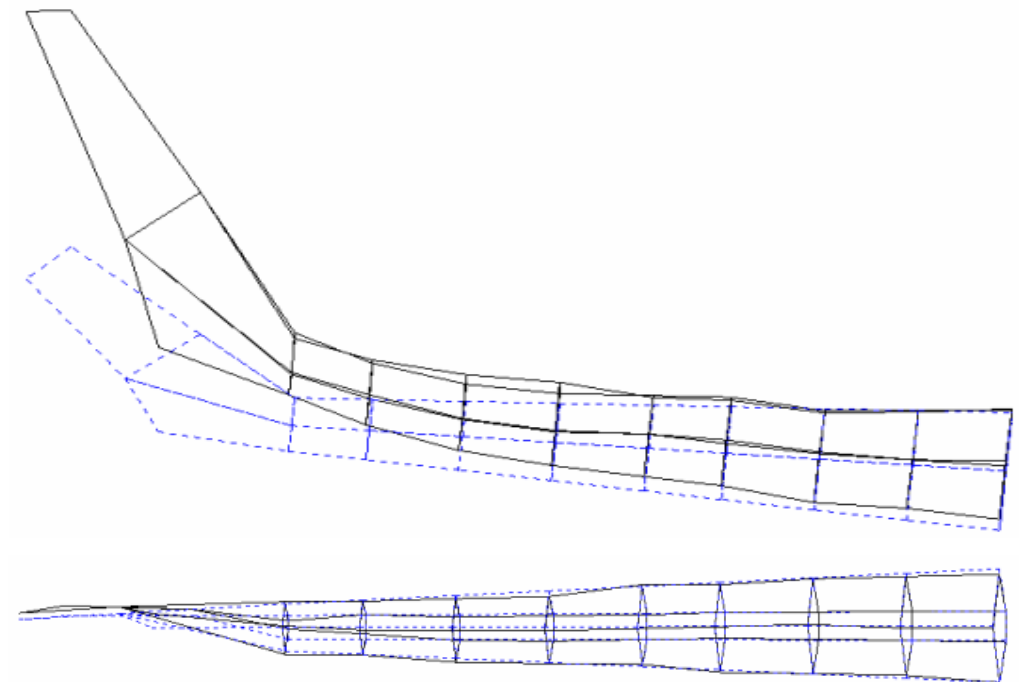


Figure 5.17 First vertical bending mode (Fourth stabilized mode) of the tail (7.2 Hz)

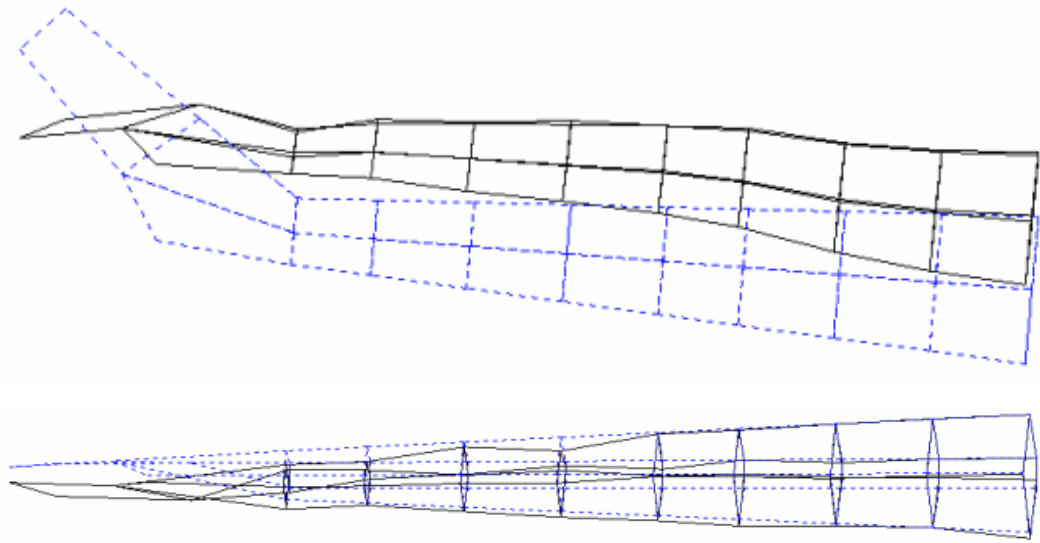


Figure 5.18 Second vertical bending mode (Sixth stabilized mode) of the tail (9.6 Hz)

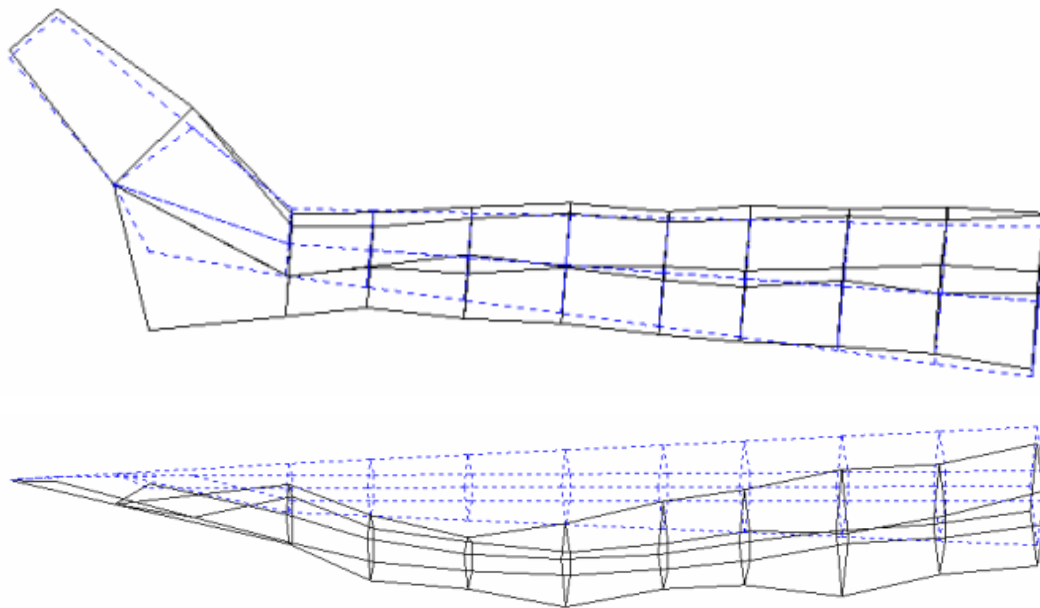


Figure 5.19 Second lateral bending mode (Twenty-fifth stabilized mode) of the tail (36.7 Hz)

Next modal analysis is carried out for the complete helicopter fuselage as shown in Figure 5.20.

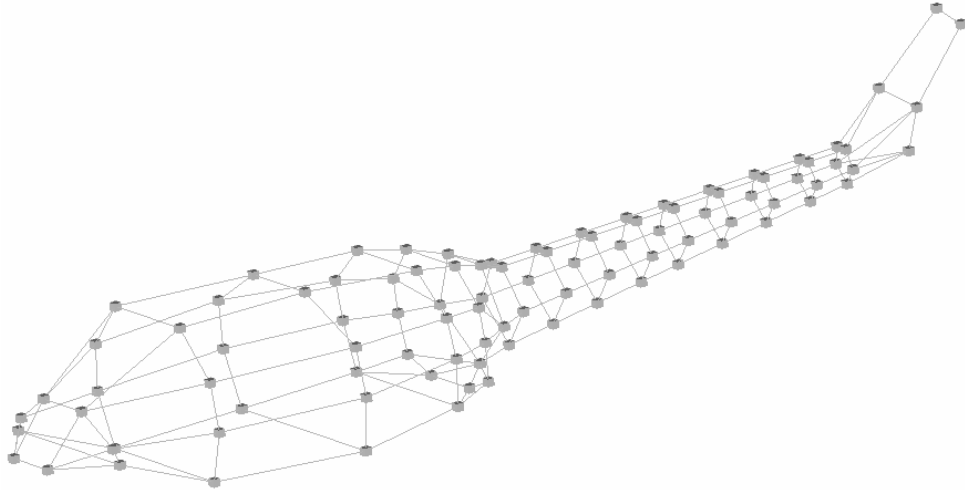


Figure 5.20 Modal analysis model of the complete helicopter fuselage

Modal analysis of the whole helicopter model is also carried out using Polymax method. This method stabilized on 27 natural frequencies as listed in Table 5.2.

Table 5.2 Stabilized natural frequencies of the complete helicopter fuselage

Mode #	Mode (Hz) with Damping Factor (%)	Mode #	Mode (Hz) with Damping Factor (%)	Mode #	Mode (Hz) with Damping Factor (%)
1	2,2-6,4	10	14,3-1,5	19	29,2-1,9
2	3,5-3,0	11	16,4-2,2	20	29,5-1,3
3	4,7-3,3	12	17,8-2,5	21	31,6-1,2
4	7,2-2,4	13	18,7-2,2	22	32,3-0,6
5	9,1-1,1	14	20,9-0,4	23	33,3-0,5
6	9,6-2,5	15	22,9-0,1	24	34,3-1,9

Table 5.2 continued

7	9,8-0,7	16	26,2-0,6	25	37,7-1,3
8	10,7-1,9	17	26,9-0,7	26	38,7-1,1
9	13,3-1,2	18	28,6-1,0	27	41,0-2,3

The reasonable mode shapes (flexible modes) were found after visual checks. 8th, 9th and 14th mode shapes, which are more meaningful, are shown in Figure 5.21, Figure 5.22 and Figure 5.23 respectively.

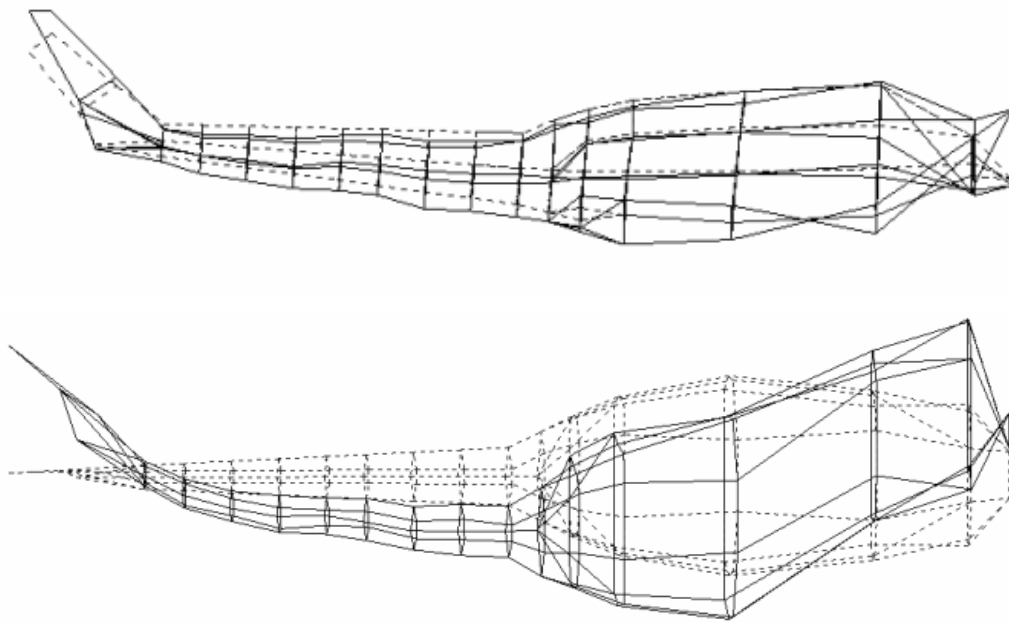


Figure 5.21 First lateral bending mode (Eighth stabilized mode shape) of the complete helicopter fuselage (10.7 Hz)

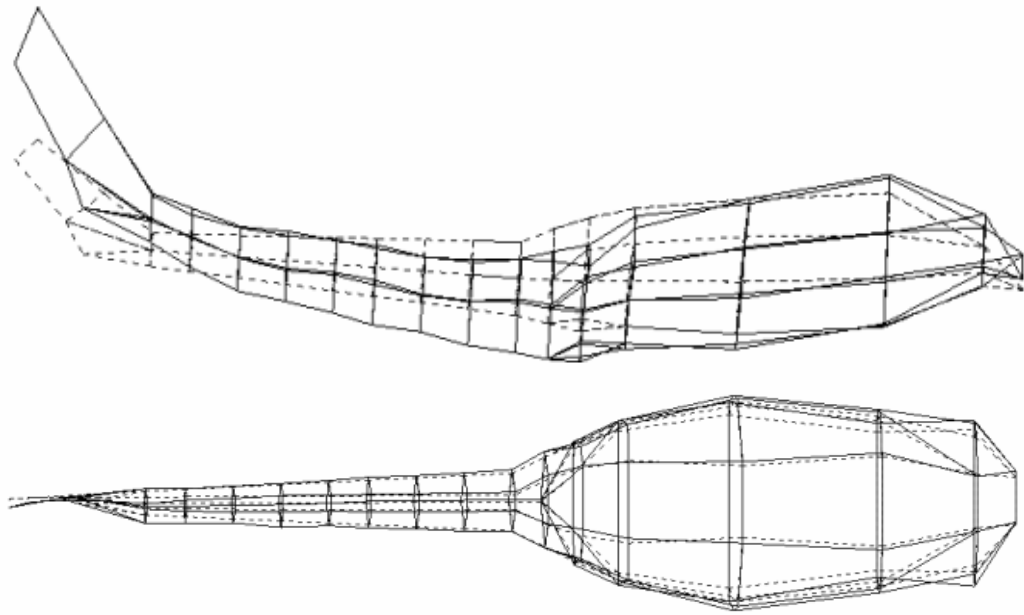


Figure 5.22 First vertical bending mode (Nineth stabilized mode shape) of the complete helicopter fuselage (13.3 Hz)

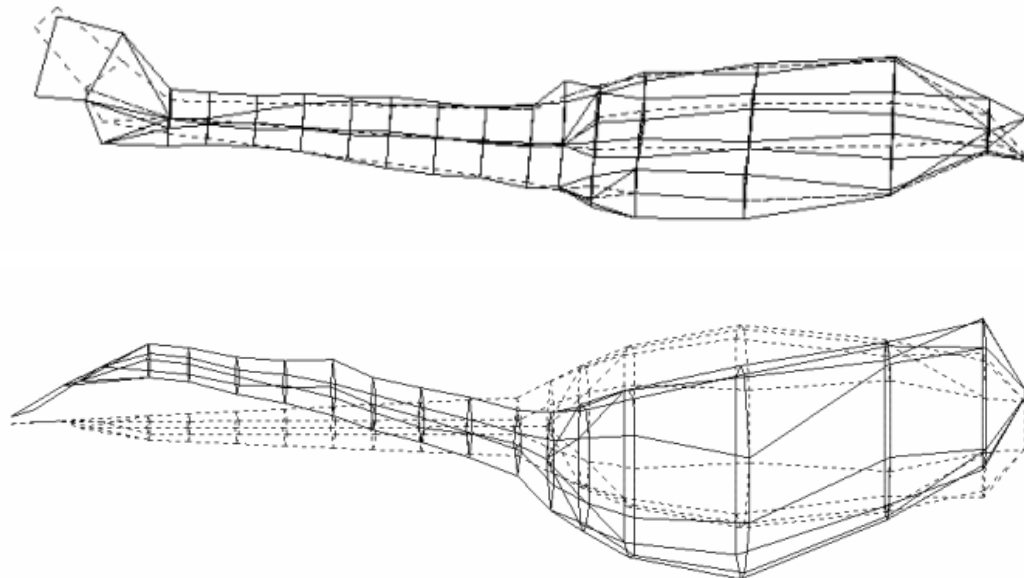


Figure 5.23 Second lateral bending mode (Fourteenth stabilized mode shape) of the complete helicopter fuselage (20.9 Hz)

In addition to these modal analysis results, one of the rigid body modes (4.7 Hz) that are found by LMS Test.Lab is given in Figure 5.24.

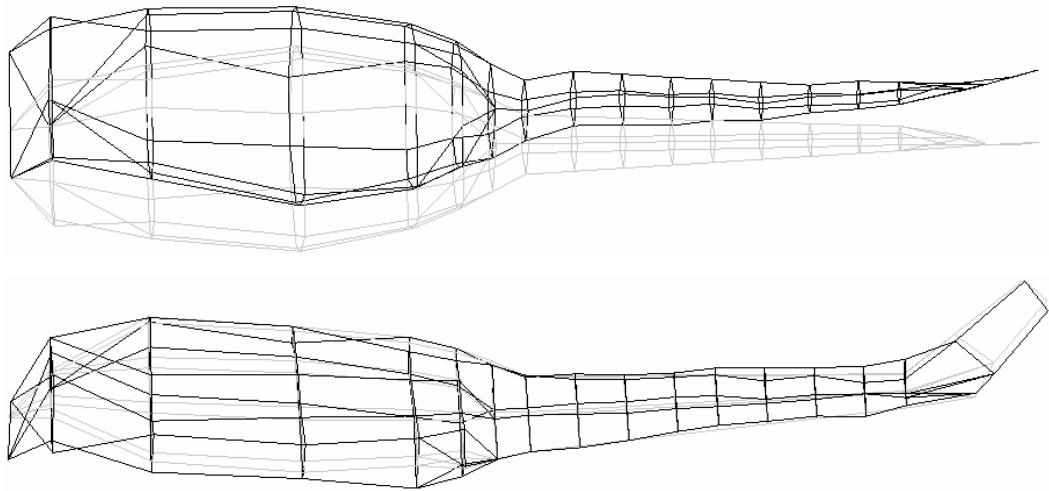


Figure 5.24 Lateral rigid body mode of the complete helicopter fuselage (4.7 Hz)

The procedure of modal analysis with LMS Test.Lab is given in Appendix C.

5.2 Finite Element Analysis

Finite element model of the helicopter was created using MSC.Patran software. This software was used for both pre and post-processing of the helicopter FEM. After model development, modal analyses were performed using commercial software MSC.Nastran.

Before meshing, surface model of the helicopter structure was created first. Scanned surface model of the helicopter was used as a base for this process. The errors in the surface model were corrected. For example, gaps inside the surface

model are stitched; vertices and edges are made compatible. In addition, most of the surfaces are generated again for better mesh quality. The generated surface model is shown in Figure 5.25.

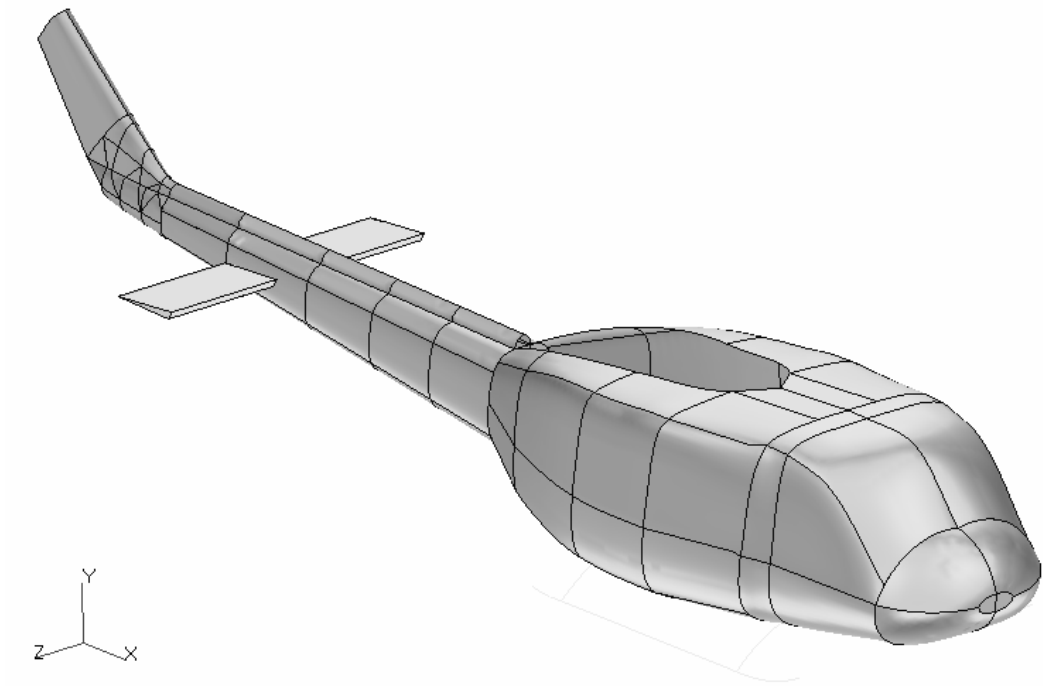


Figure 5.25 Surface model of the helicopter structure

Using the generated surface model, meshing of the tail and complete helicopter fuselage were performed as shown in Figure 5.26 and Figure 5.27.

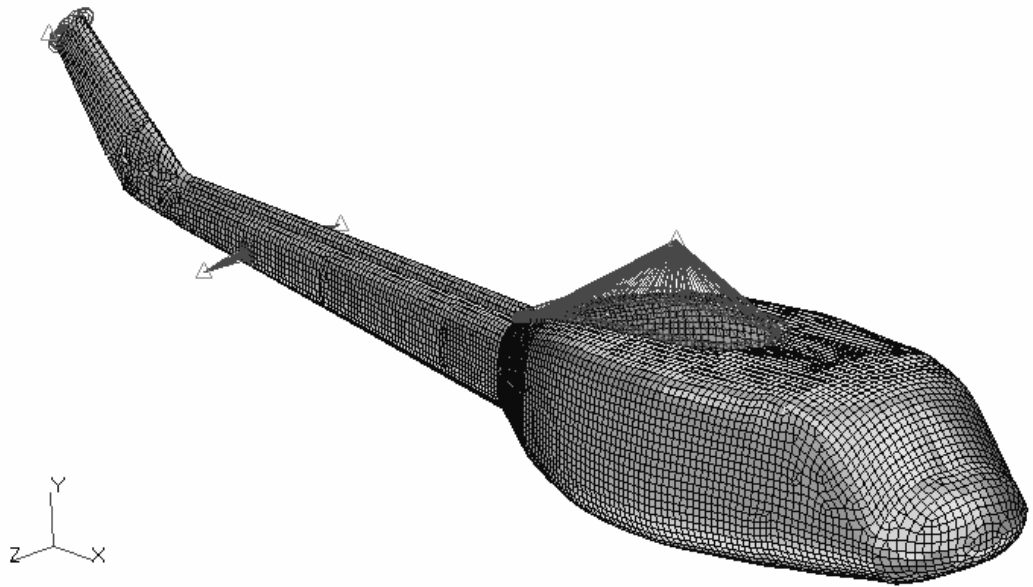


Figure 5.26 Finite element model of the complete helicopter fuselage

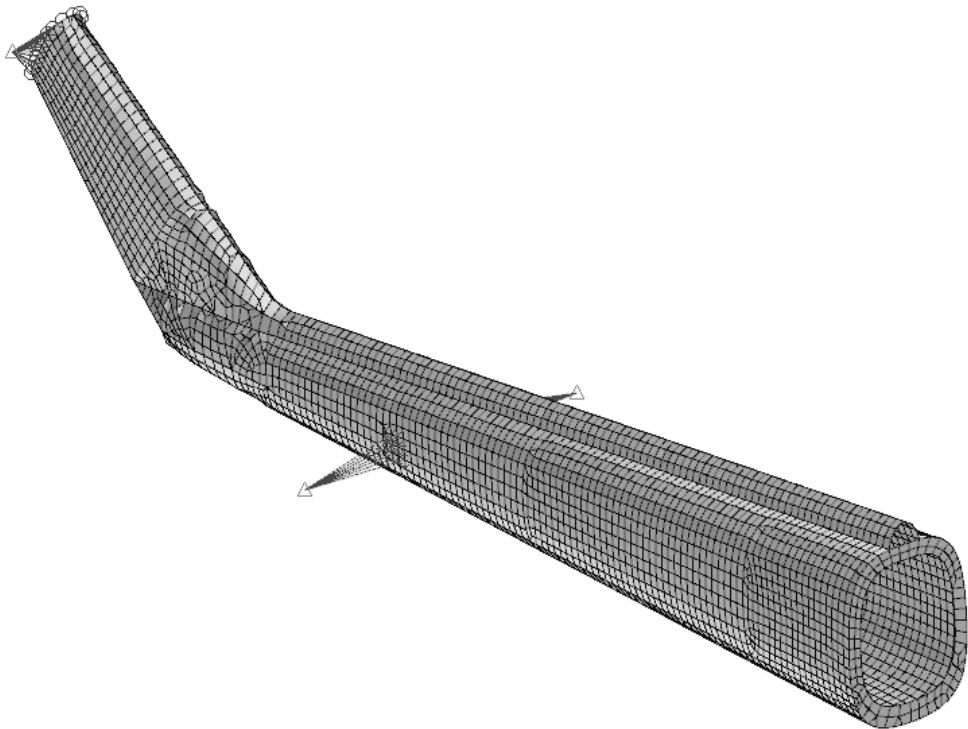


Figure 5.27 Finite element model of the tail

Main and tail motors were modeled as point masses for simplification. Since there is nonlinear connection between tail wings and the tail, tail wings were also modeled as point mass.

Helicopter structure has stiffeners all around it. In order to simulate these stiffeners, beam elements were modeled on the structure as shown in Figure 5.28.

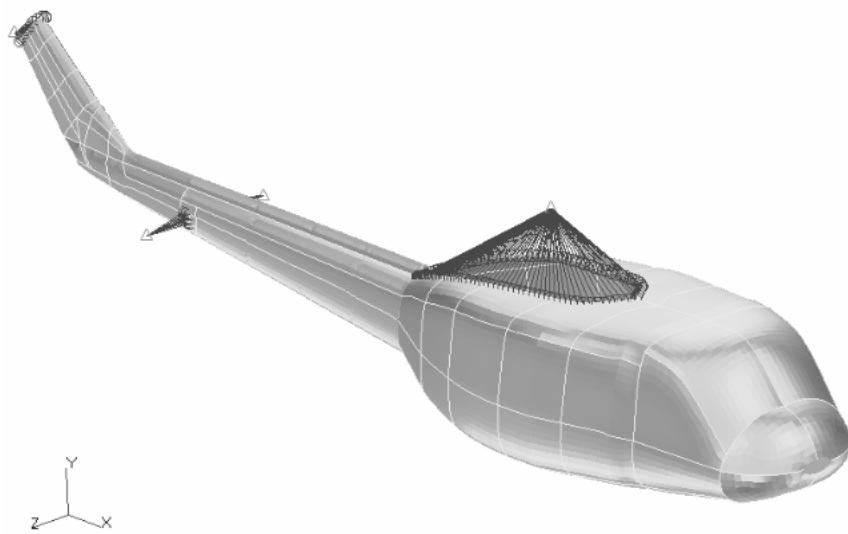


Figure 5.28 Beam elements (green in color) on the helicopter structure

After initial finite element modal analysis with MSC.Nastran, it was seen that helicopter model should be refined in order to get more global and symmetric mode shape results. For this reason, finite element model of the tail and whole helicopter model were refined with longitudinal symmetry. After refinement, finite element models with better mesh quality were obtained as shown in Figure 5.29 and Figure 5.30.

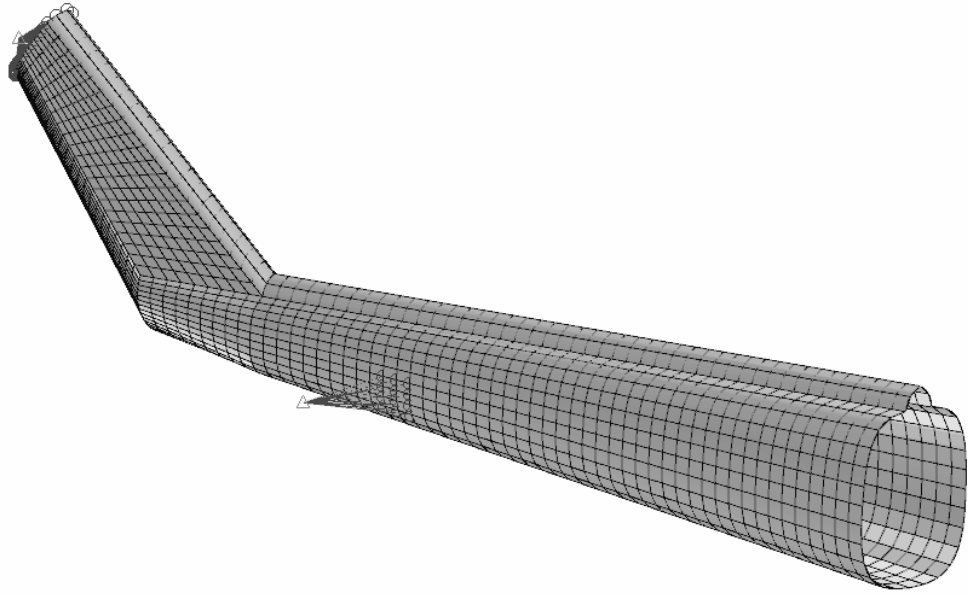


Figure 5.29 Refined finite element model of the tail

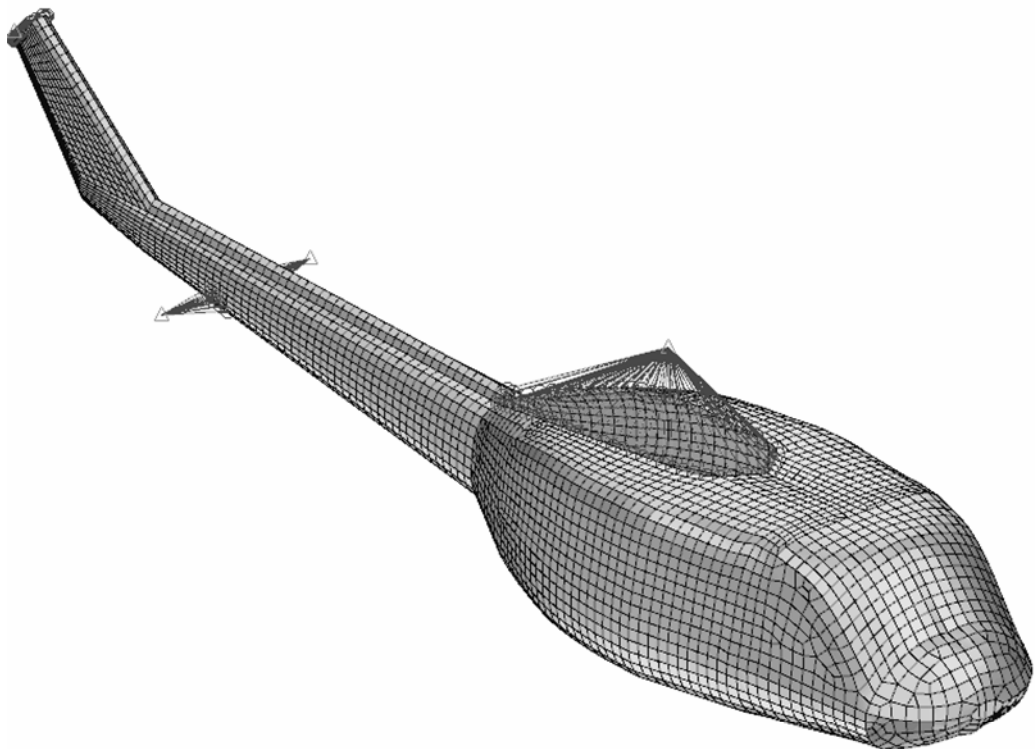


Figure 5.30 Refined finite element model of the whole helicopter

For the modal analysis of the complete helicopter, the model is solved with free boundary condition but tail is fixed in six DOF from the front section as shown in Figure 5.31. The reason for this application is that the inertia of the main body is much higher compared to the tail.

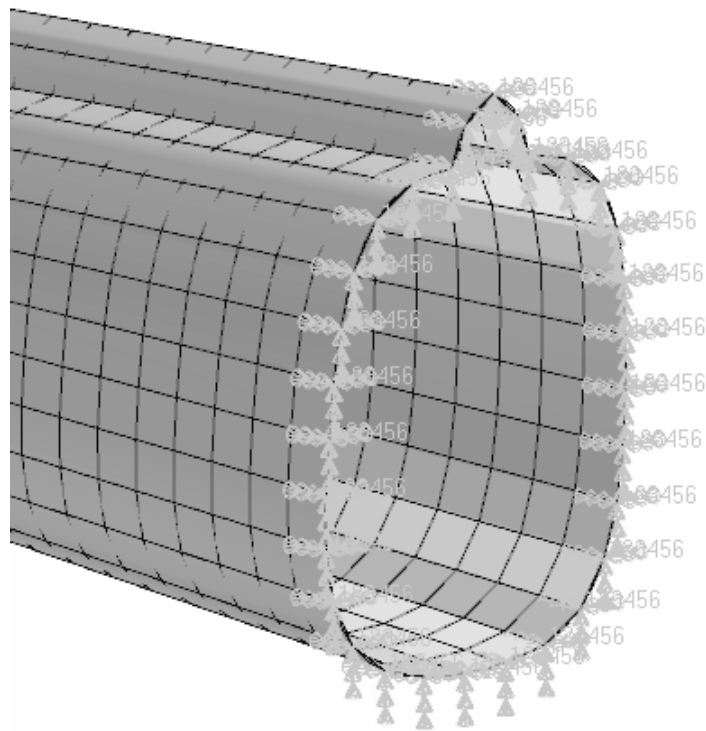


Figure 5.31 Boundary condition of the tail in all six DOF

Tail and complete fuselage finite element model properties are given in Table 5.3.

Table 5.3 Tail and complete fuselage finite element model properties

	Tail Finite Element Model	Complete Fuselage Finite Element Model
Number of Nodes	2616	5948
Number of Beam Elements (CBEAM)	1243	2471
Number of Point Mass Elements (CONM2)	3	4
Number of Shell Elements	2574 (CQUAD4)	5864 (CQUAD4) + 40 (CTRIA3)
Number of Rigid Body Elements (RBE2)	3	4

Modal analysis of the tail is carried out after generation of the mesh. First 10 natural frequencies are given in Table 5.4. First three mode shapes of the tail model are shown in Figure 5.32, Figure 5.33 and Figure 5.34 respectively.

Table 5.4 First 10 natural frequencies of the tail finite element model

Number	Natural Frequency (Hz)
1	11,4
2	14,5
3	35,6
4	58,4
5	75,7
6	110,6
7	131,5
8	134,8
9	142,6
10	151,2

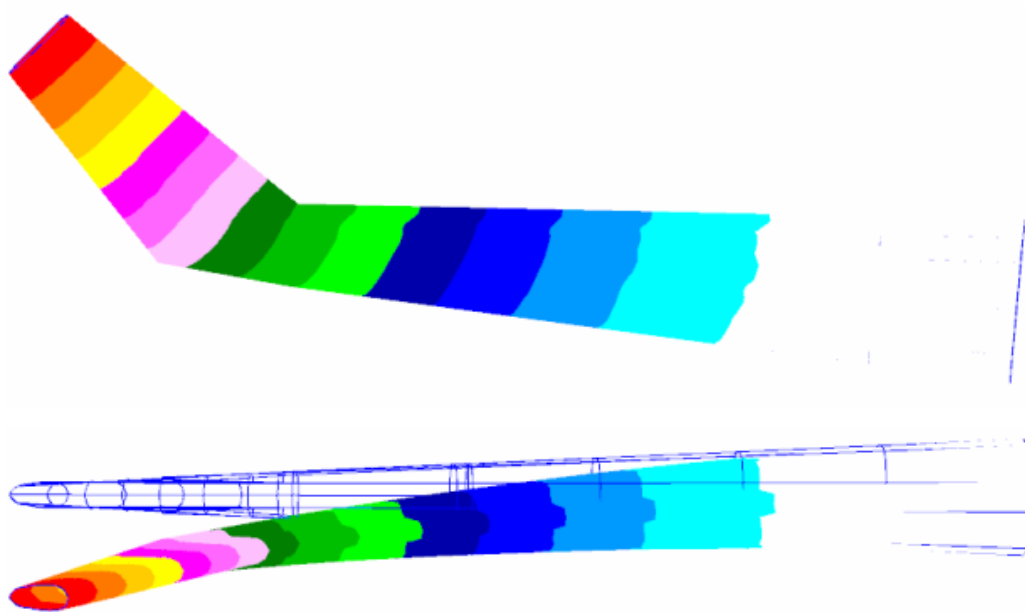


Figure 5.32 First lateral bending mode of the tail finite element model (11.4 Hz)

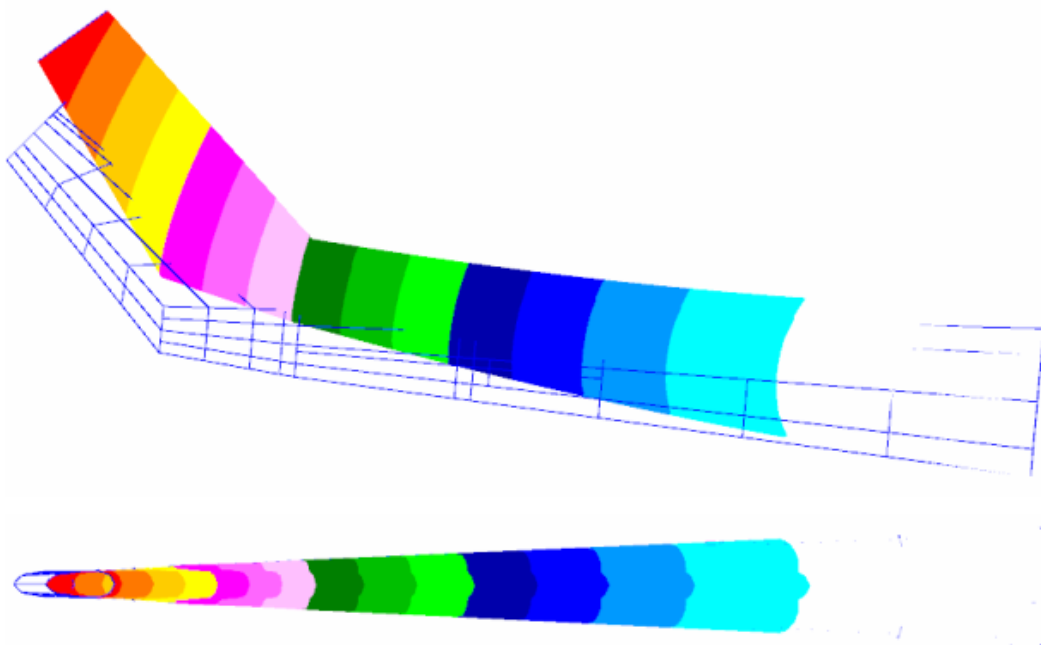


Figure 5.33 First vertical bending mode of the tail finite element model (14.5 Hz)

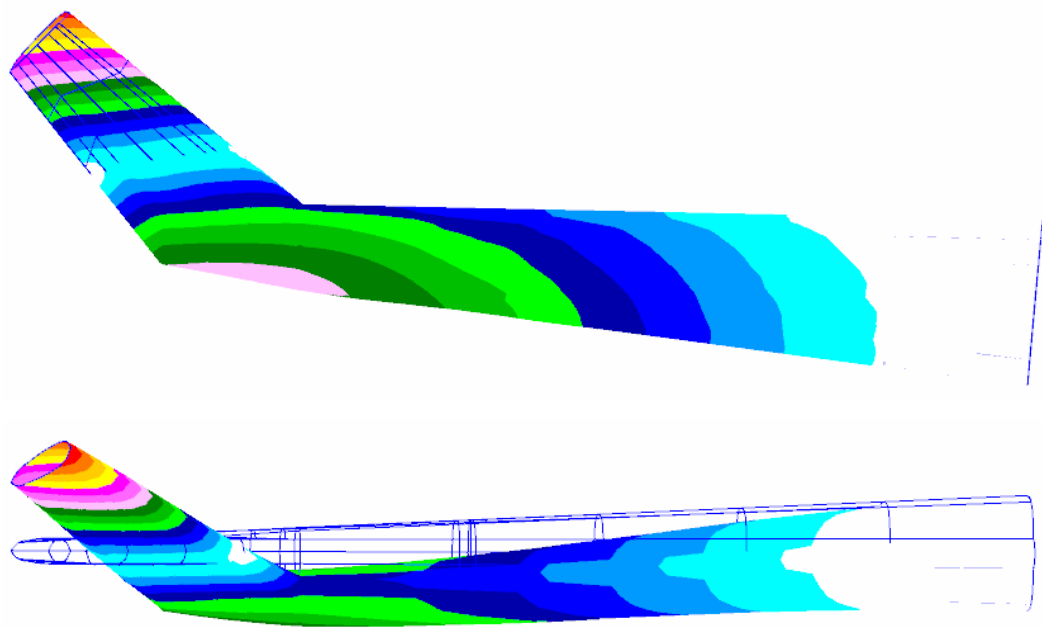


Figure 5.34 First torsion mode of the tail finite element model (35.6 Hz)

Modal analysis of the complete helicopter fuselage is carried out after generation of the mesh. First 10 natural frequencies are given in Table 5.4. First three mode shapes of the complete helicopter fuselage model are shown in Figure 5.35, Figure 5.36 and Figure 5.37 respectively.

Table 5.5 First 10 natural frequencies of the complete helicopter finite element model

Number	Natural Frequency (Hz)
1	17,6
2	22,8
3	38,3
4	40,1
5	45,0
6	45,0

Table 5.5 continued

7	48,0
8	48,3
9	55,1
10	60,1

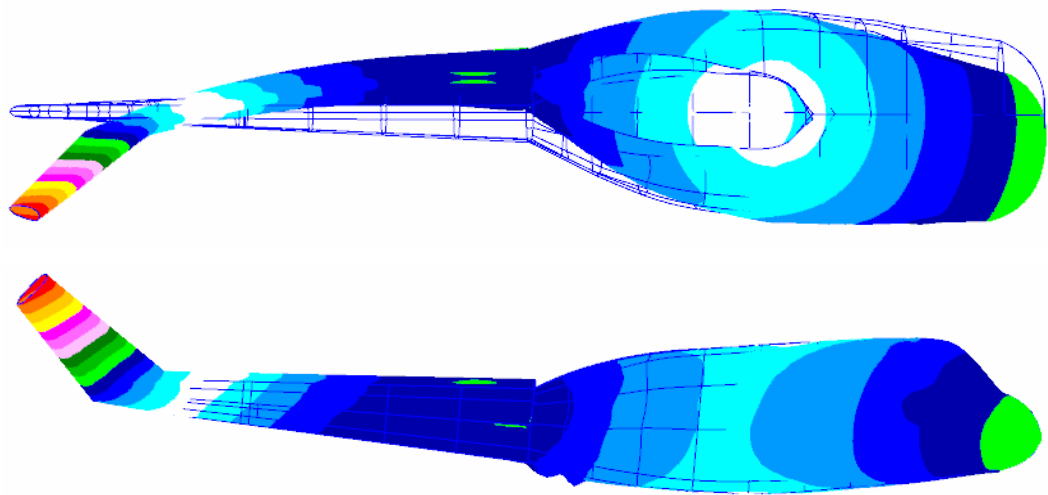


Figure 5.35 First lateral bending mode of the complete helicopter fuselage finite element model (17.6 Hz)

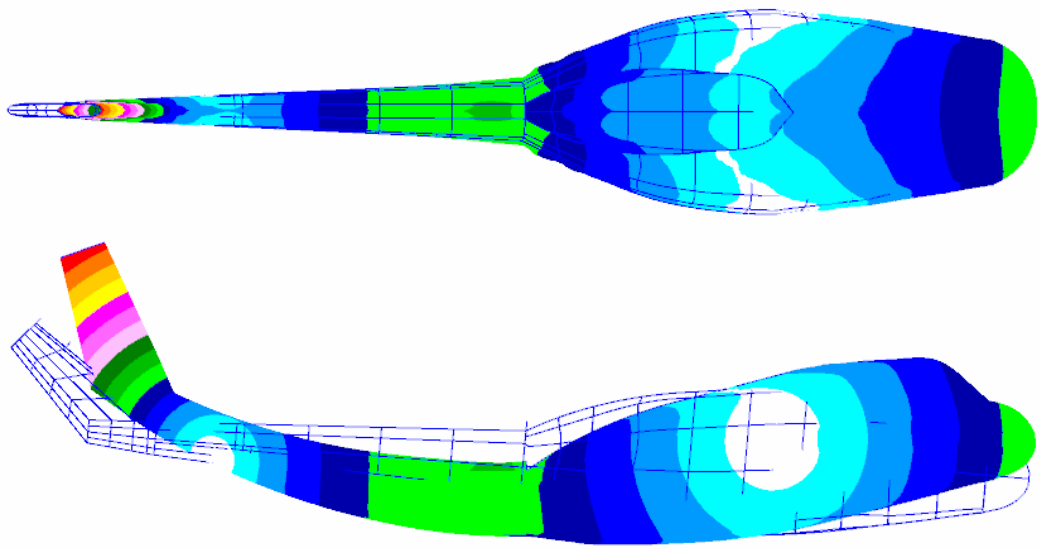


Figure 5.36 First vertical bending mode of the complete helicopter fuselage finite element model (22.8 Hz)

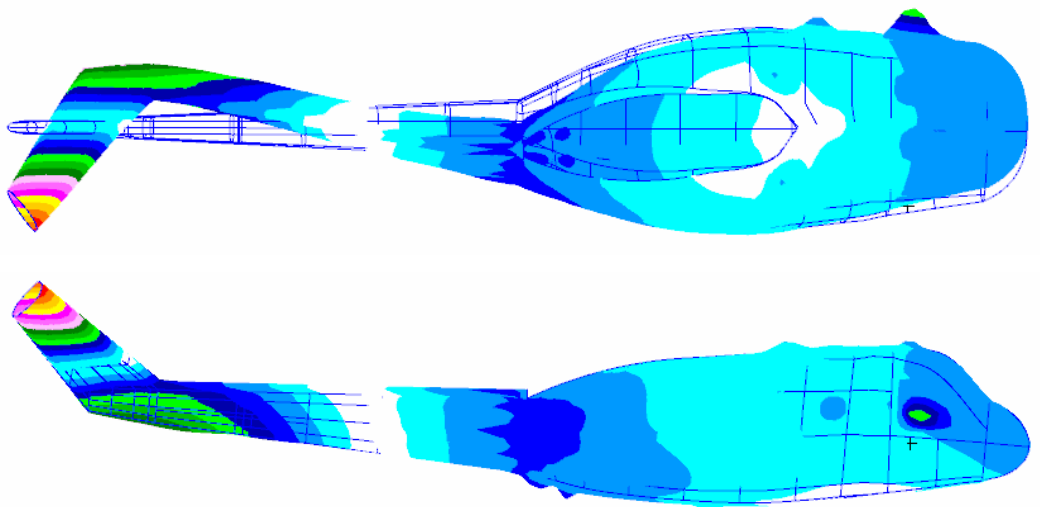


Figure 5.37 First torsion mode of the complete helicopter fuselage finite element model (38.3 Hz)

The remaining natural frequencies are mainly local modes for both tail and complete helicopter fuselage model. An example is shown in Figure 5.38.

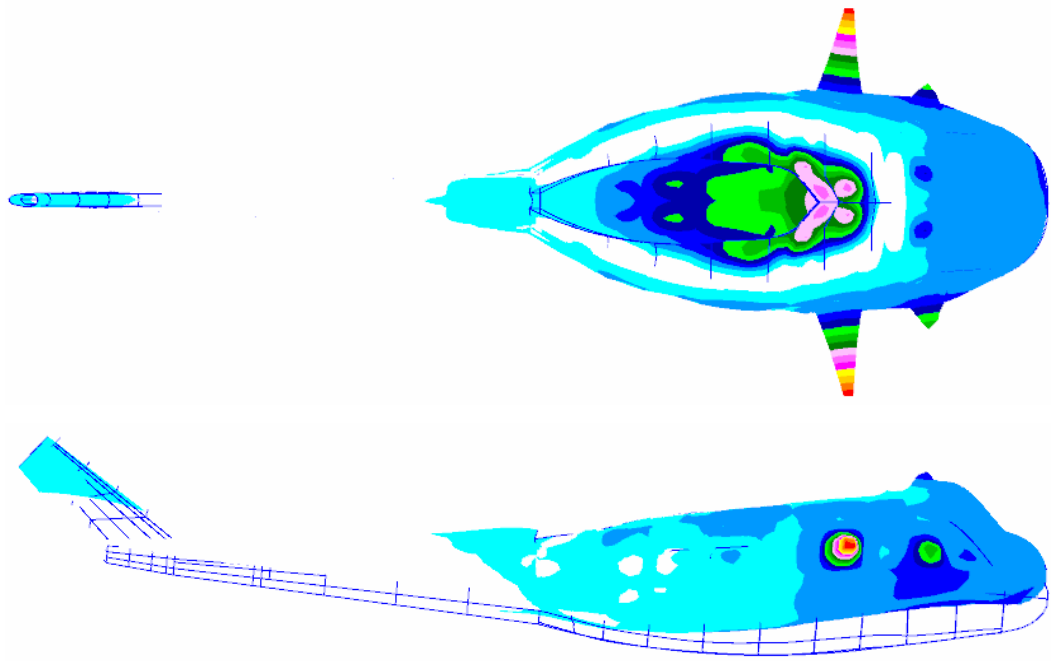


Figure 5.38 An example to a local mode (4th mode, 40.1 Hz)

The procedure of finite element model development and modal analysis with MSC.Patran&Nastran is given in Appendix E.

5.3 Model Updating

After completion of numerical and experimental modal analyses, model updating with LMS Virtual.Lab software was performed in this section. Complete helicopter fuselage and tail model were updated individually.

LMS Virtual.Lab perform reduction in order to equate the size of numerical model to the size of experimental model. In order to update the numerical and experimental models, LMS Virtual.Lab optimizes the correlation between FE and test models. This operation was performed using generalized reduced gradient (GRG) method. For the gradient calculation, sensitivities coming from MSC.Nastran were used. According to gradient calculations, the user selected design variables are optimized in order to reach the target values. Surface thickness, beam cross-section area, material properties etc. are examples to design variables. There can be different target values, for example, equating the MAC correlation to one, or the frequency difference to zero for optimization.

Modal Assurance Criterion (MAC) was used throughout the updating procedure for correlation. Software can also make correlation by using Orthogonality Criterion or Frequency Response Assurance Criterion (FRAC), but these procedures can not be used in optimization procedure.

5.3.1 Model Updating of the Complete Helicopter Fuselage

After the numerical and experimental modal analysis, models (with results) are imported to the LMS Virtual.Lab environment. Then, the MAC matrix is computed. For the complete helicopter fuselage model, computed MAC values and frequency differences are given in Table 5.6. Table also shows the correlation numbers of the numerical and experimental models.

Table 5.6 Initial MAC and frequency difference values of complete helicopter fuselage

Experimental Model Frequency Number	Experimental Model Frequency (Hz)	Numerical Model Frequency Number	Numerical Model Frequency (Hz)	MAC	Frequency Difference (Hz)
8	10,8	1	17,6	0,654	6,92
9	13,4	2	22,8	0,465	9,50

After correlation calculation, sensitivities of the natural frequencies and mode shapes are found in MSC.Nastran for 158 design variables. These design variables are tabulated in Table 5.7.

Table 5.7 Design variables for sensitivity analysis of complete helicopter fuselage model

#	Variable Name	Total Variable
1	Sheet parts elastic modulus material property	1
2	Sheet parts density material property	1
3	Sheet parts thicknesses	18
4	Stiffener (Beam) parts elastic modulus material property	1
5	Stiffener (Beam) parts density material property	1
6	Stiffener (Beam) cross section area	34
7	Stiffener (Beam) second moment of area	34
8	Stiffener (Beam) first moment of area	34
9	Stiffener (Beam) torsional stiffness	34

The complete helicopter surface and beam element property variables are shown in different colors in Figure 5.39 and Figure 5.40, respectively.

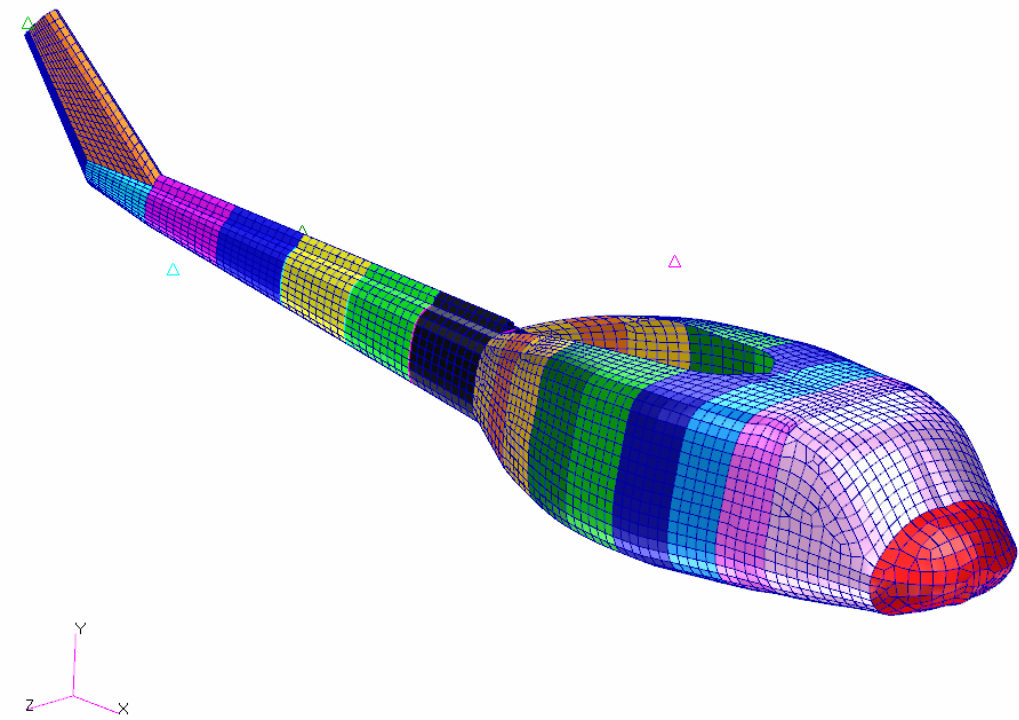


Figure 5.39 Surface element property variables in different colors

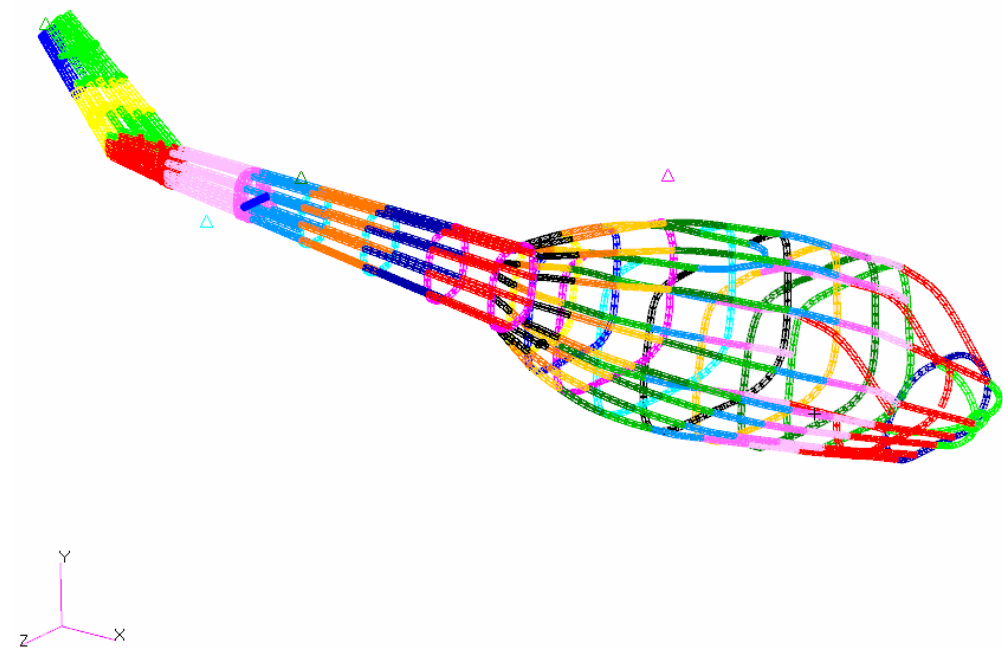


Figure 5.40 Beam element property variables in different colors

Sensitivity results for first, second, third and fourth paired mode shapes (MAC's) are tabulated in Table 5.22 through Table 5.26.

Table 5.8 Sensitivities of paired mode shapes on beam cross section areas

	MAC_1	MAC_2
Beam Cross Section Area (BCSA) 1	0,0	-0,7
Beam Cross Section Area (BCSA) 2	-0,7	-21,0
Beam Cross Section Area (BCSA) 3	-0,2	-35,6
Beam Cross Section Area (BCSA) 4	-0,1	-34,6
Beam Cross Section Area (BCSA) 5	-0,4	-28,4
Beam Cross Section Area (BCSA) 6	-0,2	-10,4
Beam Cross Section Area (BCSA) 7	-0,9	-7,9
Beam Cross Section Area (BCSA) 8	-0,1	34,6
Beam Cross Section Area (BCSA) 9	0,1	21,3
Beam Cross Section Area (BCSA) 10	0,3	33,9
Beam Cross Section Area (BCSA) 11	0,8	105,4
Beam Cross Section Area (BCSA) 12	0,4	40,9
Beam Cross Section Area (BCSA) 13	0,7	58,2
Beam Cross Section Area (BCSA) 14	-0,3	-20,6
Beam Cross Section Area (BCSA) 15	-0,2	-15,7
Beam Cross Section Area (BCSA) 16	-0,4	-20,3
Beam Cross Section Area (BCSA) 17	-0,2	-17,2
Beam Cross Section Area (BCSA) 18	-0,2	-18,0
Beam Cross Section Area (BCSA) 19	-0,2	-14,7
Beam Cross Section Area (BCSA) 20	-0,1	-7,8
Beam Cross Section Area (BCSA) 21	-0,1	-2,3
Beam Cross Section Area (BCSA) 22	0,0	0,5
Beam Cross Section Area (BCSA) 23	0,2	1,2
Beam Cross Section Area (BCSA) 24	0,5	1,0
Beam Cross Section Area (BCSA) 25	0,2	-1,9
Beam Cross Section Area (BCSA) 26	0,1	-11,3
Beam Cross Section Area (BCSA) 27	0,0	-12,0
Beam Cross Section Area (BCSA) 28	0,0	-11,2

Table 5.8 continued

Beam Cross Section Area (BCSA) 29	-0,1	-8,1
Beam Cross Section Area (BCSA) 30	0,0	-4,0
Beam Cross Section Area (BCSA) 31	0,0	-0,7
Beam Cross Section Area (BCSA) 32	0,1	0,8
Beam Cross Section Area (BCSA) 33	0,3	1,1
Beam Cross Section Area (BCSA) 34	0,2	-0,9

Table 5.9 Sensitivities of paired mode shapes on beam first moment of areas

	MAC_1	MAC_2
Beam First Moment of Area (BFAMI) 1	0,4	-6,2
Beam First Moment of Area (BFAMI) 2	-147,7	45,1
Beam First Moment of Area (BFAMI) 3	76,0	123,6
Beam First Moment of Area (BFAMI) 4	85,2	-38,7
Beam First Moment of Area (BFAMI) 5	-30,4	21,9
Beam First Moment of Area (BFAMI) 6	-218,1	-82,0
Beam First Moment of Area (BFAMI) 7	-376,8	-158,0
Beam First Moment of Area (BFAMI) 8	-180,5	-3159,9
Beam First Moment of Area (BFAMI) 9	33,3	-2544,8
Beam First Moment of Area (BFAMI) 10	-47,2	-1585,0
Beam First Moment of Area (BFAMI) 11	-283,3	-317,7
Beam First Moment of Area (BFAMI) 12	66,5	-869,6
Beam First Moment of Area (BFAMI) 13	62,7	-129,2
Beam First Moment of Area (BFAMI) 14	2152,2	21351,6
Beam First Moment of Area (BFAMI) 15	367,5	-742,1
Beam First Moment of Area (BFAMI) 16	-355,8	634,1
Beam First Moment of Area (BFAMI) 17	46,0	186,1
Beam First Moment of Area (BFAMI) 18	63,0	42,2
Beam First Moment of Area (BFAMI) 19	-102,7	-54,6
Beam First Moment of Area (BFAMI) 20	-7,1	4,1
Beam First Moment of Area (BFAMI) 21	-41,2	-29,5
Beam First Moment of Area (BFAMI) 22	-1,2	-6,2
Beam First Moment of Area (BFAMI) 23	-53,1	200,8
Beam First Moment of Area (BFAMI) 24	-375,6	-398,6

Table 5.9 continued

Beam First Moment of Area (BFAMI) 25	-23,9	0,1
Beam First Moment of Area (BFAMI) 26	374,1	3501,6
Beam First Moment of Area (BFAMI) 27	713,9	3509,9
Beam First Moment of Area (BFAMI) 28	188,7	-628,1
Beam First Moment of Area (BFAMI) 29	97,0	-3843,4
Beam First Moment of Area (BFAMI) 30	130,8	-3031,5
Beam First Moment of Area (BFAMI) 31	-91,7	-1145,3
Beam First Moment of Area (BFAMI) 32	-182,1	-812,3
Beam First Moment of Area (BFAMI) 33	-897,4	-287,3
Beam First Moment of Area (BFAMI) 34	127,7	140,5

Table 5.10 Sensitivities of paired mode shapes on beam second moment of areas

	MAC_1	MAC_2
Beam Second Moment of Area (BSAMI) 1	-13,6	6,8
Beam Second Moment of Area (BSAMI) 2	42,5	580,1
Beam Second Moment of Area (BSAMI) 3	33,0	-150,1
Beam Second Moment of Area (BSAMI) 4	3,3	-170,0
Beam Second Moment of Area (BSAMI) 5	38,8	-359,6
Beam Second Moment of Area (BSAMI) 6	-24,6	-53,9
Beam Second Moment of Area (BSAMI) 7	-88,6	-642,0
Beam Second Moment of Area (BSAMI) 8	-108,9	-462,7
Beam Second Moment of Area (BSAMI) 9	-184,1	-521,7
Beam Second Moment of Area (BSAMI) 10	51,8	-25,2
Beam Second Moment of Area (BSAMI) 11	40,9	-24,6
Beam Second Moment of Area (BSAMI) 12	-13,6	-217,2
Beam Second Moment of Area (BSAMI) 13	42,2	-47,5
Beam Second Moment of Area (BSAMI) 14	241,7	1048,2
Beam Second Moment of Area (BSAMI) 15	-2,2	-65,4
Beam Second Moment of Area (BSAMI) 16	46,3	2347,9
Beam Second Moment of Area (BSAMI) 17	-39,4	151,1
Beam Second Moment of Area (BSAMI) 18	-19,1	490,9
Beam Second Moment of Area (BSAMI) 19	-9,5	121,3
Beam Second Moment of Area (BSAMI) 20	0,5	73,2

Table 5.10 continued

Beam Second Moment of Area (BSAMI) 21	-1,2	-95,0
Beam Second Moment of Area (BSAMI) 22	-13,1	-1221,0
Beam Second Moment of Area (BSAMI) 23	-24,5	-294,1
Beam Second Moment of Area (BSAMI) 24	-24,7	-498,3
Beam Second Moment of Area (BSAMI) 25	-1,0	-98,5
Beam Second Moment of Area (BSAMI) 26	108,1	2492,3
Beam Second Moment of Area (BSAMI) 27	195,4	67,0
Beam Second Moment of Area (BSAMI) 28	151,2	-1642,4
Beam Second Moment of Area (BSAMI) 29	-9,8	-155,4
Beam Second Moment of Area (BSAMI) 30	-16,8	-1825,5
Beam Second Moment of Area (BSAMI) 31	-12,4	-183,3
Beam Second Moment of Area (BSAMI) 32	-12,6	-345,1
Beam Second Moment of Area (BSAMI) 33	-50,1	-209,3
Beam Second Moment of Area (BSAMI) 34	12,0	-6,1

Table 5.11 Sensitivities of paired mode shapes on beam torsional stiffness

	MAC_1	MAC_2
Beam Torsional Stiffness (BTS) 1	-0,3	-0,0
Beam Torsional Stiffness (BTS) 2	-152,0	209,8
Beam Torsional Stiffness (BTS) 3	-16,2	54,7
Beam Torsional Stiffness (BTS) 4	6,8	-17,8
Beam Torsional Stiffness (BTS) 5	32,6	-25,7
Beam Torsional Stiffness (BTS) 6	16,6	-40,3
Beam Torsional Stiffness (BTS) 7	-62,6	-132,7
Beam Torsional Stiffness (BTS) 8	-76,9	-734,4
Beam Torsional Stiffness (BTS) 9	42,5	-296,2
Beam Torsional Stiffness (BTS) 10	-76,7	-223,9
Beam Torsional Stiffness (BTS) 11	-31,3	-123,0
Beam Torsional Stiffness (BTS) 12	-10,1	-208,3
Beam Torsional Stiffness (BTS) 13	25,2	-77,7
Beam Torsional Stiffness (BTS) 14	88,6	114,2
Beam Torsional Stiffness (BTS) 15	9,0	-13,3

Table 5.11 continued

Beam Torsional Stiffness (BTS) 16	151,3	712,9
Beam Torsional Stiffness (BTS) 17	99,0	99,7
Beam Torsional Stiffness (BTS) 18	18,1	103,8
Beam Torsional Stiffness (BTS) 19	-3,0	128,6
Beam Torsional Stiffness (BTS) 20	-5,0	-2,2
Beam Torsional Stiffness (BTS) 21	-13,8	-70,3
Beam Torsional Stiffness (BTS) 22	-23,6	-121,0
Beam Torsional Stiffness (BTS) 23	-35,4	25,2
Beam Torsional Stiffness (BTS) 24	-75,1	-91,1
Beam Torsional Stiffness (BTS) 25	12,8	-0,2
Beam Torsional Stiffness (BTS) 26	4,0	466,3
Beam Torsional Stiffness (BTS) 27	57,6	49,0
Beam Torsional Stiffness (BTS) 28	27,6	12,4
Beam Torsional Stiffness (BTS) 29	-2,3	-41,9
Beam Torsional Stiffness (BTS) 30	-6,8	-42,6
Beam Torsional Stiffness (BTS) 31	-7,2	-68,7
Beam Torsional Stiffness (BTS) 32	-3,6	-127,3
Beam Torsional Stiffness (BTS) 33	-21,1	-0,2
Beam Torsional Stiffness (BTS) 34	3,0	-75,7

Table 5.12 Sensitivities of paired mode shapes on material properties and shell thicknesses

	MAC_1	MAC_2
Material Elastic Modulus (MEM) 1	0,0	0,0
Material Elastic Modulus (MEM) 2	0,0	0,0
Material Density (MD) 1	0,0	0,0
Material Density (MD) 2	0,0	0,0
Shell Thickness (ST) 1	1,0	43,7
Shell Thickness (ST) 2	0,5	-6,4
Shell Thickness (ST) 3	0,6	-13,1
Shell Thickness (ST) 4	-0,1	-15,6
Shell Thickness (ST) 5	-0,6	-11,6

Table 5.12 continued

Shell Thickness (ST) 6	-0,2	-0,7
Shell Thickness (ST) 7	0,0	5,9
Shell Thickness (ST) 8	0,2	13,5
Shell Thickness (ST) 9	0,2	7,9
Shell Thickness (ST) 10	0,0	-2,7
Shell Thickness (ST) 11	-0,3	-3,8
Shell Thickness (ST) 12	-0,5	-4,5
Shell Thickness (ST) 13	-0,1	-2,8
Shell Thickness (ST) 14	-0,1	-0,7
Shell Thickness (ST) 15	-0,1	0,4
Shell Thickness (ST) 16	-0,1	0,7
Shell Thickness (ST) 17	0,3	0,4
Shell Thickness (ST) 18	0,1	-0,8

Total sensitivities of similar properties on paired mode shapes are tabulated in Table 5.13 and shown in Figure 5.41.

Table 5.13 Summed sensitivities of paired mode shapes on design variables

	MAC_1	MAC_2
Summed BCSA	-0,5	-6,3
Summed BFAMI	1169,6	9891,4
Summed BSAMI	337,8	-1935,3
Summed BTS	-28,6	-558,1
Summed MEM	0	0
Summed MD	0	0
Summed ST	0,8	9,8

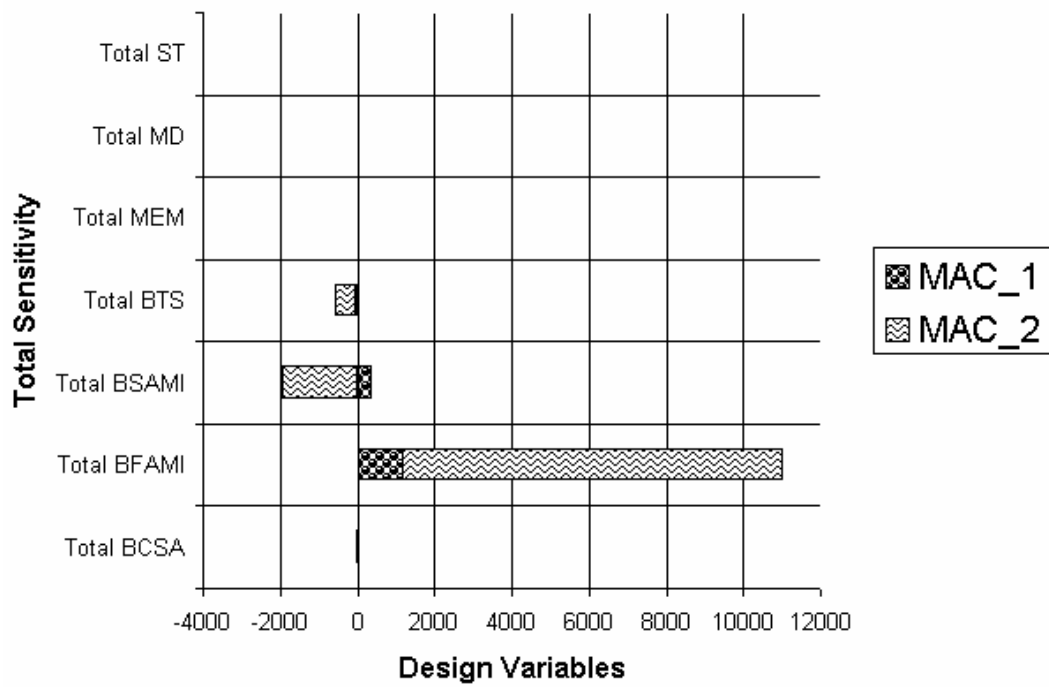


Figure 5.41 Summed sensitivities of paired mode shapes on design variables

After sensitivity analysis, updating (optimization) of these design variables are carried out. For the first optimization, sensitivity based algorithm is chosen. But except Freq_Diff_1 objective function, the algorithm could not update for any of the objective functions. Change of objective functions for this optimization try is shown in Figure 5.42 and Figure 5.43.

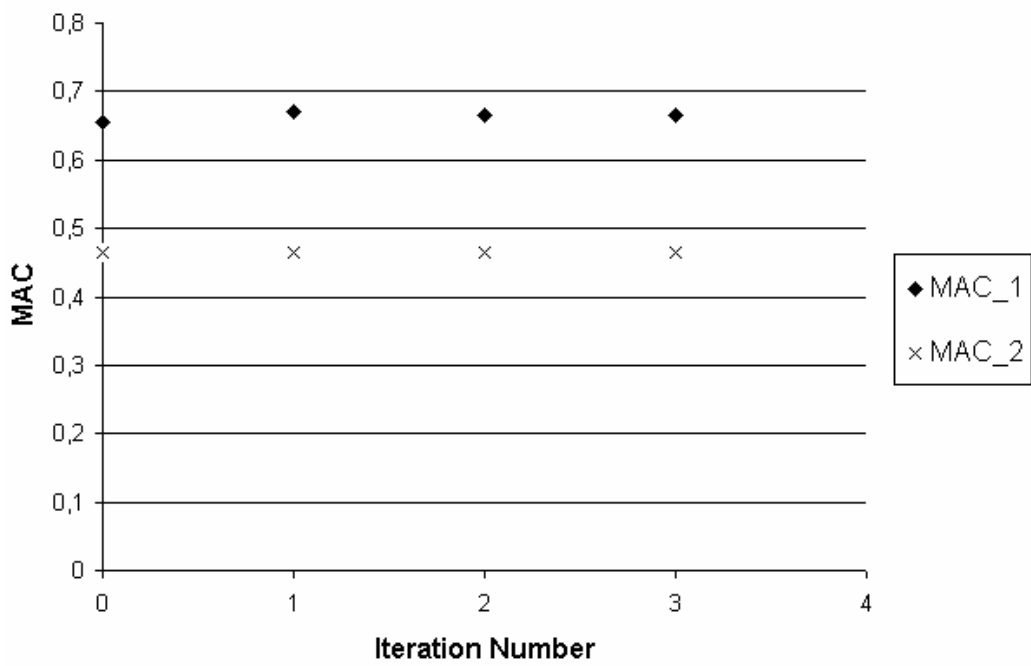


Figure 5.42 Change of MAC's for sensitivity based optimization

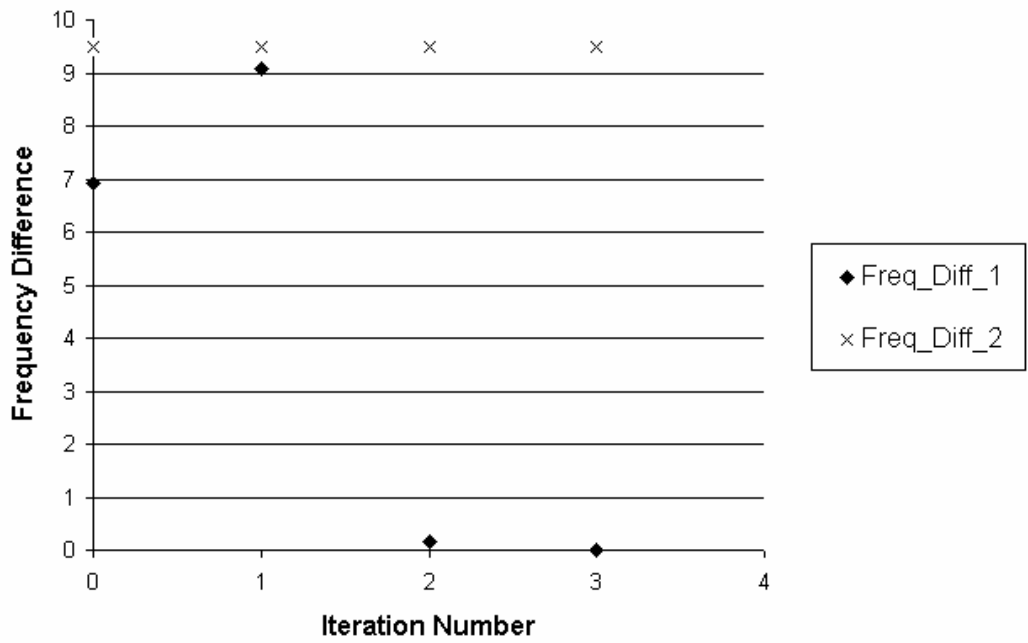


Figure 5.43 Change of frequency differences for sensitivity based optimization

After updating problem with the sensitivity based algorithm, finite difference algorithm was chosen for optimization. Updating was tried for the objective functions of increasing all MAC values and decreasing all frequency differences between reference and verification models. First optimization results are found as tabulated in Table 5.14 and Table 5.15 and shown in Figure 5.44 and Figure 5.45.

Table 5.14 MAC updating results with objective functions of increasing all MAC and decreasing all frequency differences

Iteration	MAC_1	MAC_2
0	0,654	0,465
1	0,654	0,464
2	0,656	0,462
3	0,657	0,461
4	0,657	0,461
5	0,657	0,461
6	0,658	0,460
7	0,658	0,459
8	0,659	0,458
9	0,660	0,457
10	0,661	0,455

Table 5.15 Frequency difference updating results with objective functions of increasing all MAC and decreasing all frequency differences

Iteration	Freq_Diff_1	Freq_Diff_2
0	6,92	9,50
1	6,69	9,22
2	5,62	7,88
3	5,27	7,43
4	5,22	7,37
5	5,13	7,25
6	5,01	7,11

Table 5.15 continued

7	4,96	7,05
8	4,86	6,92
9	4,83	6,88
10	4,69	6,69

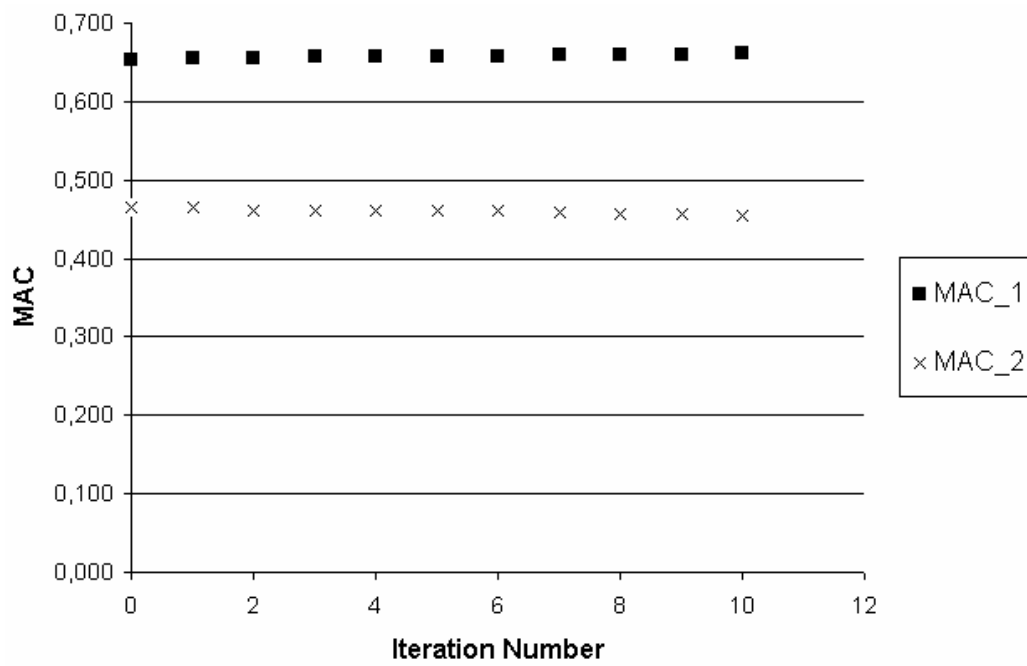


Figure 5.44 MAC updating results with objective functions of increasing all MAC and decreasing all frequency differences

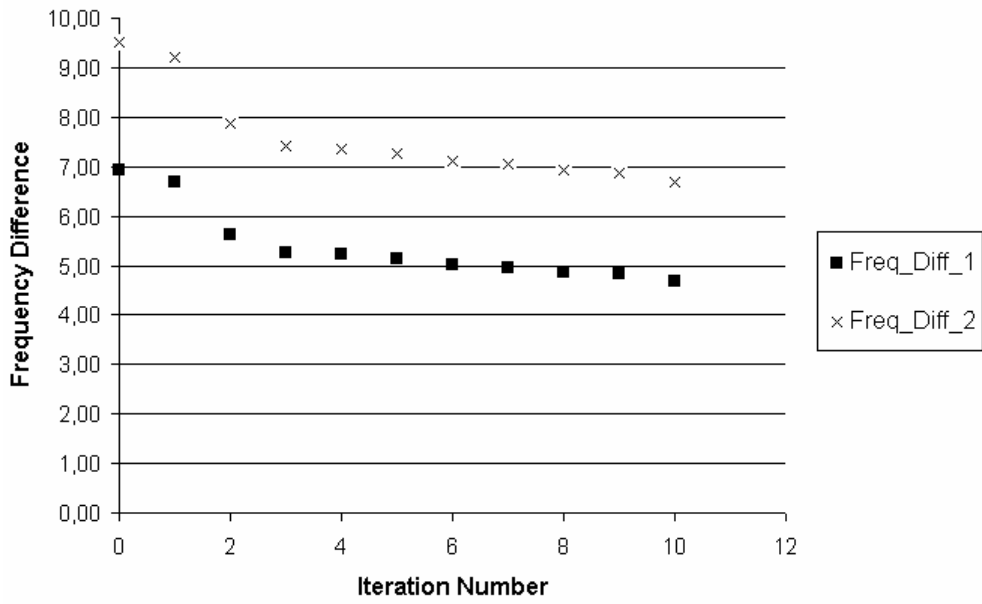


Figure 5.45 Frequency difference results with objective functions of increasing all MAC and decreasing all frequency differences

Change of design variables for this updating run are shown in Figure 5.46 through Figure 5.52.

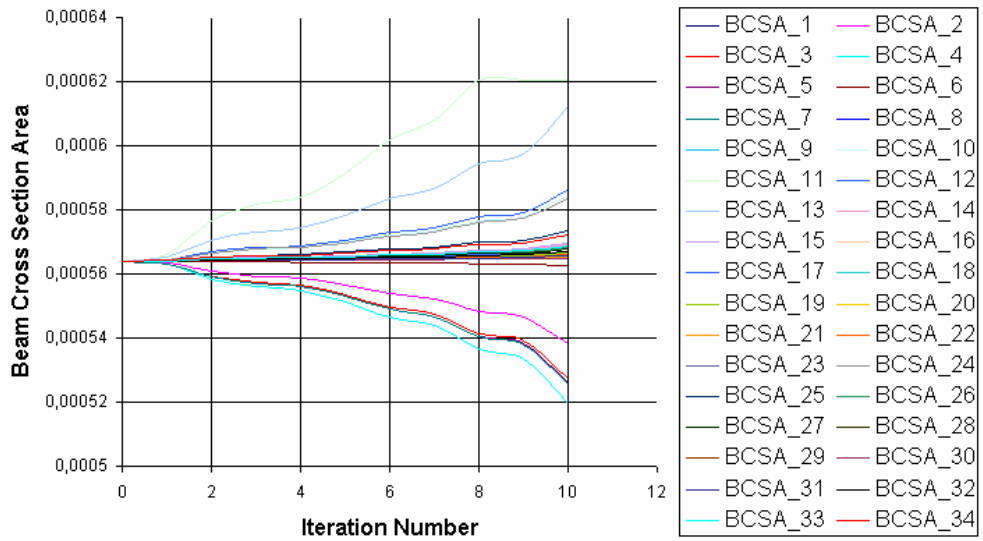


Figure 5.46 Change of beam cross-section areas for first optimization

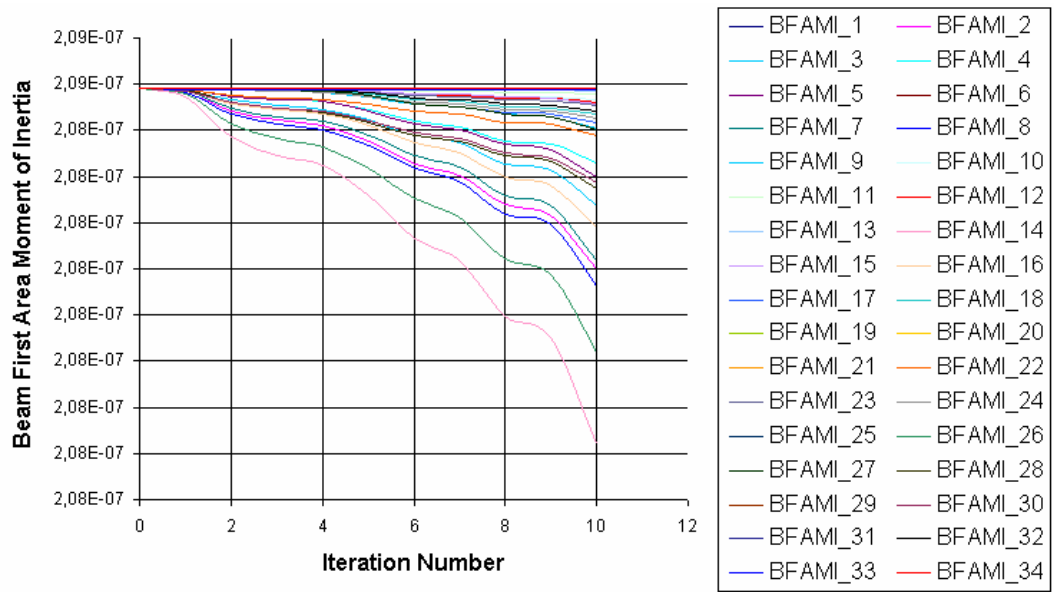


Figure 5.47 Change of beam first moment of areas for first optimization

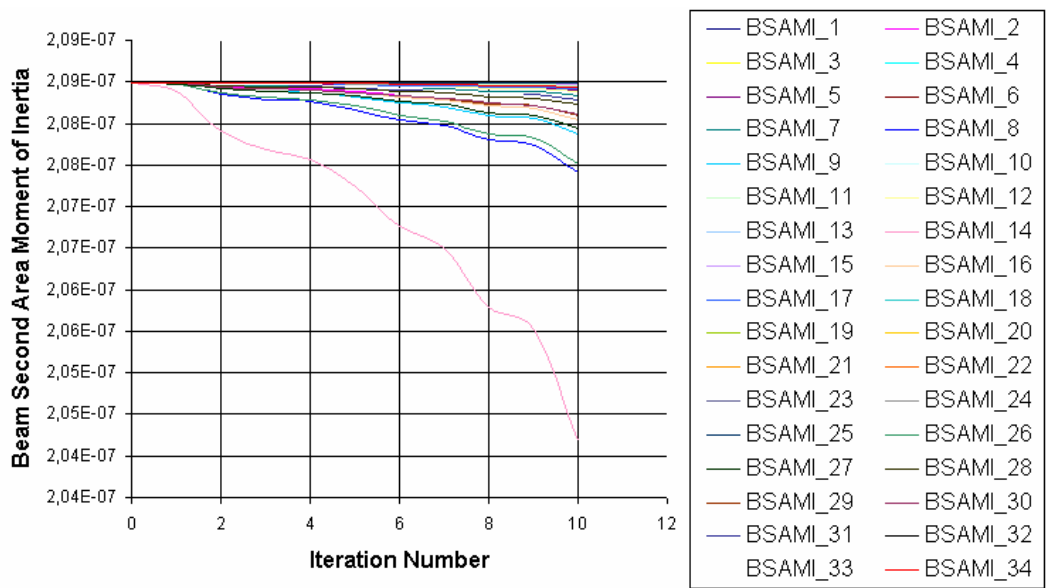


Figure 5.48 Change of beam second moment of areas for first optimization

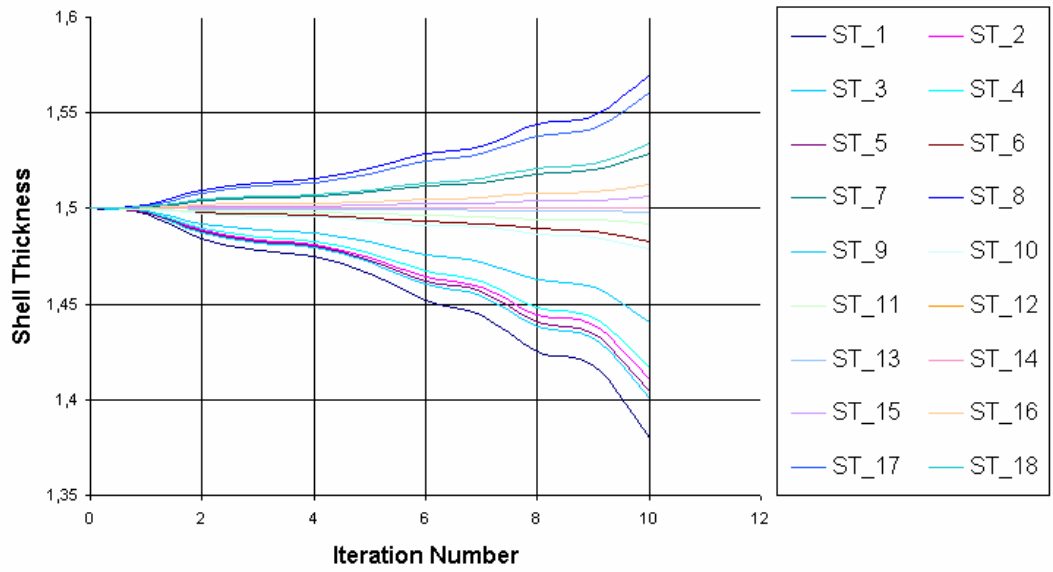


Figure 5.49 Change of shell thicknesses for first optimization

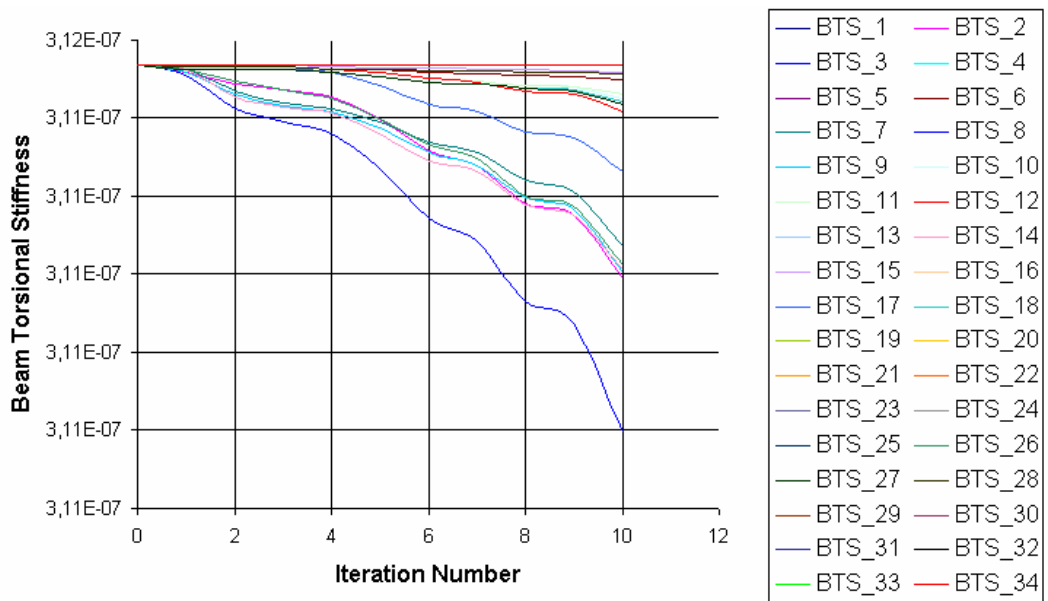


Figure 5.50 Change of beam torsional stiffnesses for first optimization

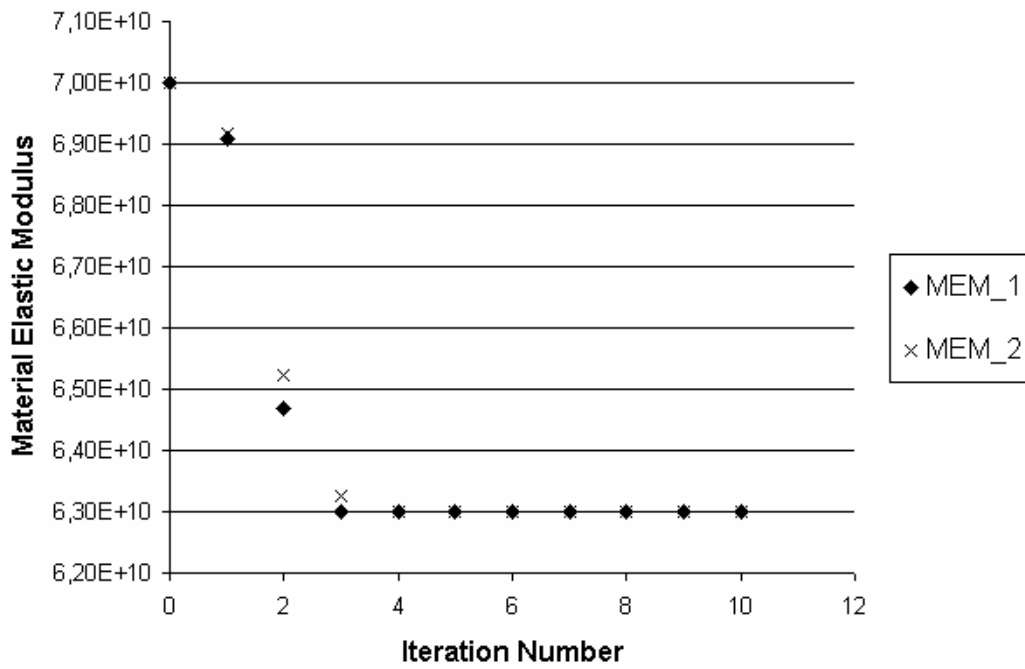


Figure 5.51 Change of material elastic modulus for first optimization

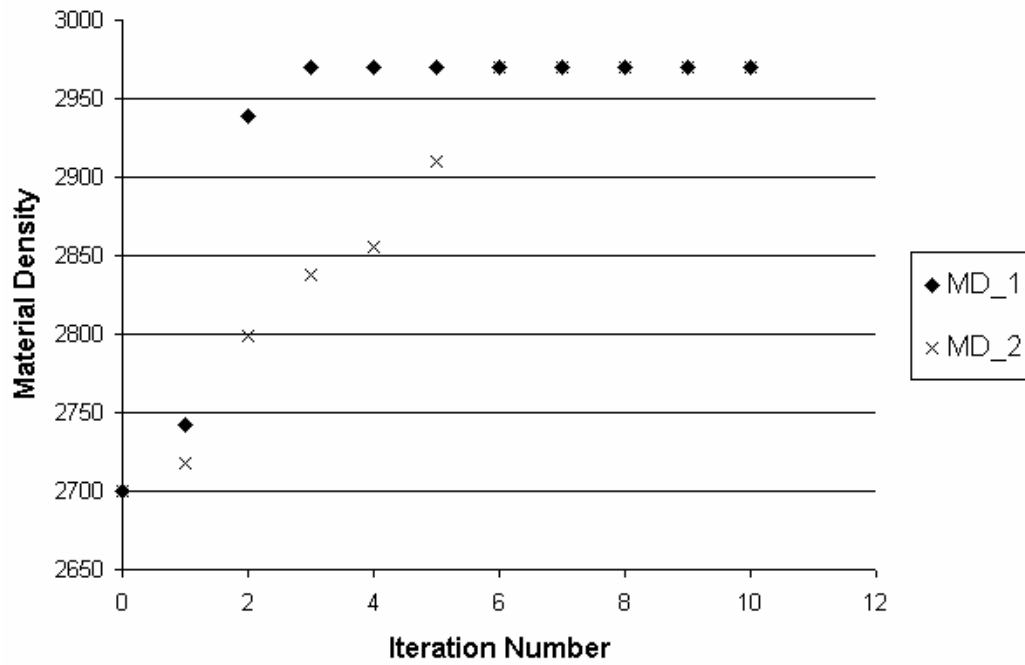


Figure 5.52 Change of material density for first optimization

As a second updating strategy, only increase of MAC values are chosen as objective functions. Results of this work are tabulated in Table 5.16 and shown in Figure 5.53.

Table 5.16 MAC updating results with objective functions of increasing all MAC

Iteration	MAC_1	MAC_2
0	0,654	0,465
1	0,654	0,465
2	0,654	0,466
3	0,653	0,468
4	0,656	0,478
5	0,657	0,479
6	0,660	0,480
7	0,661	0,481
8	0,665	0,484
9	0,665	0,484
10	0,667	0,485
11	0,668	0,486
12	0,669	0,486
13	0,670	0,488
14	0,671	0,488
15	0,671	0,488

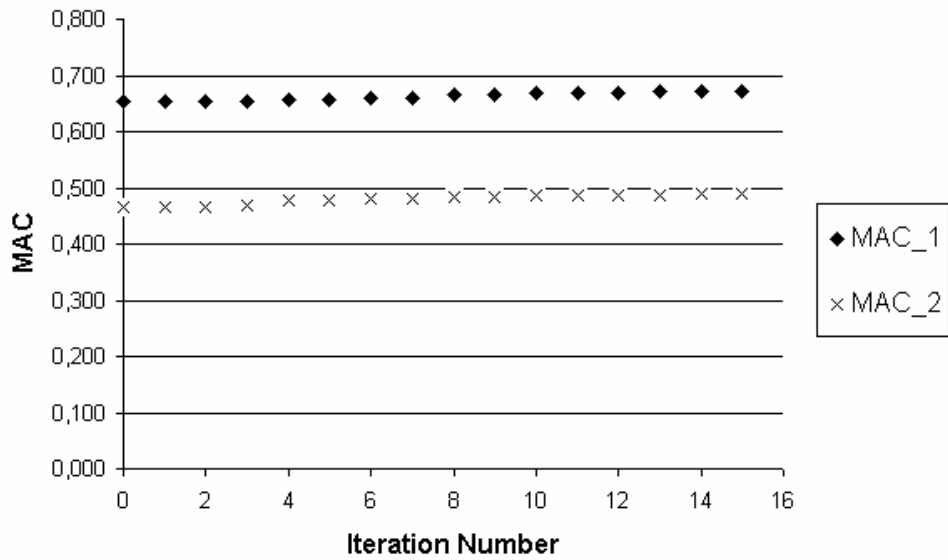


Figure 5.53 MAC updating results with objective functions of increasing all MAC

After only MAC updating, the decrease of frequency difference values are chosen as the lone objective function. Results of this work are tabulated in Table 5.17 and shown in Figure 5.54.

Table 5.17 Frequency difference updating results with objective functions of decreasing all frequency differences

Iteration	Freq_Diff_1	Freq_Diff_2
0	6,92	9,50
1	6,69	9,22
2	5,62	7,88
3	5,27	7,43
4	5,22	7,37
5	5,13	7,25
6	5,01	7,11
7	4,96	7,05
8	4,86	6,92
9	4,83	6,88
10	4,69	6,69

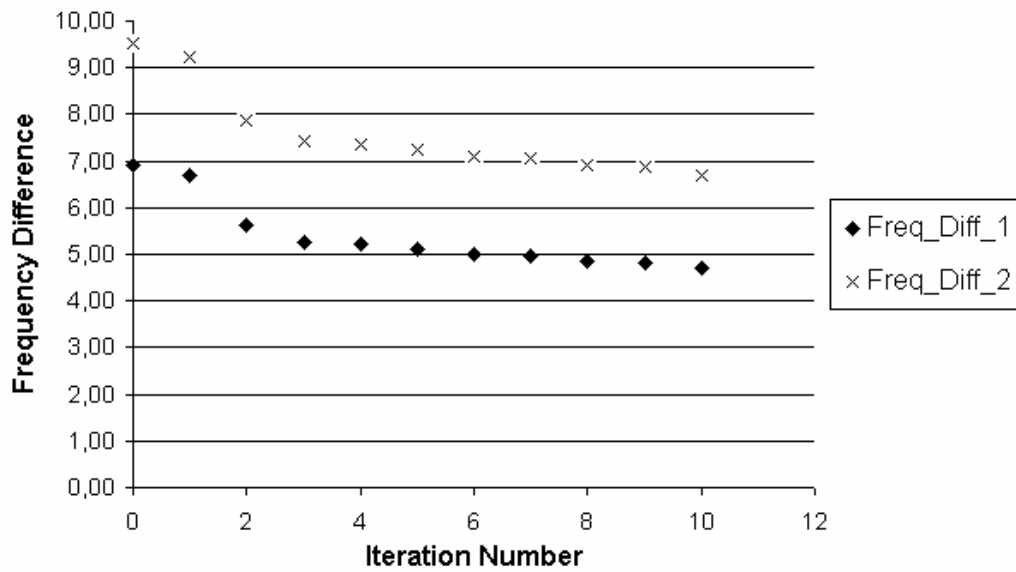


Figure 5.54 Frequency difference updating results with objective functions of decreasing all frequency differences

Then, decrease of frequency difference of 2 is chosen as the objective function. Results of this work are tabulated in Table 5.18 and shown in Figure 5.55.

Table 5.18 Updating results for objective function of decreasing frequency difference 2

Iteration	Freq_Diff_2
0	9,50
1	4,48
2	0,63
3	0,35
4	0,02
5	0,01

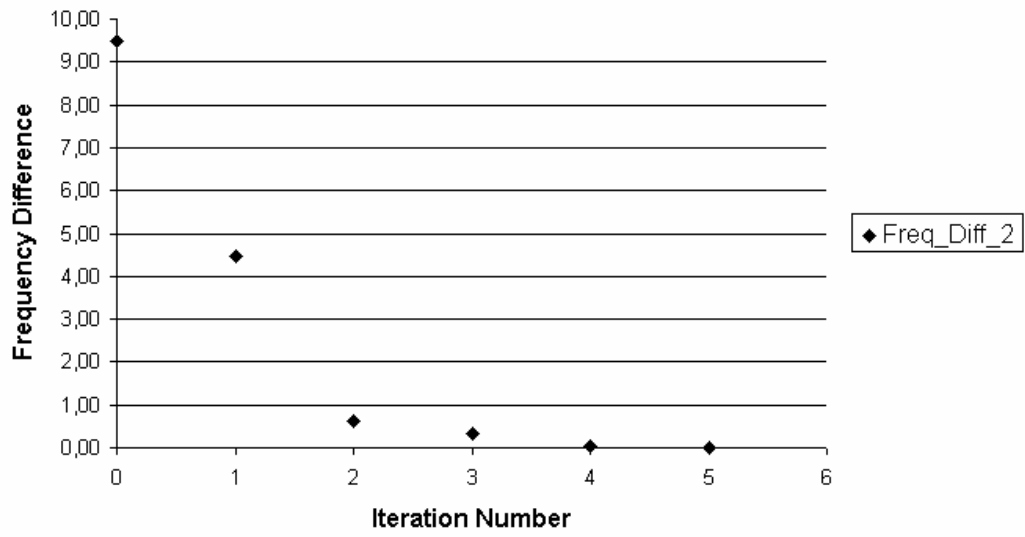


Figure 5.55 Updating results for objective function of decreasing frequency difference 2

Then, the increase of only MAC_1 is chosen as the objective function. Results of this work are tabulated in Table 5.19 and shown in Figure 5.56.

Table 5.19 Updating results for objective function of increasing only MAC_1

Iteration	MAC_1
0	0,654
1	0,662
2	0,683
3	0,689
4	0,691
5	0,692
6	0,693
7	0,694
8	0,694
9	0,694

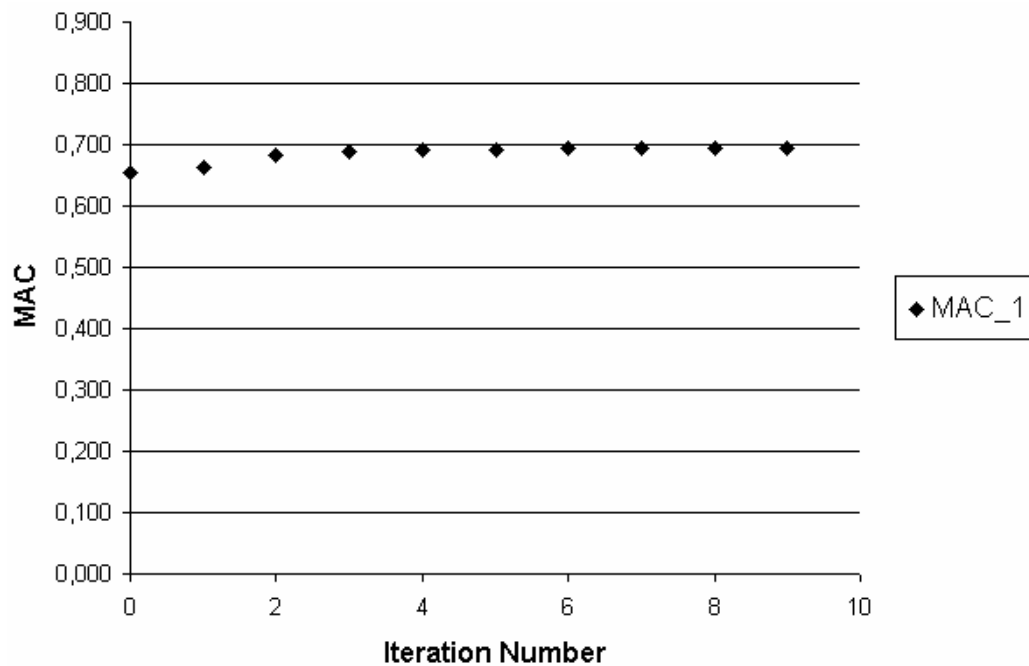


Figure 5.56 Updating results for objective function of increasing only MAC_1

After model updating trials for different design variables, objective functions and optimization methods, proper results could not be achieved. Especially MAC updating results shows very little improvement. The reasons for this problem are:

- Experimental modal analysis problems such as cabin and cockpit could not be excited properly using one shaker at the tail.
- Since the helicopter is very old and all of its devices are removed, cabin and cockpit fuselage has excessive local nonlinearities (e.g. vibration of large plates because of loosens in joints).

In order to solve this problem, cabin and cockpit region is removed from model updating calculations. From this point on, only model updating of the tail is studied.

5.3.2 Model Updating of the Tail

In this case study, model updating of the tail is performed. The procedure of model updating is exactly the same as the complete helicopter fuselage model updating study discussed previously.

At the beginning of the updating process, correlation calculation is performed. According to this calculation, MAC results are shown in Table 5.20. The correlation numbers of the numerical and experimental models are also shown in the table.

Table 5.20 Initial MAC and frequency difference values of the tail model

Experimental Model Frequency Number	Experimental Model Frequency (Hz)	Numerical Model Frequency Number	Numerical Model Frequency (Hz)	MAC	Frequency Difference (Hz)
1	3,6	1	11,4	0,779	7,9
2	7,3	2	14,5	0,548	7,3
3	9,6	4	58,4	0,607	48,8
4	36,7	5	75,7	0,414	39,0

72 design variables are introduced inside LMS Virtual.Lab to be used for optimization. These design variables are summarized in Table 5.21.

Table 5.21 Design variables of the tail model

#	Variable Name	Total Variable
1	Sheet parts elastic modulus material property	1
2	Sheet parts density material property	1
3	Sheet part thicknesses	8

Table 5.21 continued

4	Stiffener (Beam) parts elastic modulus material property	1
5	Stiffener (Beam) parts density material property	1
6	Stiffener (Beam) cross section area	15
7	Stiffener (Beam) second moment of area	15
8	Stiffener (Beam) first moment of area	15
9	Stiffener (Beam) torsional stiffness	15

Tail surface and beam element property variables are shown in Figure 5.57 and Figure 5.58 as different colors.

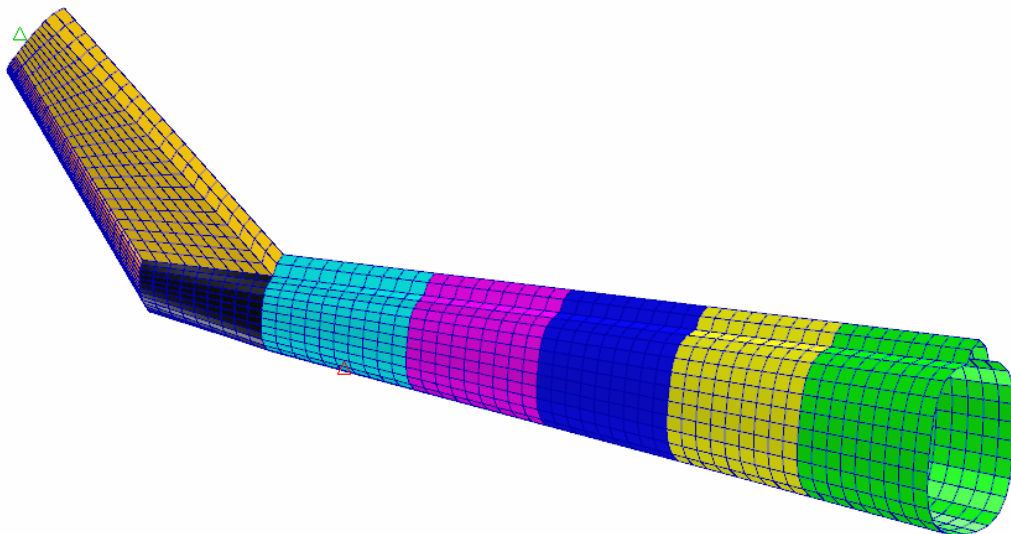


Figure 5.57 Surface element property variables in different colors

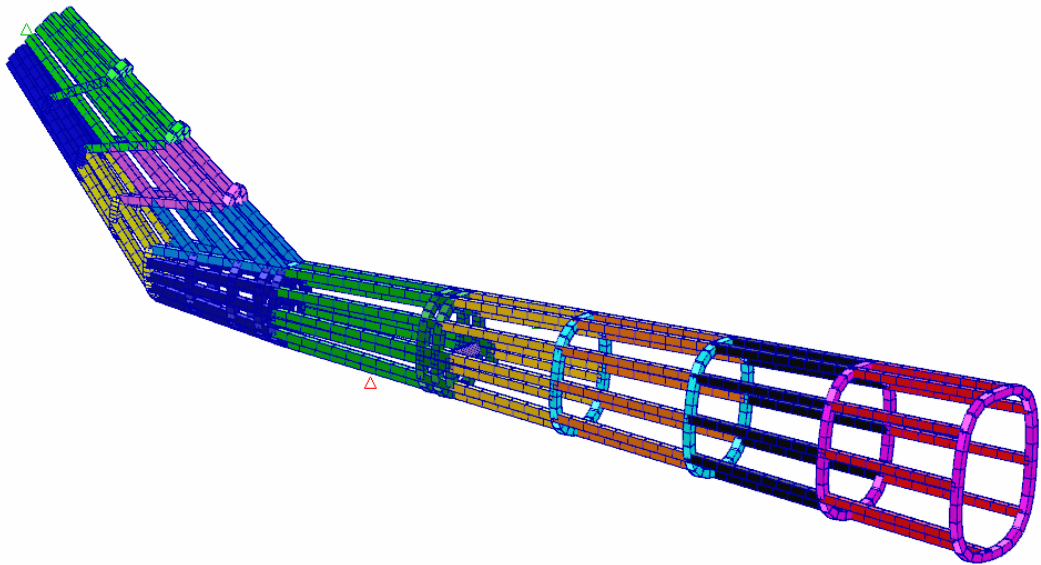


Figure 5.58 Beam element property variables in different colors

After introduction of design variables to the software, sensitivities of the natural frequencies and mode shapes are found in MSC.Nastran for desired design variables. Sensitivity results for the first, second, third and fourth paired mode shapes (MAC's) are tabulated in Table 5.22 through Table 5.26.

Table 5.22 Sensitivities of paired mode shapes on beam cross section areas

	MAC_1	MAC_2	MAC_3	MAC_4
Beam Cross-Section Area (BCSA) 1	0,3	-0,2	-0,6	-4,1
Beam Cross-Section Area (BCSA) 2	-59,0	30,5	-12,7	18,5
Beam Cross-Section Area (BCSA) 3	-27,7	13,3	19,4	10,5
Beam Cross-Section Area (BCSA) 4	1,3	-7,1	7,7	-45,3
Beam Cross-Section Area (BCSA) 5	17,5	-20,1	-13,5	-73,8
Beam Cross-Section Area (BCSA) 6	4,8	-4,3	-8,6	-58,1
Beam Cross-Section Area (BCSA) 7	34,6	-31,0	-13,4	17,2
Beam Cross-Section Area (BCSA) 8	23,6	-7,8	-8,1	151,6
Beam Cross-Section Area (BCSA) 9	12,3	-3,1	-0,9	13,8
Beam Cross-Section Area (BCSA) 10	0,9	0,5	2,9	-0,3

Table 5.22 continued

Beam Cross-Section Area (BCSA) 11	-29,7	9,3	27,8	104,3
Beam Cross-Section Area (BCSA) 12	3,3	1,2	10,3	18,9
Beam Cross-Section Area (BCSA) 13	-11,9	5,5	20,2	-41,1
Beam Cross-Section Area (BCSA) 14	-0,1	0,0	0,6	1,0
Beam Cross-Section Area (BCSA) 15	0,7	-0,6	4,8	-12,2

Table 5.23 Sensitivities of paired mode shapes on beam first moment of areas

	MAC_1	MAC_2	MAC_3	MAC_4
Beam First Moment of Area (BFAMI) 1	1,1	-0,2	2,5	-180,9
Beam First Moment of Area (BFAMI) 2	-2005,1	-0,1	-342,3	-8958,9
Beam First Moment of Area (BFAMI) 3	-706,1	18,6	-135,5	-3995,9
Beam First Moment of Area (BFAMI) 4	-311,1	23,8	132,2	-745,5
Beam First Moment of Area (BFAMI) 5	980,0	6,5	512,9	5719,0
Beam First Moment of Area (BFAMI) 6	524,3	0,4	771,2	704,4
Beam First Moment of Area (BFAMI) 7	2447,2	116,7	4821,4	3115,9
Beam First Moment of Area (BFAMI) 8	16939,3	-1616,3	9213,5	-3859,7
Beam First Moment of Area (BFAMI) 9	9376,3	-657,7	1524,2	-12095,8
Beam First Moment of Area (BFAMI) 10	632,4	-164,5	344,5	4097,7
Beam First Moment of Area (BFAMI) 11	369,3	-21,4	0,3	5338,4
Beam First Moment of Area (BFAMI) 12	1215,1	-171,1	562,4	-1383,9
Beam First Moment of Area (BFAMI) 13	181,9	3,3	83,1	1773,3
Beam First Moment of Area (BFAMI) 14	-68,3	-6,5	-962,1	-6230,7
Beam First Moment of Area (BFAMI) 15	-183,5	53,4	-1704,1	-4508,0

Table 5.24 Sensitivities of paired mode shapes on beam second moment of areas

	MAC_1	MAC_2	MAC_3	MAC_4
Beam Second Moment of Area (BSAMI) 1	28,8	-0,1	8,6	145,9
Beam Second Moment of Area (BSAMI) 2	149,6	382,9	-5039,7	97,1
Beam Second Moment of Area (BSAMI) 3	248,8	163,4	-2351,4	-297,3
Beam Second Moment of Area (BSAMI) 4	246,2	-84,9	-1409,0	-1581,8

Table 5.24 continued

Beam Second Moment of Area (BSAMI) 5	383,1	-320,5	1447,3	-1025,2
Beam Second Moment of Area (BSAMI) 6	404,7	84,0	1405,9	-851,2
Beam Second Moment of Area (BSAMI) 7	1965,1	-1881,8	5981,3	-1849,0
Beam Second Moment of Area (BSAMI) 8	3092,2	-2579,0	4730,5	-4229,4
Beam Second Moment of Area (BSAMI) 9	3568,6	-211,7	2612,5	152,4
Beam Second Moment of Area (BSAMI) 10	253,5	-1,6	192,4	328,0
Beam Second Moment of Area (BSAMI) 11	187,0	-1,1	669,6	611,7
Beam Second Moment of Area (BSAMI) 12	335,1	-65,2	859,7	2587,9
Beam Second Moment of Area (BSAMI) 13	153,6	2,7	645,7	378,4
Beam Second Moment of Area (BSAMI) 14	68,4	47,3	-1420,1	-610,9
Beam Second Moment of Area (BSAMI) 15	319,9	124,6	-246,8	210,9

Table 5.25 Sensitivities of paired mode shapes on beam torsional stiffness

	MAC_1	MAC_2	MAC_3	MAC_4
Beam Torsional Stiffness (BTS) 1	4,9	0,0	0,0	-2,5
Beam Torsional Stiffness (BTS) 2	47,0	0,1	-24,8	-382,4
Beam Torsional Stiffness (BTS) 3	108,8	-0,1	-45,1	-140,0
Beam Torsional Stiffness (BTS) 4	124,5	-7,1	-88,7	-32,5
Beam Torsional Stiffness (BTS) 5	385,5	-3,3	-26,3	-419,3
Beam Torsional Stiffness (BTS) 6	131,2	-0,3	374,1	-229,6
Beam Torsional Stiffness (BTS) 7	1768,4	-15,1	117,7	-1932,1
Beam Torsional Stiffness (BTS) 8	3191,1	-264,3	1466,7	-809,6
Beam Torsional Stiffness (BTS) 9	2577,3	-66,9	455,3	-3647,5
Beam Torsional Stiffness (BTS) 10	266,6	-45,0	-4,6	532,4
Beam Torsional Stiffness (BTS) 11	221,6	-2,4	127,9	661,2
Beam Torsional Stiffness (BTS) 12	320,6	-10,8	7,3	-615,5
Beam Torsional Stiffness (BTS) 13	67,2	0,1	87,0	37,1
Beam Torsional Stiffness (BTS) 14	-23,3	10,3	-56,5	-157,8
Beam Torsional Stiffness (BTS) 15	37,0	3,7	135,1	363,1

Table 5.26 Sensitivities of paired mode shapes on material properties and shell thicknesses

	MAC_1	MAC_2	MAC_3	MAC_4
Material Density (MD) 1	0,0	0,0	0,0	0,0
Material Density (MD) 2	0,0	0,0	0,0	0,0
Material Elastic Modulus (MEM) 1	0,0	0,0	0,0	0,0
Material Elastic Modulus (MEM) 2	0,0	0,0	0,0	0,0
Shell Thickness (ST) 1	-18,8	12,7	-31,2	-20,2
Shell Thickness (ST) 2	-7,4	5,7	-6,7	-4,1
Shell Thickness (ST) 3	1,9	-0,3	4,0	-1,8
Shell Thickness (ST) 4	6,7	-4,2	2,7	-12,7
Shell Thickness (ST) 5	16,3	-6,6	5,9	-16,7
Shell Thickness (ST) 6	4,6	-2,7	3,0	10,3
Shell Thickness (ST) 7	0,2	0,3	2,4	2,1
Shell Thickness (ST) 8	0,4	0,2	5,5	8,8

Additionally, sensitivities of paired mode shapes for Shell Thickness (ST), Material Properties(MD, MEM), Beam Cross-Section Area (BCSA), Beam Torsional Stiffness (BTS), Beam First Moment of Area (BFAMI) and Beam Second Moment of Area (BSAMI) are shown in Figure 5.59 through Figure 5.63 respectively.

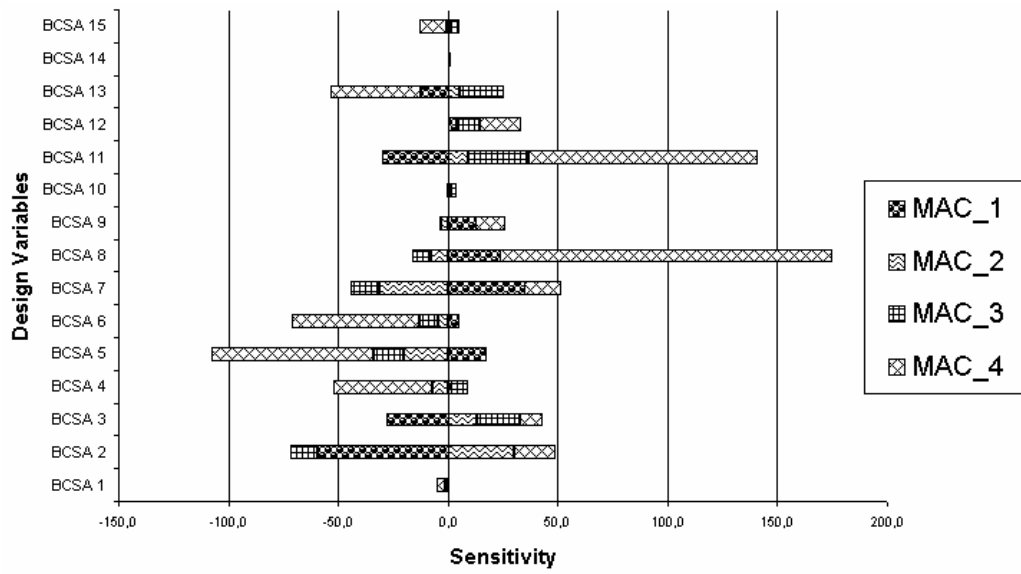


Figure 5.59 Sensitivities of paired mode shapes on beam cross section areas

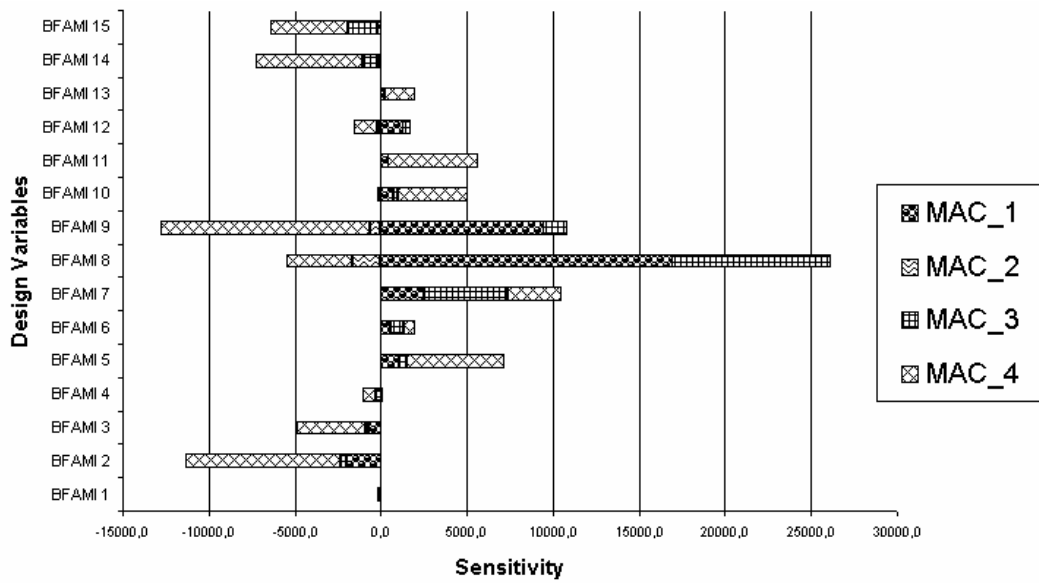


Figure 5.60 Sensitivities of paired mode shapes on beam first moment of area

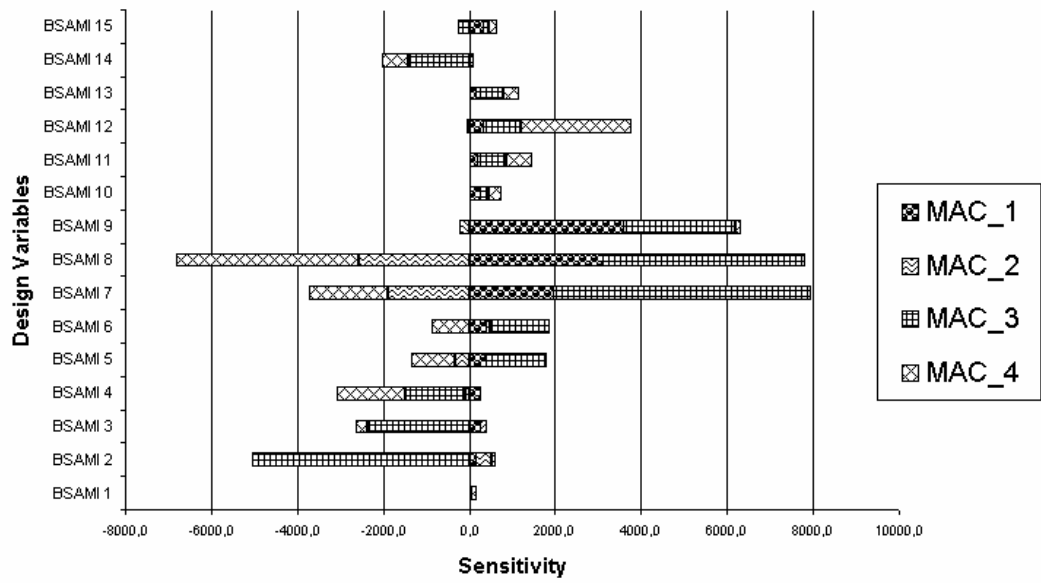


Figure 5.61 Sensitivities of paired mode shapes on beam second moment of area

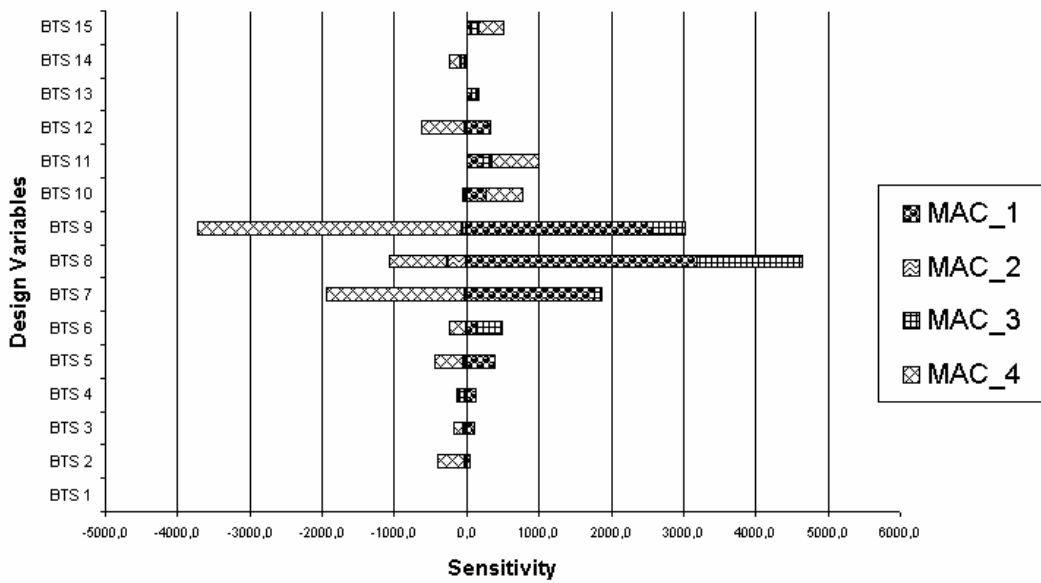


Figure 5.62 Sensitivities of paired mode shapes on beam torsional stiffness

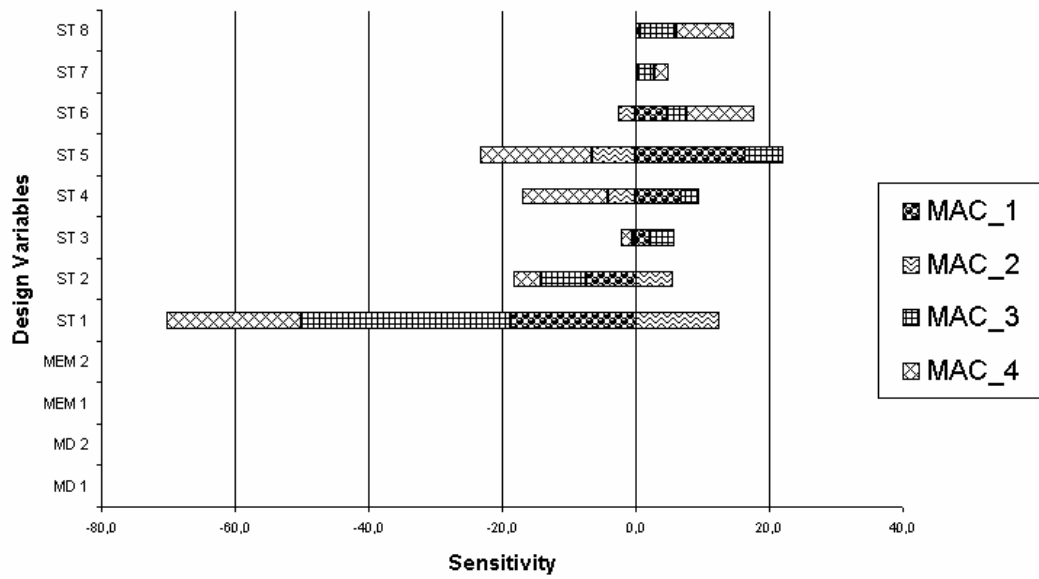


Figure 5.63 Sensitivities of paired mode shapes on material properties and shell thicknesses

Total sensitivities of similar properties on paired mode shapes are tabulated in Table 5.27 and shown in Figure 5.64.

Table 5.27 Summed sensitivities of paired mode shapes on design variables

	MAC_1	MAC_2	MAC_3	MAC_4
Beam Cross-Section Area (BCSA)	-29,3	-13,9	35,9	100,9
Beam First Moment of Area (BFAMI)	29392,9	-2415,1	14823,7	-21210,4
Beam Second Moment of Area (BSAMI)	11404,5	-4341,0	8086,5	-5932,6
Beam Torsional Stiffness (BTS)	9228,4	-401,0	2525,1	-6774,9
Material Density (MD)	0,0	0,0	0,0	0,0
Material Elastic Modulus (MEM)	0,0	0,0	0,0	0,0
Shell Thickness (ST)	3,9	5,1	-14,3	-34,4

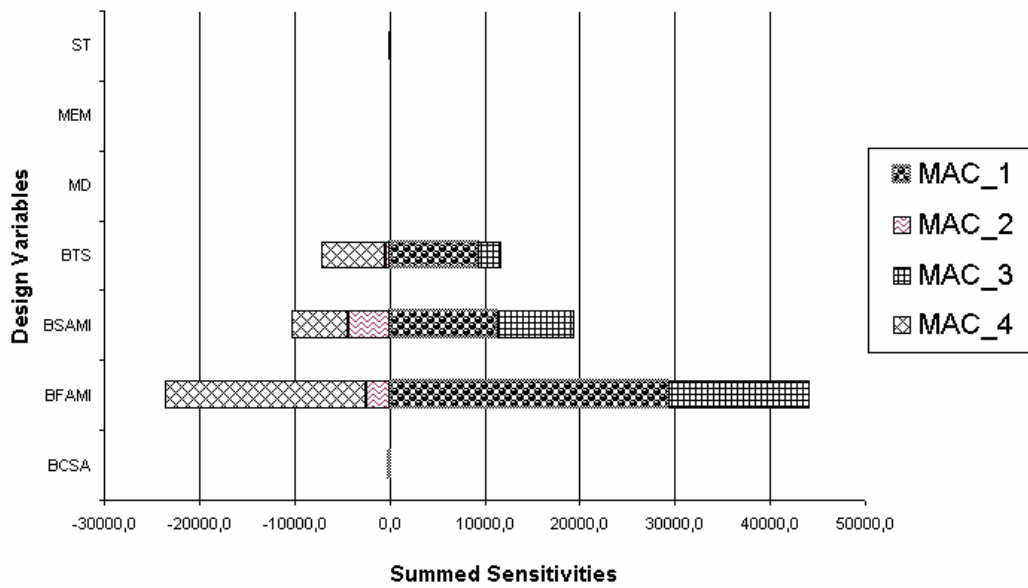


Figure 5.64 Summed sensitivities of paired mode shapes on design variables

After the sensitivity analysis, updating of these design variables are carried out. For the first optimization, gradient sensitivity algorithm is chosen. But, the algorithm could not converge for any of the objective functions. Changes in objective functions with number of iterations for this optimization try are shown in Figure 5.65 and Figure 5.66.

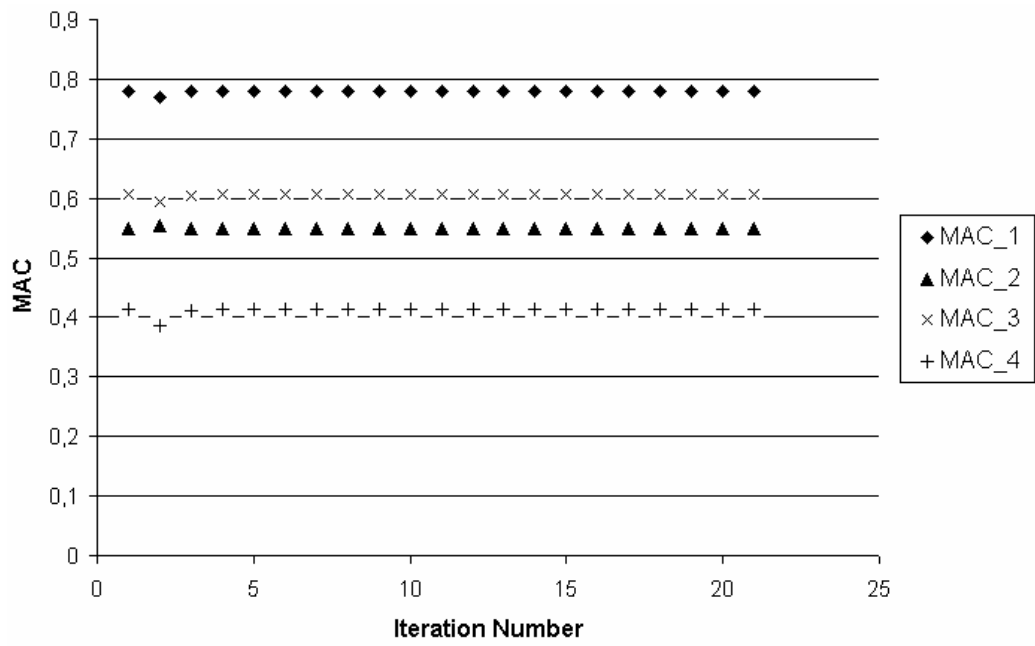


Figure 5.65 Change of MAC's for gradient sensitivity based optimization

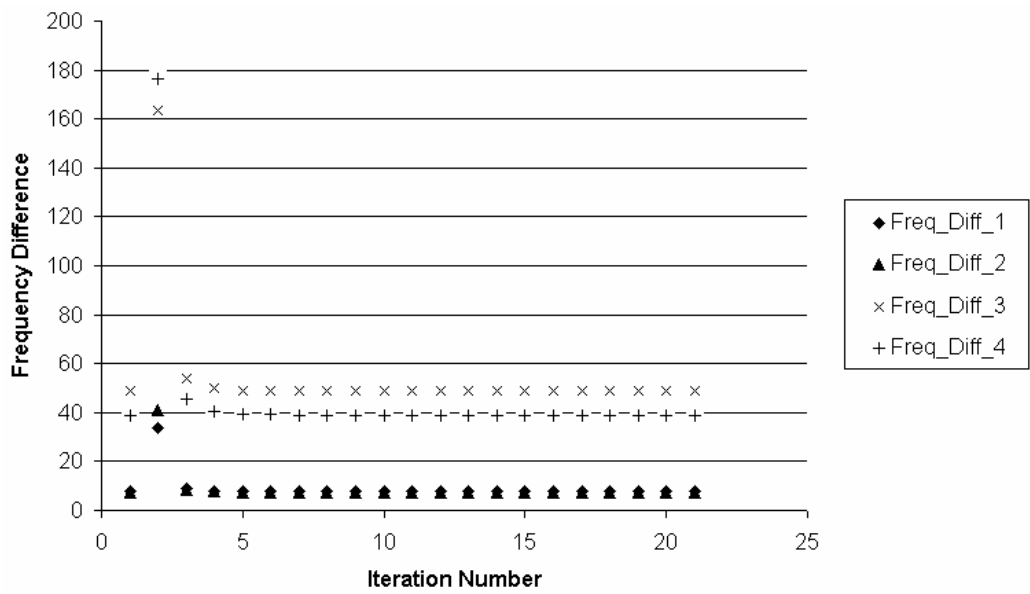


Figure 5.66 Change of frequency differences for gradient sensitivity based optimization

After convergence problem with the sensitivity based algorithm is faced, the finite difference algorithm was chosen for optimization. First, updating was tried for the objective functions of increasing all MAC values and decreasing all frequency differences between reference and verification results. Optimization results are found as tabulated in Table 5.28 and Table 5.29 and shown in Figure 5.67 and Figure 5.68.

Table 5.28 MAC updating results with objective functions of increasing all MAC and decreasing all frequency differences

Iteration	MAC_1	MAC_2	MAC_3	MAC_4
0	0,779	0,548	0,607	0,414
1	0,768	0,535	0,647	0,463
2	0,777	0,540	0,634	0,449
3	0,780	0,541	0,629	0,442
4	0,777	0,553	0,599	0,394
5	0,781	0,550	0,607	0,403
6	0,778	0,552	0,601	0,395
7	0,764	0,557	0,590	0,389
8	0,767	0,556	0,592	0,387
9	0,765	0,557	0,591	0,385
10	0,758	0,559	0,588	0,376

Table 5.29 Frequency difference updating results with objective functions of increasing all MAC and decreasing all frequency differences

Iteration	Freq_Diff_1	Freq_Diff_2	Freq_Diff_3	Freq_Diff_4
0	7,9	7,3	48,9	39,0
1	0,7	1,7	11,5	10,7
2	0,9	1,5	13,2	7,8
3	0,8	1,6	12,8	7,9
4	0,1	2,5	10,1	9,9
5	0,4	2,2	11,5	8,3

Table 5.29 continued

6	0,3	2,2	11,3	8,3
7	0,2	2,2	11,0	8,5
8	0,3	2,1	11,5	7,7
9	0,4	2,0	11,8	7,0
10	0,5	1,8	12,3	5,6

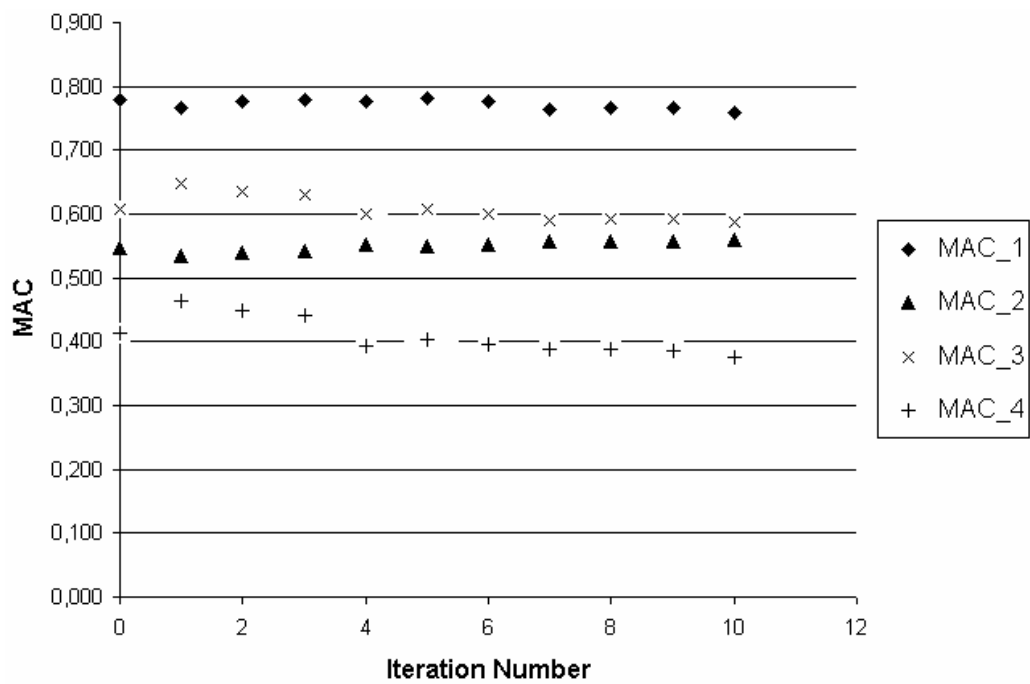


Figure 5.67 MAC updating results with objective functions of increasing all MAC and decreasing all frequency differences

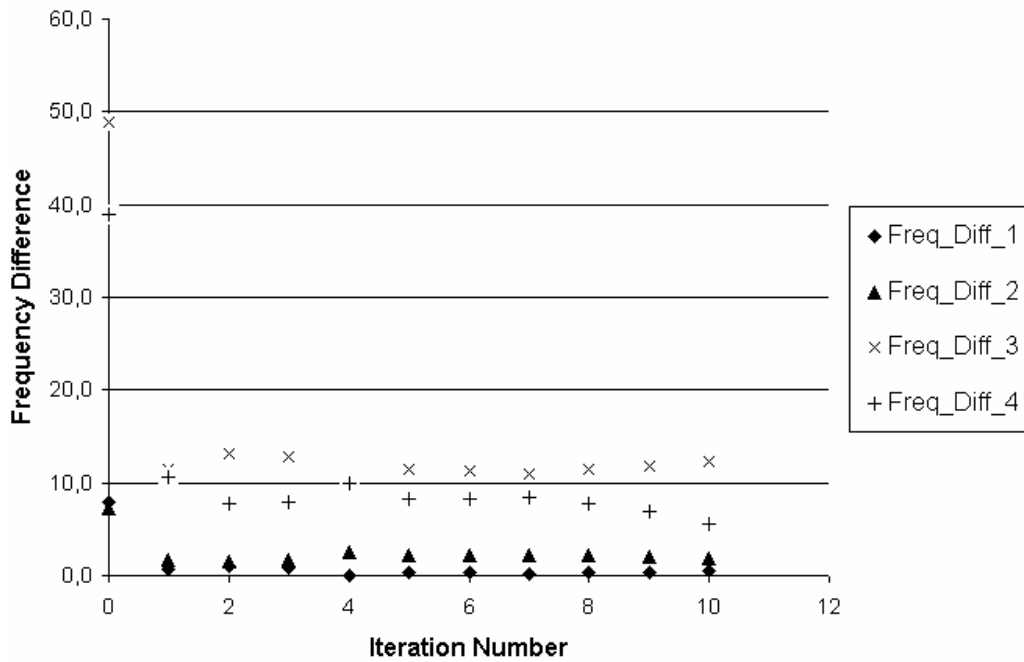


Figure 5.68 Frequency difference updating results with objective functions of increasing all MAC and decreasing all frequency differences

Change of design variables for this updating run is tabulated in Table 5.30 and shown in Figure 5.69 through Figure 5.75.

Table 5.30 Changes of design variables for the first optimization

Iteration	0	5	10
BCSA_1	5,64E-04	5,14E-04	5,56E-04
BCSA_2	5,64E-04	4,98E-04	4,65E-04
BCSA_3	5,64E-04	5,59E-04	5,21E-04
BCSA_4	5,64E-04	5,97E-04	5,74E-04
BCSA_5	5,64E-04	5,93E-04	6,14E-04
BCSA_6	5,64E-04	6,12E-04	6,39E-04
BCSA_7	5,64E-04	5,14E-04	5,56E-04
BCSA_8	5,64E-04	5,62E-04	4,43E-04
BCSA_9	5,64E-04	5,63E-04	5,38E-04
BCSA_10	5,64E-04	5,81E-04	5,85E-04
BCSA_11	5,64E-04	6,99E-04	8,19E-04

Table 5.30 continued

BCSA_12	5,64E-04	5,84E-04	4,65E-04
BCSA_13	5,64E-04	6,29E-04	6,89E-04
BCSA_14	5,64E-04	5,65E-04	5,63E-04
BCSA_15	5,64E-04	5,84E-04	5,67E-04
BFAMI_1	2,08E-07	2,07E-07	2,05E-07
BFAMI_2	2,08E-07	2,08E-07	2,07E-07
BFAMI_3	2,08E-07	2,08E-07	2,08E-07
BFAMI_4	2,08E-07	2,08E-07	2,08E-07
BFAMI_5	2,08E-07	2,08E-07	2,07E-07
BFAMI_6	2,08E-07	2,08E-07	2,08E-07
BFAMI_7	2,08E-07	2,07E-07	2,05E-07
BFAMI_8	2,08E-07	2,07E-07	2,06E-07
BFAMI_9	2,08E-07	2,08E-07	2,07E-07
BFAMI_10	2,08E-07	2,08E-07	2,08E-07
BFAMI_11	2,08E-07	2,08E-07	2,08E-07
BFAMI_12	2,08E-07	2,08E-07	2,08E-07
BFAMI_13	2,08E-07	2,08E-07	2,08E-07
BFAMI_14	2,08E-07	2,08E-07	2,08E-07
BFAMI_15	2,08E-07	2,08E-07	2,08E-07
BSAMI_1	2,08E-07	2,08E-07	2,09E-07
BSAMI_2	2,08E-07	2,09E-07	2,10E-07
BSAMI_3	2,08E-07	2,09E-07	2,09E-07
BSAMI_4	2,08E-07	2,08E-07	2,10E-07
BSAMI_5	2,08E-07	2,08E-07	2,09E-07
BSAMI_6	2,08E-07	2,08E-07	2,08E-07
BSAMI_7	2,08E-07	2,08E-07	2,09E-07
BSAMI_8	2,08E-07	2,07E-07	2,06E-07
BSAMI_9	2,08E-07	2,08E-07	2,10E-07
BSAMI_10	2,08E-07	2,08E-07	2,09E-07
BSAMI_11	2,08E-07	2,08E-07	2,10E-07
BSAMI_12	2,08E-07	2,08E-07	2,09E-07
BSAMI_13	2,08E-07	2,08E-07	2,09E-07
BSAMI_14	2,08E-07	2,09E-07	2,09E-07
BSAMI_15	2,08E-07	2,08E-07	2,10E-07

Table 5.30 continued

ST_1	1,5	1,230	1,225
ST_2	1,5	1,348	1,420
ST_3	1,5	1,412	1,553
ST_4	1,5	1,441	1,538
ST_5	1,5	1,348	1,222
ST_6	1,5	1,415	1,356
ST_7	1,5	1,533	1,532
ST_8	1,500	1,557	1,549
MEM_1	7,00E+10	1,30E+10	7,51E+09
MEM_2	7,00E+10	2,45E+10	3,87E+10
MD_1	2700,00	5346,00	5346,00
MD_2	2700,00	3562,46	3531,57
BTS_1	3,11E-07	3,11E-07	3,12E-07
BTS_2	3,11E-07	3,11E-07	3,12E-07
BTS_3	3,11E-07	3,11E-07	3,12E-07
BTS_4	3,11E-07	3,11E-07	3,12E-07
BTS_5	3,11E-07	3,11E-07	3,12E-07
BTS_6	3,11E-07	3,11E-07	3,11E-07
BTS_7	3,11E-07	3,11E-07	3,12E-07
BTS_8	3,11E-07	3,11E-07	3,10E-07
BTS_9	3,11E-07	3,11E-07	3,13E-07
BTS_10	3,11E-07	3,11E-07	3,12E-07
BTS_11	3,11E-07	3,11E-07	3,12E-07
BTS_12	3,11E-07	3,11E-07	3,12E-07
BTS_13	3,11E-07	3,11E-07	3,12E-07
BTS_14	3,11E-07	3,11E-07	3,12E-07
BTS_15	3,11E-07	3,11E-07	3,12E-07

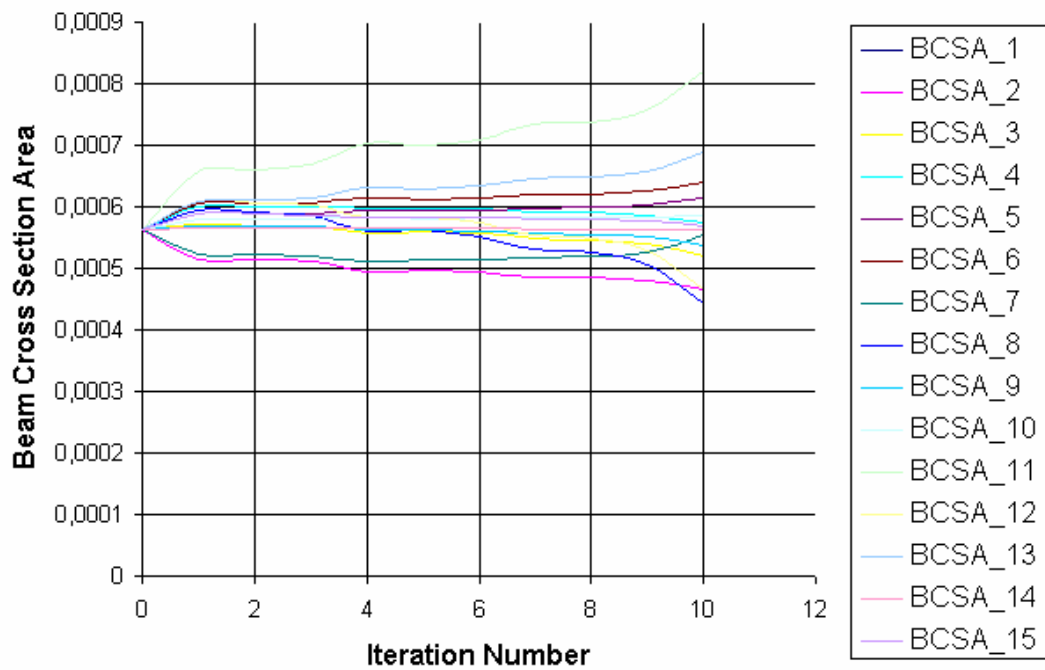


Figure 5.69 Change of beam cross-section areas for the first optimization

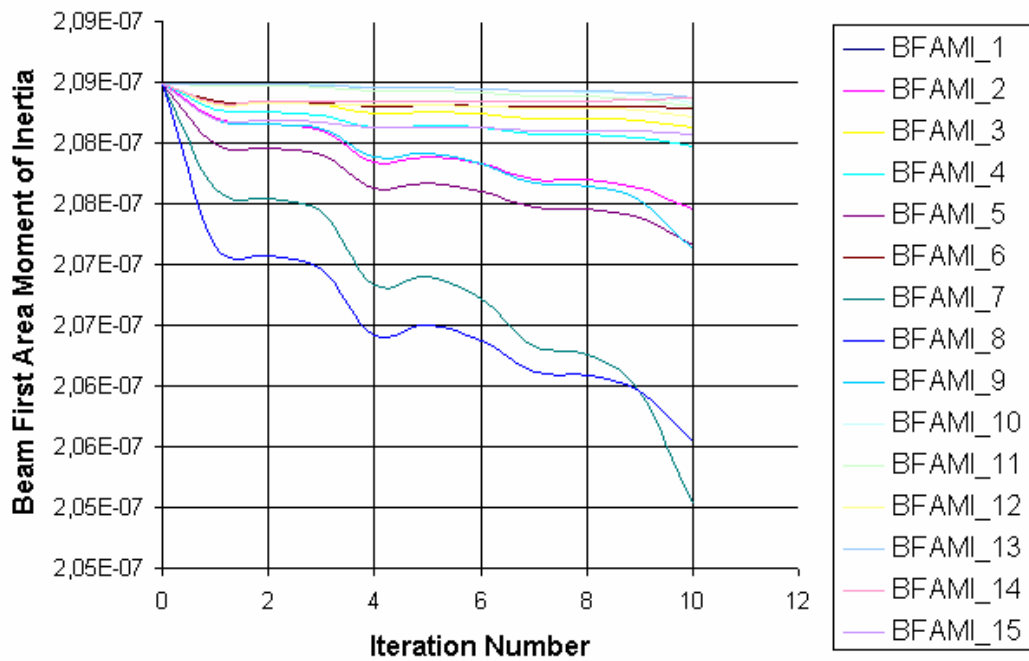


Figure 5.70 Change of beam first moment of areas for the first optimization

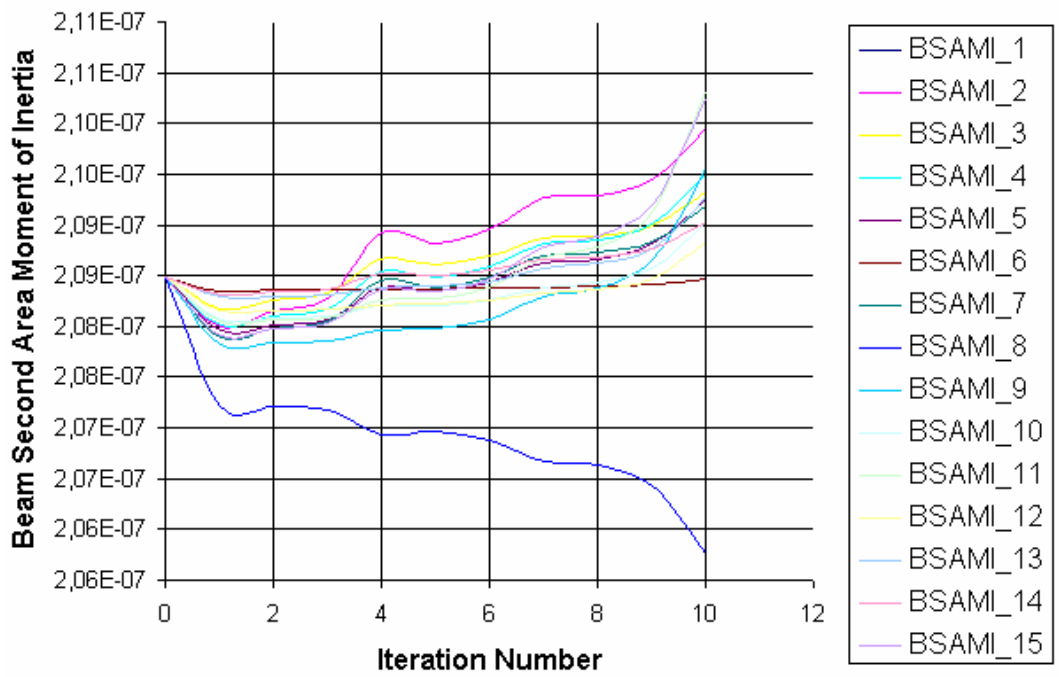


Figure 5.71 Change of beam second moment of areas for the first optimization

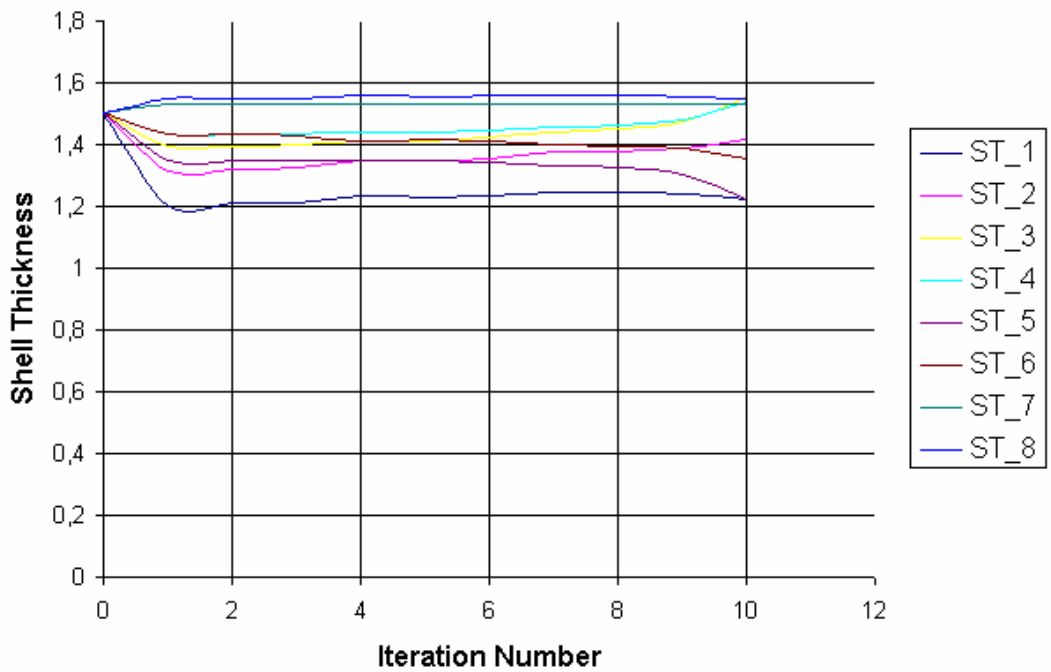


Figure 5.72 Change of shell thicknesses for the first optimization

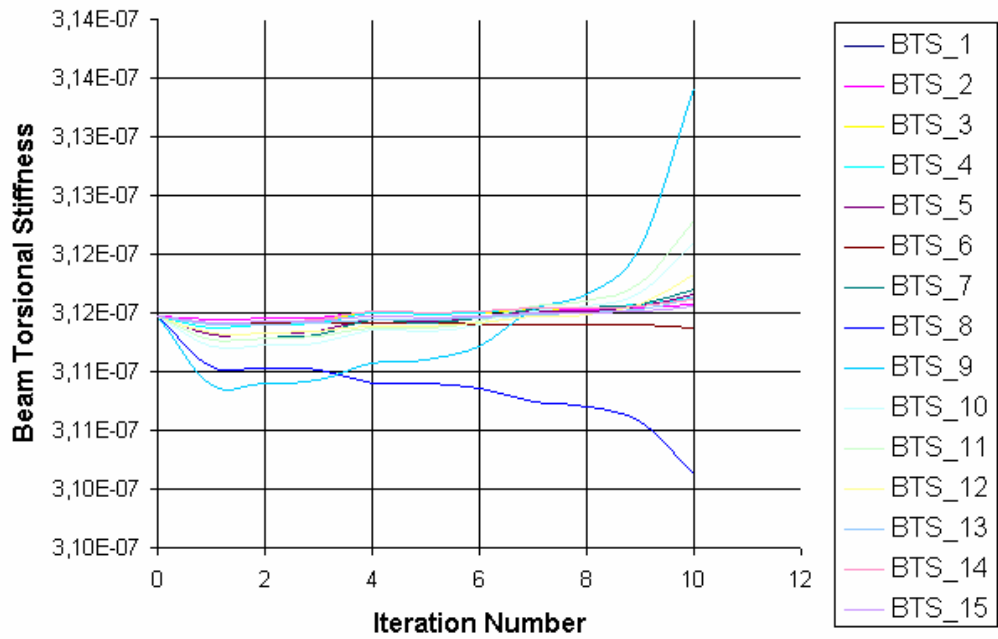


Figure 5.73 Change of beam torsional stiffnesses for the first optimization

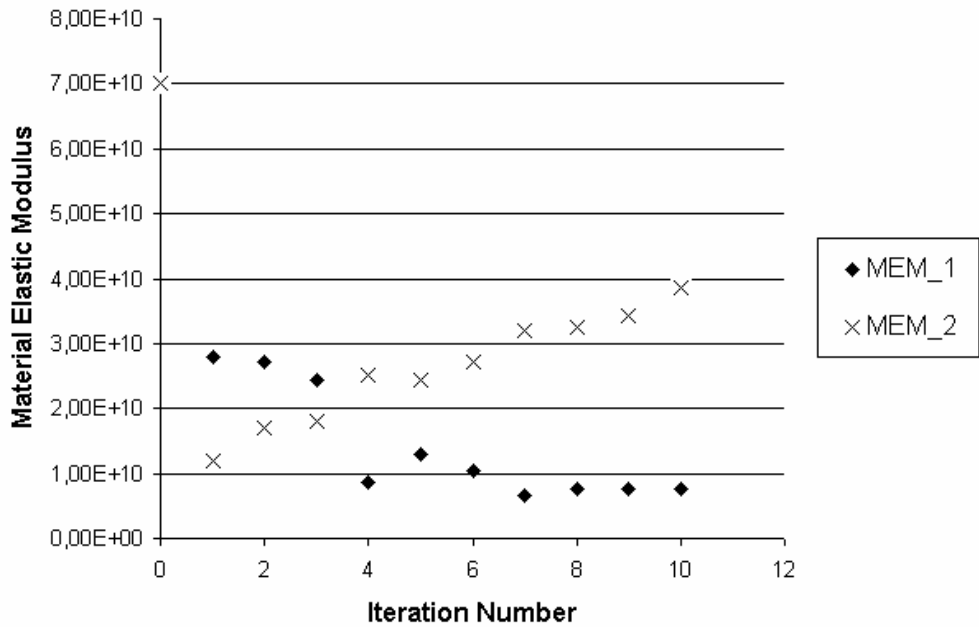


Figure 5.74 Change of material elastic modulus for the first optimization (N/m^2)

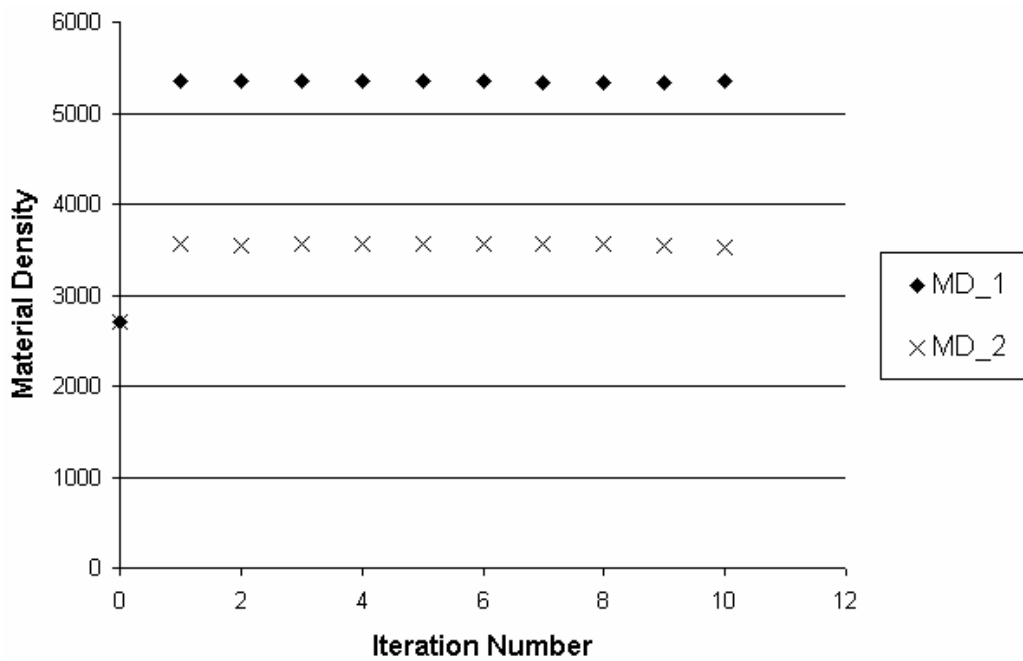


Figure 5.75 Change of material density for the first optimization (kg/m³)

As a second updating strategy, only increase of MAC values are chosen as objective functions. Results of this work are tabulated in Table 5.31 and shown in Figure 5.76.

Table 5.31 MAC updating results with objective functions of increasing all MAC

Iteration	MAC_1	MAC_2	MAC_3	MAC_4
0	0,779	0,548	0,607	0,414
1	0,779	0,547	0,617	0,448
2	0,755	0,543	0,699	0,581
3	0,734	0,542	0,744	0,602
4	0,718	0,557	0,769	0,617
5	0,715	0,579	0,769	0,634
6	0,715	0,582	0,766	0,639
7	0,713	0,588	0,757	0,649
8	0,715	0,591	0,750	0,658

Table 5.31 continued

9	0,715	0,591	0,761	0,659
10	0,710	0,589	0,778	0,658
11	0,719	0,586	0,775	0,659
12	0,713	0,591	0,775	0,661
13	0,707	0,595	0,775	0,662
14	0,699	0,601	0,774	0,667
15	0,698	0,601	0,774	0,668

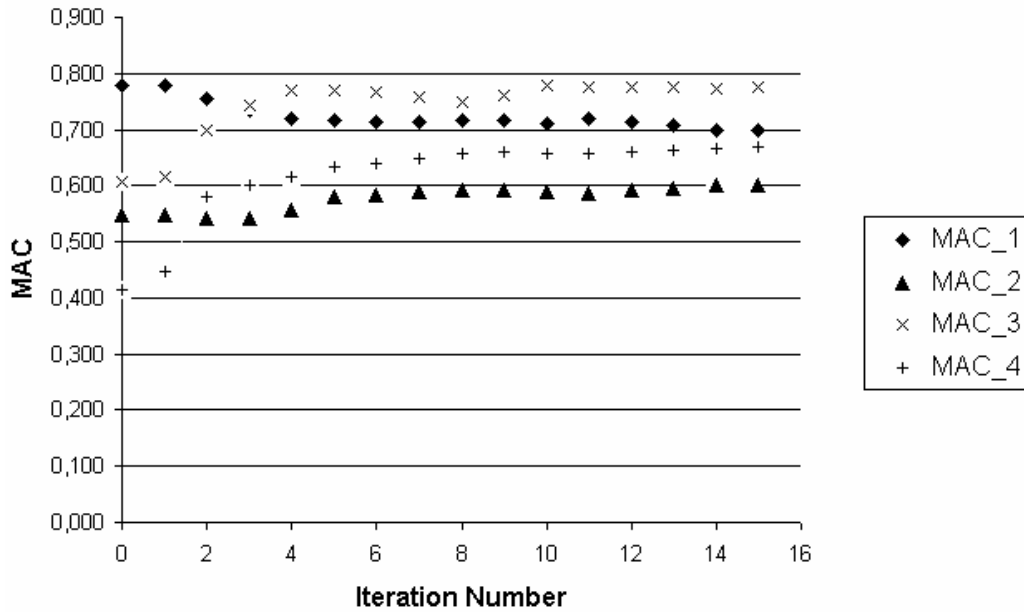


Figure 5.76 MAC updating results with objective functions of increasing all MAC

After only MAC updating, only decrease of frequency difference values are chosen as objective functions. Results of this work are tabulated in Table 5.32 and shown in Figure 5.77.

Table 5.32 Frequency difference updating results with objective functions of decreasing all frequency differences

Iteration	Freq_Diff_1	Freq_Diff_2	Freq_Diff_3	Freq_Diff_4
0	7,91	7,33	48,85	39,01
1	0,70	1,74	11,46	10,66
2	0,94	1,49	13,21	7,75
3	0,83	1,65	12,84	7,88
4	0,07	2,51	10,14	9,87
5	0,38	2,17	11,45	8,28
6	0,30	2,22	11,26	8,28
7	0,19	2,25	11,01	8,45
8	0,30	2,13	11,48	7,69
9	0,37	2,02	11,83	6,98
10	0,49	1,80	12,29	5,57
11	0,60	1,43	12,32	3,28
12	0,60	1,43	12,32	3,28

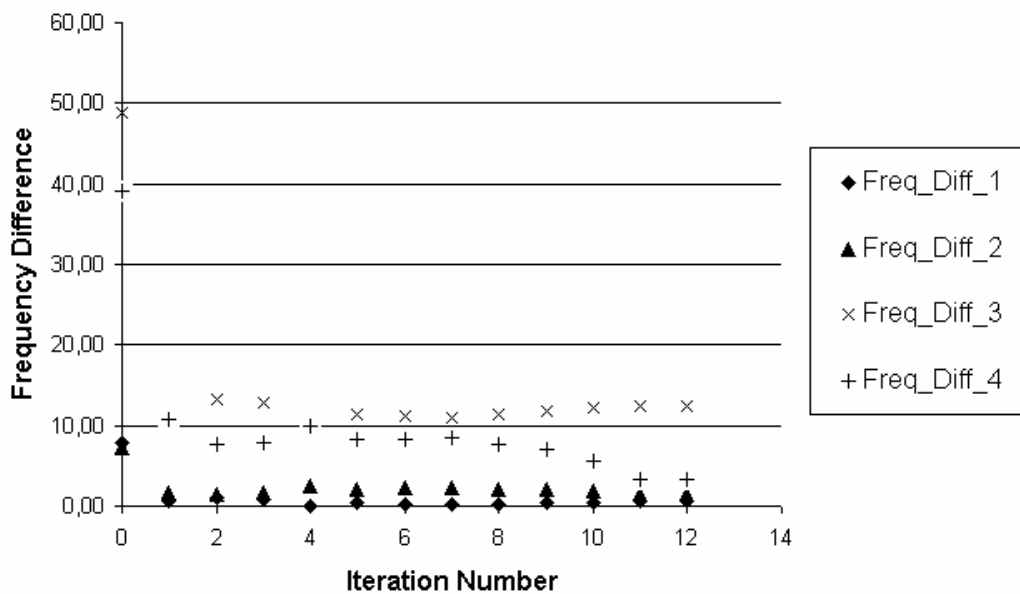


Figure 5.77 Frequency difference updating results with objective functions of decreasing all frequency differences

Then, decrease of frequency differences 1 and 2 are chosen as objective functions. Results of this work are tabulated in Table 5.33 and shown in Figure 5.78.

Table 5.33 Frequency difference 1 and 2 updating results for objective functions of decreasing Freq_Diff_1 and 2

Iteration	Freq_Diff_1	Freq_Diff_2
0	7,90	7,33
1	0,63	3,44
2	1,32	1,01
3	1,32	1,01
4	1,26	1,08
5	1,22	1,12
6	0,95	1,32
7	0,20	1,56
8	0,82	1,26
9	0,48	0,99
10	0,56	0,82
11	0,76	0,38
12	0,77	0,34
13	0,79	0,25
14	0,77	0,10
15	0,77	0,09
16	0,76	0,09
17	0,74	0,08
18	0,72	0,09
19	0,70	0,09
20	0,70	0,10
21	0,69	0,10
22	0,69	0,10
23	0,69	0,10
24	0,69	0,10
25	0,68	0,11

Table 5.33 continued

26	0,68	0,11
27	0,68	0,11
28	0,68	0,11

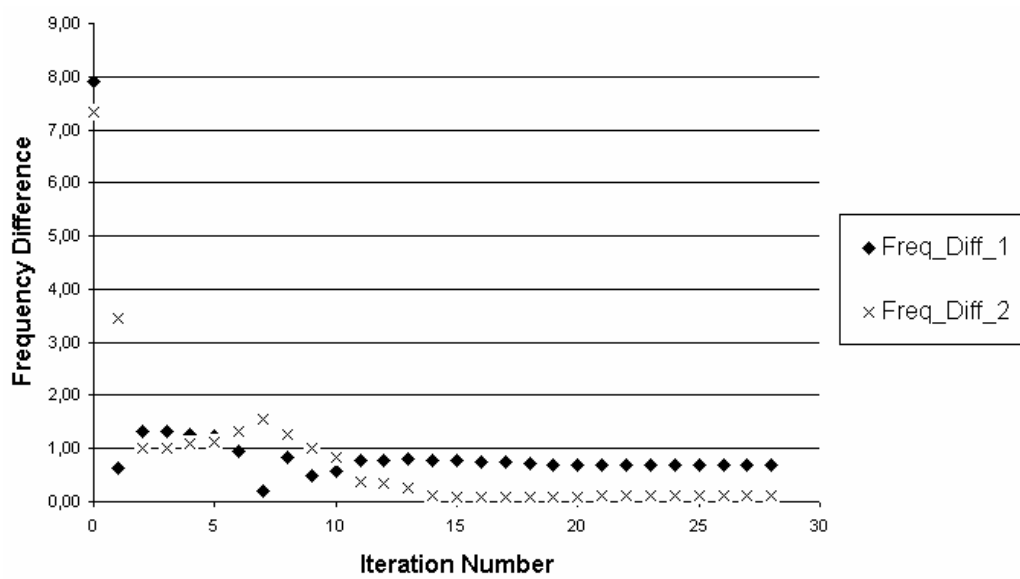


Figure 5.78 Frequency difference 1 and 2 updating results for objective functions of decreasing Freq_Diff_1 and 2

Then, increase of only MAC 4 is chosen as objective function. Results of this work are tabulated in Table 5.34 and shown in Figure 5.79.

Table 5.34 Updating results for objective function of increasing only MAC_4

Iteration	MAC_4
0	0,414
1	0,478
2	0,614
3	0,628
4	0,656
5	0,660
6	0,664
7	0,671
8	0,673
9	0,674
10	0,678
11	0,678
12	0,679
13	0,679
14	0,680
15	0,680

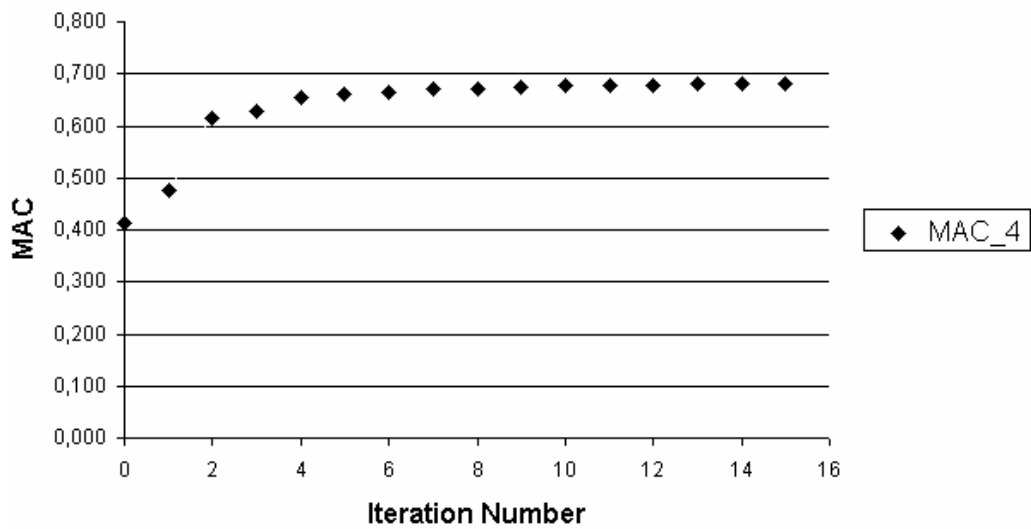


Figure 5.79 Updating results for objective function of increasing only MAC_4

As seen from the results, there are problems with the updating. They are mainly because of the mentioned errors in the modal tests. In order to solve this problem and improve the MAC results, these erroneous locations should be removed from both MAC calculation and updating. Finding these erroneous locations can be performed by the coMAC and the nrMAC, that is, the proposed algorithm described in Section 4.

When written matlab code is performed for the tail model, first 20 nodes that can be removed according to coMAC are found as given in Table 5.35.

Table 5.35 coMAC node removals and related MAC values

Node Removal Number	Node Number	MAC 1	MAC 2	MAC 3	MAC 4
1	70	0,785	0,578	0,715	0,417
2	78	0,788	0,580	0,715	0,417
3	62	0,793	0,581	0,715	0,413
4	68	0,796	0,582	0,715	0,407
5	72	0,801	0,583	0,715	0,408
6	80	0,805	0,584	0,716	0,408
7	66	0,809	0,586	0,716	0,403
8	60	0,814	0,587	0,716	0,396
9	74	0,817	0,588	0,716	0,398
10	64	0,822	0,589	0,716	0,396
11	58	0,824	0,591	0,716	0,381
12	36	0,826	0,592	0,717	0,363
13	48	0,828	0,594	0,717	0,347
14	56	0,831	0,596	0,717	0,334
15	26	0,833	0,598	0,717	0,314
16	38	0,834	0,599	0,717	0,289
17	40	0,836	0,600	0,717	0,269
18	46	0,837	0,601	0,718	0,241
19	28	0,841	0,603	0,718	0,218
20	50	0,843	0,604	0,718	0,199

Changes of MAC values according to node removals by coMAC calculation are shown in Figure 5.80.

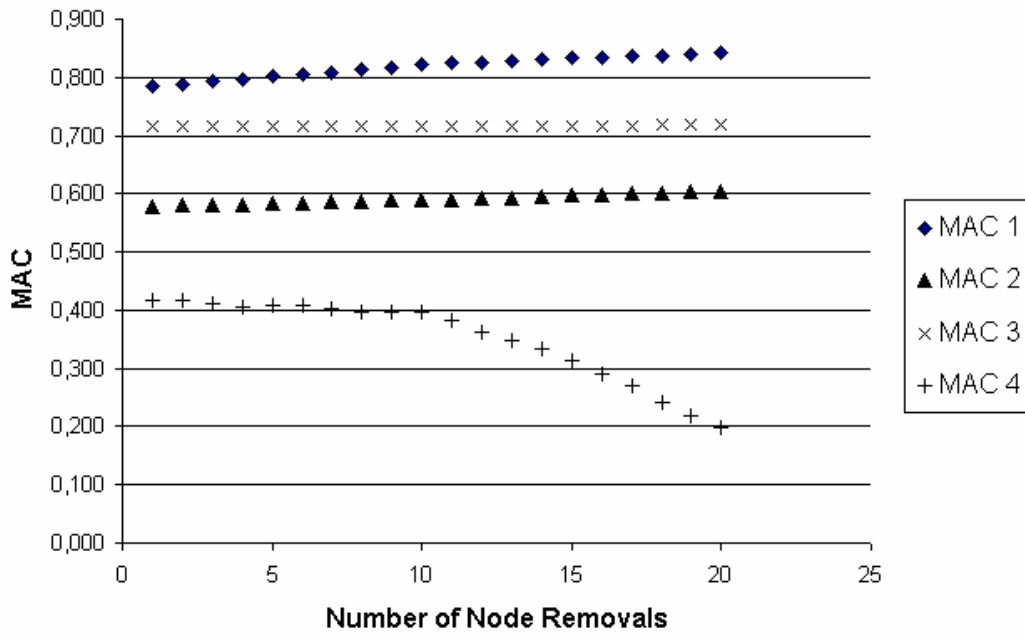


Figure 5.80 Changes of MAC values according to node removals by coMAC

Additionally, first 20 nodes that can be removed according to nrMAC are found as given in Table 5.36. Weights of all MAC values are taken as equal for this calculation.

Table 5.36 nrMAC node removals and related MAC values with weights
0,25;0,25;0,25;0,25

Node Removal Number	Node Number	MAC 1	MAC 2	MAC 3	MAC 4
1	99	0,781	0,584	0,707	0,418
2	3	0,781	0,592	0,701	0,418
3	85	0,781	0,592	0,718	0,418

Table 5.36 continued

4	2	0,769	0,594	0,718	0,451
5	13	0,769	0,602	0,716	0,451
6	6	0,781	0,603	0,720	0,547
7	7	0,782	0,537	0,713	0,590
8	83	0,782	0,537	0,728	0,591
9	75	0,782	0,539	0,722	0,593
10	87	0,783	0,540	0,735	0,593
11	8	0,817	0,541	0,737	0,626
12	76	0,808	0,541	0,738	0,648
13	73	0,808	0,541	0,750	0,648
14	95	0,810	0,547	0,749	0,650
15	70	0,816	0,548	0,750	0,651
16	23	0,816	0,556	0,747	0,651
17	81	0,816	0,556	0,760	0,651
18	89	0,816	0,557	0,772	0,652
19	17	0,816	0,564	0,767	0,653
20	91	0,817	0,566	0,762	0,655

Changes of MAC values according to node removals by nrMAC calculation are shown in Figure 5.81.

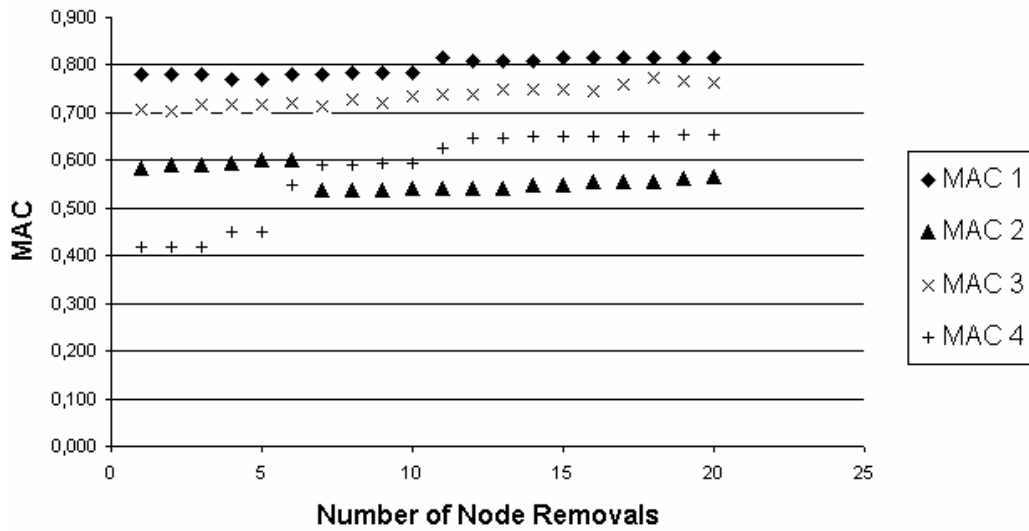


Figure 5.81 Changes of MAC values according to node removals by nrMAC with weights 0,25;0,25;0,25;0,25

If weights of MACs are changed to 0,1;0,4;0,4;0,1 which shows second and third mode are more important, then node removals by nrMAC are calculated as tabulated in Table 5.37.

Table 5.37 nrMAC node removals and related MAC values with weights 0,1;0,4;0,4;0,1

Node Removal Number	Node Number	MAC 1	MAC 2	MAC 3	MAC 4
1	99	0,781	0,584	0,707	0,418
2	3	0,781	0,592	0,701	0,418
3	85	0,781	0,592	0,718	0,418
4	13	0,781	0,600	0,716	0,418
5	83	0,782	0,600	0,731	0,419
6	75	0,782	0,607	0,725	0,420
7	87	0,782	0,607	0,738	0,421
8	73	0,782	0,607	0,750	0,421
9	95	0,784	0,615	0,749	0,422
10	23	0,784	0,623	0,746	0,422

Table 5.37 continued

11	81	0,784	0,623	0,759	0,422
12	89	0,784	0,623	0,771	0,422
13	2	0,772	0,626	0,771	0,455
14	17	0,772	0,633	0,765	0,456
15	91	0,773	0,640	0,761	0,457
16	71	0,773	0,640	0,772	0,457
17	93	0,775	0,648	0,770	0,458
18	77	0,776	0,648	0,782	0,458
19	6	0,788	0,649	0,787	0,556
20	7	0,789	0,567	0,781	0,600

Changes of MAC values according to node removals by nrMAC with MAC weights 0,1;0,4;0,4;0,1 are shown in Figure 5.82.

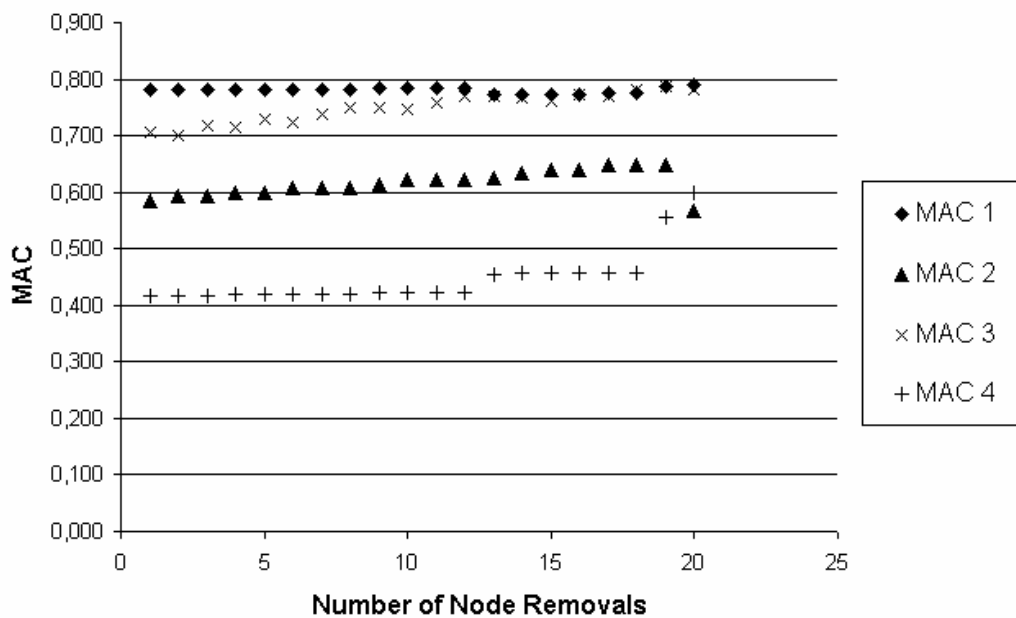


Figure 5.82 Changes of MAC values according to node removals by nrMAC with weights 0,1;0,4;0,4;0,1

If mode shape results computed by finite element analysis and experimental modal analysis are studied carefully, it is seen that some of the accelerometer locations move different from expected global modes. As an example, unexpected motion of 33rd, 102nd and 103rd locations are shown in Figure 5.83 and Figure 5.84.

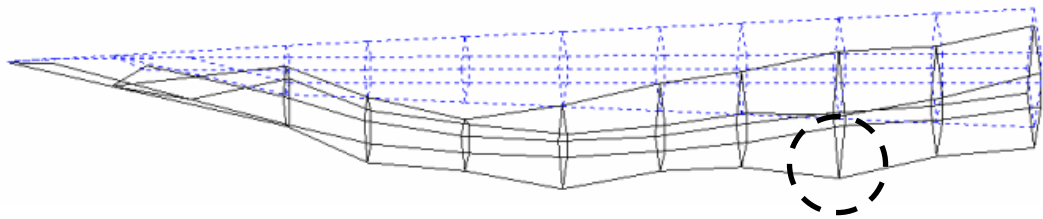


Figure 5.83 Different motion of 33rd accelerometer location from global mode

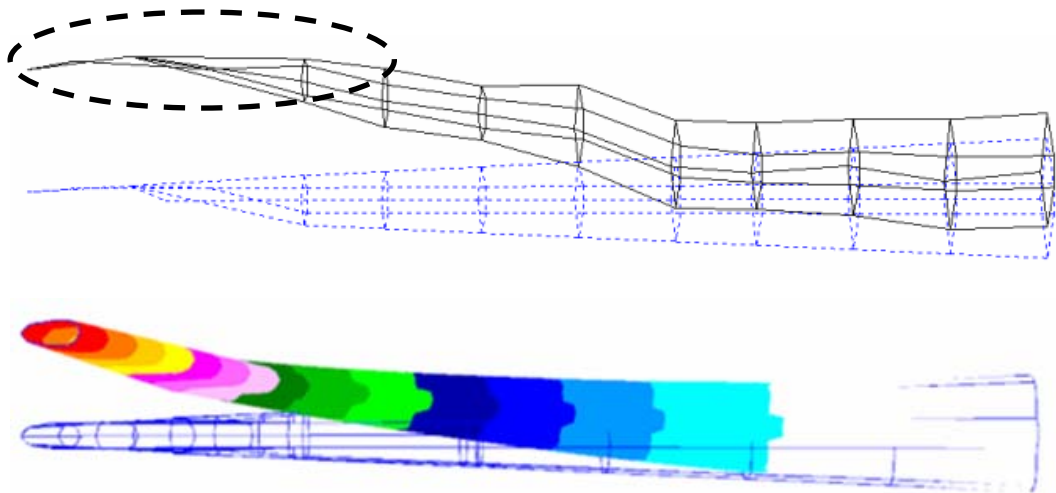


Figure 5.84 Different motions of 102nd and 103rd accelerometer locations from global mode

After finding node numbers to be removed for coMAC and nrMAC, these nodes are removed from the updating studies. Firstly, 10 nodes are removed according to coMAC results. For this configuration, the increase of all MAC values is chosen as objective functions. Updating results are tabulated in Table 5.38 and shown in Figure 5.85.

Table 5.38 Updating of MAC values under removal of 10 nodes according to coMAC

Iteration	MAC_1	MAC_2	MAC_3	MAC_4
0	0,822	0,565	0,654	0,398
1	0,828	0,563	0,655	0,409
2	0,855	0,547	0,658	0,464
3	0,868	0,537	0,658	0,488
4	0,875	0,530	0,659	0,501
5	0,881	0,524	0,659	0,511
6	0,886	0,519	0,661	0,518
7	0,890	0,515	0,662	0,526
8	0,894	0,510	0,665	0,534
9	0,912	0,484	0,673	0,564
10	0,897	0,505	0,680	0,557
11	0,895	0,508	0,683	0,558
12	0,881	0,521	0,693	0,566
13	0,851	0,544	0,709	0,572
14	0,786	0,591	0,733	0,578
15	0,760	0,603	0,739	0,601

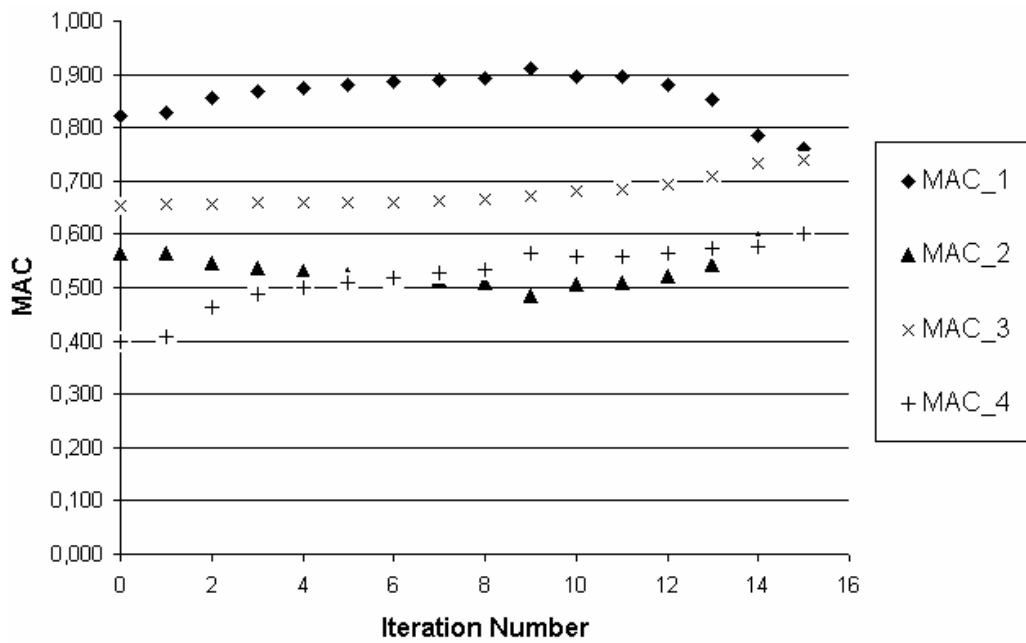


Figure 5.85 Updating of MAC values under removal of 10 nodes according to coMAC

The same updating strategy was carried out again for 20 node removals according to coMAC. Results are tabulated in Table 5.39 and shown in Figure 5.86.

Table 5.39 Updating of MAC values under removal of 20 nodes according to coMAC

Iteration	MAC_1	MAC_2	MAC_3	MAC_4
0	0,846	0,603	0,590	0,379
1	0,850	0,602	0,588	0,387
2	0,866	0,595	0,581	0,423
3	0,910	0,554	0,538	0,500
4	0,889	0,577	0,569	0,469
5	0,893	0,573	0,571	0,478
6	0,911	0,551	0,583	0,513
7	0,898	0,566	0,600	0,497
8	0,891	0,572	0,610	0,493
9	0,854	0,599	0,638	0,484

Table 5.39 continued

10	0,844	0,603	0,645	0,483
11	0,838	0,606	0,648	0,483
12	0,818	0,618	0,654	0,486
13	0,830	0,612	0,651	0,504
14	0,845	0,605	0,641	0,530
15	0,839	0,609	0,640	0,543

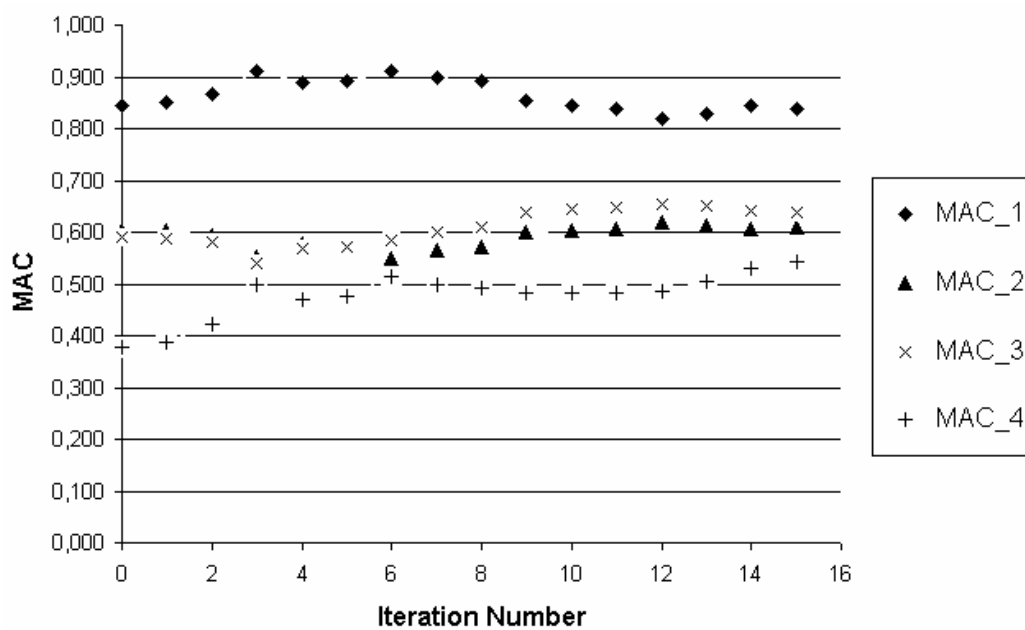


Figure 5.86 Updating of MAC values under removal of 20 nodes according to coMAC

Then, 10 nodes are removed according to nrMAC results with weights 0,25;0,25;0,25;0,25. For this configuration, the increase of all MAC values is chosen as objective functions. Updating results are tabulated in Table 5.40 and shown in Figure 5.87.

Table 5.40 Updating of MAC values under removal of 10 nodes according to nrMAC with weights 0,25;0,25;0,25;0,25

Iteration	MAC_1	MAC_2	MAC_3	MAC_4
0	0,800	0,477	0,727	0,681
1	0,803	0,475	0,737	0,696
2	0,821	0,461	0,837	0,752
3	0,813	0,425	0,845	0,679
3	0,821	0,460	0,844	0,752
4	0,807	0,468	0,867	0,772
5	0,713	0,519	0,874	0,821
6	0,779	0,485	0,869	0,801
6	0,752	0,501	0,875	0,814
6	0,737	0,508	0,875	0,818
7	0,736	0,509	0,880	0,817
8	0,735	0,510	0,884	0,816
9	0,733	0,512	0,889	0,815
10	0,729	0,516	0,892	0,817
11	0,713	0,529	0,895	0,822
12	0,727	0,522	0,901	0,817
13	0,743	0,516	0,890	0,819
14	0,734	0,523	0,888	0,822
15	0,735	0,523	0,895	0,820

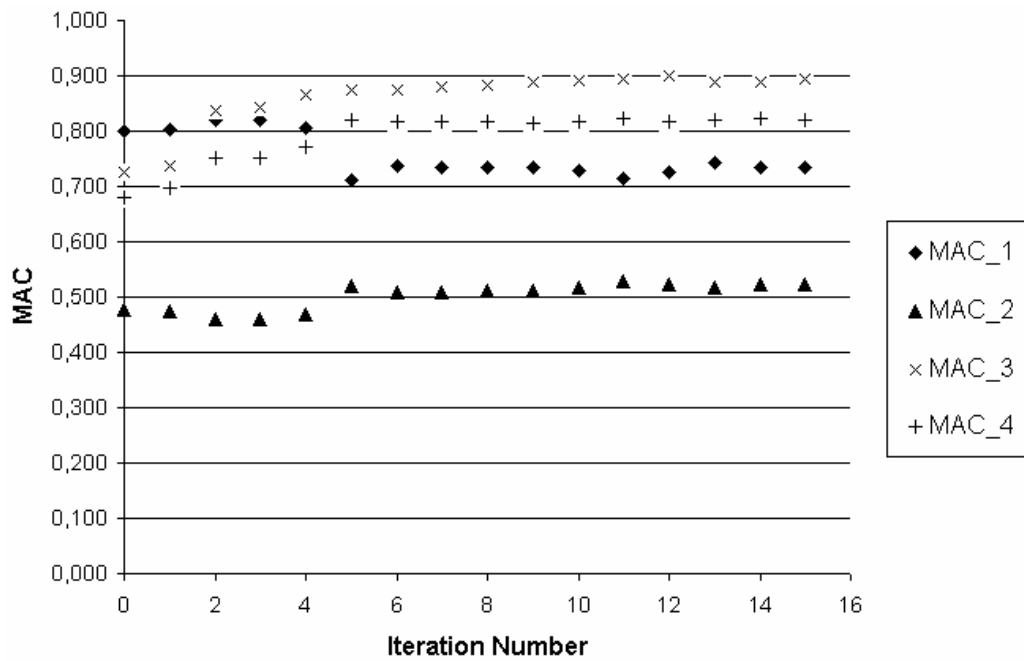


Figure 5.87 Updating of MAC values under removal of 10 nodes according to nrMAC with weights 0,25;0,25;0,25;0,25

Then, 10 nodes are removed according to nrMAC results with weights 0,1;0,4;0,4;0,1. For this configuration, the increase of all MAC values is chosen as objective functions. Updating results are tabulated in Table 5.41 and shown in Figure 5.88.

Table 5.41 Updating of MAC values under removal of 10 nodes according to nrMAC with weights 0,1;0,4;0,4;0,1

Iteration	MAC_1	MAC_2	MAC_3	MAC_4
0	0,766	0,597	0,612	0,429
1	0,767	0,594	0,628	0,468
2	0,729	0,569	0,783	0,594
3	0,745	0,580	0,758	0,598
4	0,750	0,585	0,774	0,611
5	0,726	0,609	0,804	0,632
6	0,725	0,620	0,784	0,642
7	0,724	0,620	0,791	0,643

Table 5.41 continued

8	0,716	0,618	0,808	0,649
9	0,735	0,613	0,800	0,653
10	0,716	0,627	0,799	0,659
11	0,730	0,619	0,800	0,658
12	0,726	0,621	0,802	0,660
13	0,708	0,632	0,804	0,667
14	0,713	0,630	0,805	0,668
15	0,715	0,629	0,804	0,670

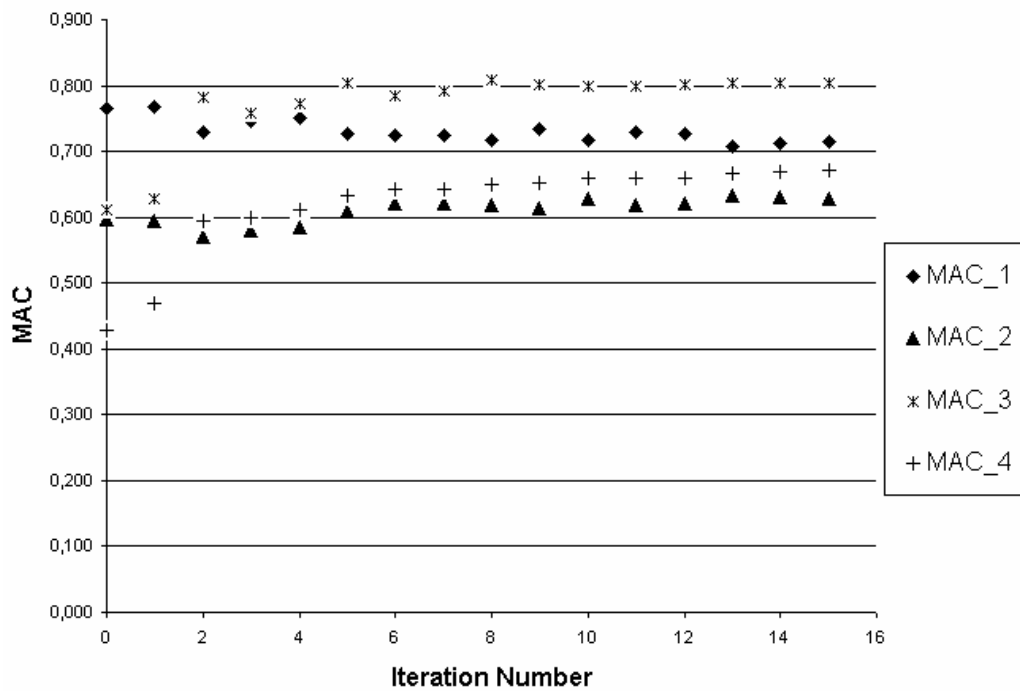


Figure 5.88 Updating of MAC values under removal of 10 nodes according to nrMAC with weights 0,1;0,4;0,4;0,1

Then, 20 nodes are removed according to nrMAC results with weights 0,25;0,25;0,25;0,25. For this configuration, the increase of all MAC values is chosen as objective functions. Updating results are tabulated in Table 5.42 and shown in Figure 5.89.

Table 5.42 Updating of MAC values under removal of 20 nodes according to nrMAC with weights 0,25;0,25;0,25;0,25

Iteration	MAC_1	MAC_2	MAC_3	MAC_4
0	0,793	0,504	0,763	0,713
1	0,797	0,501	0,775	0,728
2	0,819	0,484	0,873	0,779
3	0,814	0,486	0,890	0,785
4	0,689	0,553	0,889	0,843
5	0,752	0,523	0,890	0,834
6	0,751	0,524	0,901	0,833
7	0,739	0,532	0,917	0,831
8	0,734	0,535	0,911	0,836
9	0,733	0,537	0,909	0,837
10	0,736	0,538	0,903	0,838
11	0,735	0,541	0,903	0,839
12	0,728	0,552	0,910	0,840
13	0,733	0,551	0,908	0,842
14	0,764	0,536	0,916	0,833
15	0,763	0,539	0,910	0,839

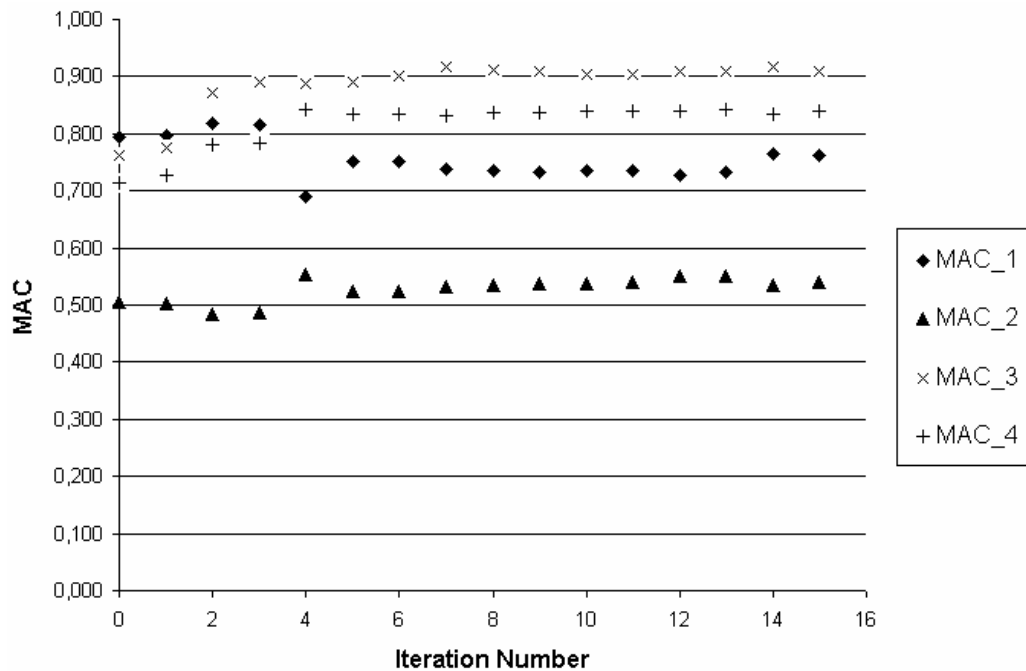


Figure 5.89 Updating of MAC values under removal of 20 nodes according to nrMAC with weights 0,25;0,25;0,25;0,25

Material elastic modulus variable change without and with node removal optimization is shown in Figure 5.90.

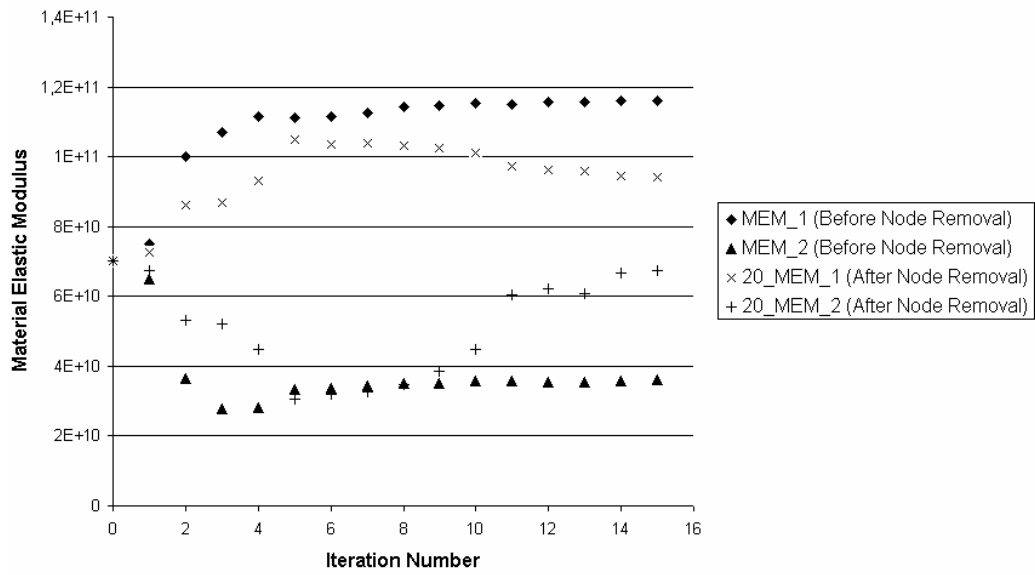


Figure 5.90 Change of material elastic modulus without and with node removal

CHAPTER 6

DISCUSSION AND CONCLUSIONS

Today, numerical methods are used in many engineering problems for optimum designs. Finite element method is one of the leading numerical methods to simulate real world cases. The more realistic the finite element method simulations are, the more opportunities the engineers have for optimum design solutions. For this reason, numerical models are verified and updated according to experimental results in order to improve the power of numerical methods and get the realistic simulation results.

In this thesis, application of model updating on a helicopter structure is performed. Finite element model of a helicopter structure is tried to be updated according to modal test results. Updating is performed separately for global modes of the tail and the complete helicopter fuselage models.

For the verification and updating of the numerical model, modal tests are carried out on the helicopter. Excitation is performed from the tail end of the craft resting on soft foam for free-free boundary condition and the acceleration data is acquired in two directions for 102 locations. These test results are used for experimental modal analysis. Then, an experimental model is developed according to mode shapes and corresponding natural frequencies obtained from modal analysis.

In order to compare and correlate the numerical and experimental models, Modal Assurance Criterion (MAC) is used. This correlation method is also used as an objective function for the optimization problem. In addition to optimization of MAC values, frequency differences of the two models are tried to be reduced as a second objective function. Optimization process was carried out by optimizing the various design variables like shell thickness, material properties, etc.

In addition to model updating studies, a new diagnostic tool (nrMAC) was proposed for optimum node removal in order to get better MAC values. After providing information about the theory behind the proposed algorithm, results are investigated on the tail model updating case study after the algorithm is implemented in Matlab. Moreover, applicability of this method is evaluated and compared with the coordinate modal assurance criterion (coMAC).

Model updating was then applied on the complete helicopter fuselage. Since cabin and cockpit region could not be excited appropriately and these areas have been associated with excessive local nonlinearities, updating procedure gave poor results. Then cabin, cockpit and nose of the helicopter is subtracted from model updating studies and the tail model updating is performed for different cases.

There is always certain level of mis-correlation between numerical and experimental model results. This mis-correlation is mostly because of the errors introduced in the numerical model. However, there are errors in experimental results as well due to nonlinearities and poor signal-to-noise ratios. The level of mis-correlation is tried to be reduced by the updating procedure. Nevertheless, sometimes the errors in these models are hard to correct. Trying to eliminate these errors is accompanied with some other problems. According to the tail model updating case study results, these problems are anticipated as:

- Updating of design variables to unrealistic values. This occurs mainly because, in order to eliminate the serious errors and improve the correlation, updating algorithm changes the design variable to unreasonable values. This problem is clearly seen in the tail updating case study.
- Correlation cannot be updated to reasonable levels for most of the optimization cases. Even updating to reasonable levels is realized computationally, the numerical model loses its physical meaning.
- Wrong sensitivity results are obtained. For this reason, model updating fails, because optimization of objective functions cannot converge to accepted values.
- The locations that have serious errors do not only affect the elements close to them, but also they can disturb the nearby regions.

Summary of MAC change for tail model updating is given in Table 6.1. As seen from the results, nrMAC has generally better correlation.

Table 6.1 MAC change summary for tail model updating

Objective Function	Node Removal	MAC_1	MAC_2	MAC_3	MAC_4
Initial Values		0,779	0,548	0,607	0,414
All MAC and Freq. Diff.	No	0,758	0,559	0,588	0,376
All MAC	No	0,698	0,601	0,774	0,668
MAC 4					0,68
All MAC	coMAC – 10 nodes	0,76	0,6	0,739	0,601
All MAC	coMAC – 20 nodes	0,839	0,609	0,64	0,543
All MAC	nrMAC – 10 nodes 0,25;0,25;0,25;0,25	0,735	0,523	0,895	0,82
All MAC	nrMAC – 10 nodes 0,1;0,4;0,4;0,1	0,715	0,629	0,804	0,670
All MAC	nrMAC – 20 nodes 0,25;0,25;0,25;0,25	0,763	0,539	0,910	0,839

Also Table 6.2 shows the total MAC change for different objective functions. Performance of nrMAC is seen clearly for a target value of 4.

Table 6.2 Total MAC change summary for tail model updating

Objective Functions	Total MAC	Target in Percentage
Initial Total	2,35	58,70%
Updating All W/out Node Removal	2,28	57,03%
Updating All MAC W/out Node Removal	2,74	68,53%
Updating All MAC W\ 10 coMAC Node Removal	2,70	67,50%
Updating All MAC W\ 20 coMAC Node Removal	2,63	65,78%
Updating All MAC W\ 10 nrMAC(0,25;0,25; 0,25;0,25) Node Removal	2,97	74,33%
Updating All MAC W\ 10 nrMAC(0,1;0,4; 0,1;0,4) Node Removal	2,82	70,46%
Updating All MAC W\ 20 nrMAC(0,25;0,25; 0,25;0,25) Node Removal	3,05	76,28%

In order to eliminate the problems contributed by erroneous locations, uncorrelated coordinates are removed from the correlation and updating calculations. This operation was carried out using coMAC and nrMAC algorithms for the tail model updating case study. According to the results:

- The performance of nrMAC is compared with the coMAC. Same number of nodes is removed from the tail model for both methods. In order to make a fair comparison, nrMAC node removal was performed for equal weights of modes. According to updated results in total, new method gives better results than coMAC.

- Removal of erroneous coordinates from correlation calculation and updating increases the accuracy of the model updating and consequently saves computing time.
- Having discovered that some coordinates possess erroneous data should not force the engineer to repeat the tests. These coordinates should be removed from mode correlation and updating in order not to cause extra test time and cost.

Sometimes, importance of one or two natural frequencies is more than remaining frequencies. For these types of applications, weighting of frequencies becomes necessary. For example, fourth harmonic of the main rotor i.e. the main excitation frequency of a helicopter can be more important than other modes. For such cases, opportunities of having the ability to weight modes gain importance. Because of its theory, weighting is not possible for coMAC algorithm. Coordinate based correlation is calculated by using coMAC. However, nrMAC algorithm has the advantage of the possibility of weighting modes. This method calculates the optimum node removals according to the input weights of paired modes. In order to see the applicability of weighting, different updating runs were performed for different weights of the modes according to nrMAC algorithm and successful results are obtained.

In addition to updating and correlation problems, there have been problems with the numerical technique, that is, finite element analysis. The problems and solutions to them can be summarized as:

- Unsymmetric modes are generated. In order to get rid of this problem, symmetric mesh is created for tail and complete helicopter finite element model.
- Local modes are found because of shell element properties. In order to solve this problem, realistic beam element distribution is created on the model.

- Local modes affect accelerometer locations. The related locations are removed from the correlation and updating studies

The newly proposed method finds the degrees of freedom for removal. According to the algorithm, calculated DOF should be removed from updating. However in current version of LMS Virtual.Lab software, it is not possible to remove only one DOF for an accelerometer location. For this reason, nodes that include the calculated axis are removed with other axes. If for a location, 3-axial accelerometer is used and all of the axes are removed instead of one calculated axis, this may decrease correlation. If the other two degrees of freedom have perfect correlation, removals of them decrease the total correlation. When this problem is solved, performance of coMAC and nrMAC should be examined in the future.

REFERENCES

- [1] M. Baruch, Optimization Procedure to Correct Stiffness and Flexibility Matrices Using Vibration Tests, *AIAA Journal*, Vol. 16, pp. 1208-1210, 1978
- [2] A. Berman, E. J. Nagy, Improvement of a Large Analytical Model Using Test Data, *AIAA Journal*, Vol. 21, No. 8, pp. 1168-1173, 1983
- [3] R. M. Lin, J. Zhu, Model Updating of Damped Structures using FRF Data, *Mechanical Systems and Signal Processing*, Vol.20, pp. 2200-2218, 2006
- [4] T. Uhl, W. Bochniak, W. Lisowski, L. Hermans, H. V. Auweraer, J. Malecki, FE-Model Correlation of a Helicopter Using Ground Test Results, *17th International Modal Analysis Conference*, Vol. 3727 (2), pp. 940-946, 1999
- [5] D. Göge, M. Link, Assessment of Computational Model Updating Procedures With Regard to Model Validation, *Aerospace Science And Technology*, Vol.7, 47-61, 2003
- [6] D. Göge, Automatic Updating of Large Aircraft Models Using Experimental Data from Ground Vibration Testing, *Aerospace Science and Technology*, Vol. 7, pp. 33-45, 2003
- [7] G. W. Brown, C. Farhat, F. M. Hemez et al., Overcoming Difficulties in the Updating of FE Models for Industrial Applications, *American Institute of Aeronautics and Astronautics*, 1033, 1997
- [8] M. T. Kozak, M. D. Cömert, H. N. Özgüven, A Modal Updating Routine Based on the Minimization of a New Frequency Response Based Index for Error Localization, *25th International Modal Analysis Conference*, Orlando, Florida, 2007

- [9] J. Lopez-Diez, V. Marco-Comez, P. Luengo, Modal Effective Mass Applied to Error Localization of Finite Element Models, American Institute of Aeronautics & Astronautics, 24684, 1999
- [10] D. Göge, M. Link, Results Obtained by Minimizing Natural Frequency and Mode Shape Errors of a Beam Model, Mechanical Systems And Signal Processing, Vol.17(1), 21-27, 2003
- [11] M. T. Kozak, Investigation of Model Updating Techniques and Their Applications to Aircraft Structures, MSc Thesis, Mechanical Engineering Department, Middle East Technical University, TR, Ankara, 2006
- [12] S. Köksal, M. D. Cömert, H. N. Özgüven, Comparison and Application of Reanalysis Methods, Proceedings of the 25th International Modal Analysis Conference, Orlando, Florida, 2007
- [13] S. Z. Rad, Methods for Updating Numerical Models in Structural Dynamics, PhD Thesis, Mechanical Engineering Department, Imperial College of Science, Technology and Medicine, London, UK, 1997
- [14] H. Grafe, “Modal Updating of Large Structural Dynamics Models Using Measured Response Functions”, PhD Thesis, Mechanical Engineering Department, Imperial College of Science, Technology and Medicine, London, UK, 1998
- [15] H. G. Natke, Problems of Model Updating Procedures: A Perspective Resumption, Mechanical Systems and Signal Processing, Vol.12(1), pp. 65-74, 1998
- [16] S. V. Modak, T. K. Kundra, B. C. Nakra, Comparative study of model updating methods using simulated experimental data, Computers & Structures, Vol. 80, pp. 437-447, 2002
- [17] C. M. Harris, A. G. Piersol, Harris’ Shock and Vibration Handbook, McGraw-Hill, Fifth Edition, 2002

- [18] Robert D. Cook, Finite Element Modeling for Stress Analysis, John Wiley & Sons Inc. Press, 1994
- [19] D. J. Ewins, Modal Testing Second Edition, Research Studies Press, 2000
- [20] N. Imamovic, Validation of Large Structural Dynamics Models Using Modal Test Data, PhD Thesis, Mechanical Engineering Department, Imperial College of Science, Technology and Medicine, London, UK, 1998
LMS Virtual.Lab Technical Data Sheet
- [21] N. M. M. Maia, J. M. M. e Silva, Theoretical and Experimental Modal Analysis, Research Studies Press Ltd., 1998
- [22] C. Zang, H. Grafe, M. Imregün, Frequency-Domain Criteria for Correlating and Updating Dynamic Finite Element Models, Mechanical Systems and Signal Processing, Vol 15, pp. 139-155, 2001
- [23] H. C. Frey, S. R. Patil, Identification and Review of Sensitivity Analysis Methods, Risk Analysis, v22 i3, pp. 553-578, 2002
- [24] J. E. Mottershead, C. Mares, M. I. Friswell, S. James, Selection and Updating of Parameters for Aluminum Space-Frame Model, Mechanical Systems and Signal Processing, Volume 14, Number 6, pp. 923-944(22), 2000
- [25] J. K. Sinha, A. R. Rao, R. K. Sinha, Advantage of a Updated Model of Structure: A Case Study, Nuclear Engineering and Design, Vol. 232, pp. 1-6, 2004
- [26] MSC.Nastran Design Sensitivity and Optimization User's Guide, MSC.Software, 2004
- [27] NAS107, Design Sensitivity and Optimization in MSC.Nastran Course Notes, MSC.Software, 2003
- [28] S. C. Chapra, R. P. Canale, Numerical Methods for Engineers With Programming and Software Applications Third Edition, McGraw-Hill International Editions, 1998

[29] C. R. Pickrel, Airplane Ground Vibration Testing: Correlation With Nominal Modal Model, Conference on Structural Dynamics No 20, Los Angeles CA, 2002

APPENDIX A

USED EQUIPMENT THROUGHOUT MODAL TESTS

- 1) Iotech data acquisition system
 - a. Maximum Aggregate Speed : 500 kHz
 - b. 24 analog channels.



Figure A.1 Iotech data acquisition system

- 2) 3-Axial ICP Type Piezoelectric Accelerometers
 - a. PCB Piezotronics Model 356A16

- b. Measurement Range : $\pm 490 \text{ m/s}^2 \text{ pk}$
- c. Frequency Range (Y&Z Axis) : 0.5-5000 Hz
- d. Frequency Range (X Axis) : 0.5-4500 Hz
- e. Resonant Frequency : $\geq 25 \text{ kHz}$
- f. Sensing Element : Ceramic
- g. Sensing Geometry : Shear
- h. Weight : 7.4 gram
- i. Nonlinearity $\leq 1 \%$



Figure A.2 3-axial piezoelectric accelerometer

- 3) One-axis force transducer
 - a. Compression Range : 4448 N
 - b. Tension Range : 2224 N



Figure A.3 Single axis force transducer

- 4) Modal hammer
 - a. PCB Piezotronics Model 086C04
 - b. Measurement Range : +/- 4400 N pk
 - c. Resonant Frequency : ≥ 22 kHz
 - d. Sensing Element : Quartz
 - e. Hammer Mass : 0.16 kg
 - f. Nonlinearity ≤ 1 %

- 5) Data Physics shaker and amplifier system
 - a. DP-V070 Shaker
 - i. Peak force = 440N at sine, 310 at random
 - ii. Armature travel = 25.4 mm (pk-pk)
 - iii. Frequency range = DC-6500 Hz
 - iv. Max acceleration = 100g at sine, 79g at random
 - v. Resonance frequency = 5500 Hz
 - b. A-10C Amplifier
 - i. Power rating = 1000 VA

- ii. Frequency range = DC-20kHz
 - iii. Signal to noise ratio = >90 dB
- 6) Tira shaker and amplifier system
- a. TV 51110 Shaker
 - i. Peak force = 100N at sine, 70N at random
 - ii. Armature travel = 25.4 mm (pk-pk)
 - iii. Frequency range = DC-5000 Hz
 - iv. Max acceleration = 43g at sine, 30g at random
 - v. Resonance frequency = > 6000 Hz
 - b. BAA 120 Amplifier
 - i. Power rating = 120 VA
 - ii. Frequency range = DC-20kHz
 - iii. Signal to noise ratio = >90 dB

APPENDIX B

FRF GRAPHS OF MODAL TESTS

The stabilization graph of the tail is shown in Figure B.1.

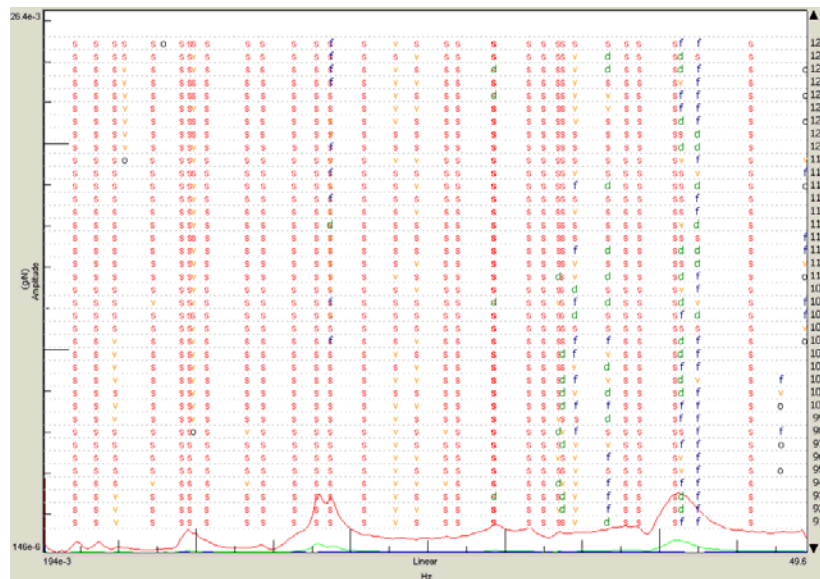


Figure B.1 Stabilization graph of the tail modal analysis

The stabilization graph of the entire helicopter fuselage is shown in Figure B.2.

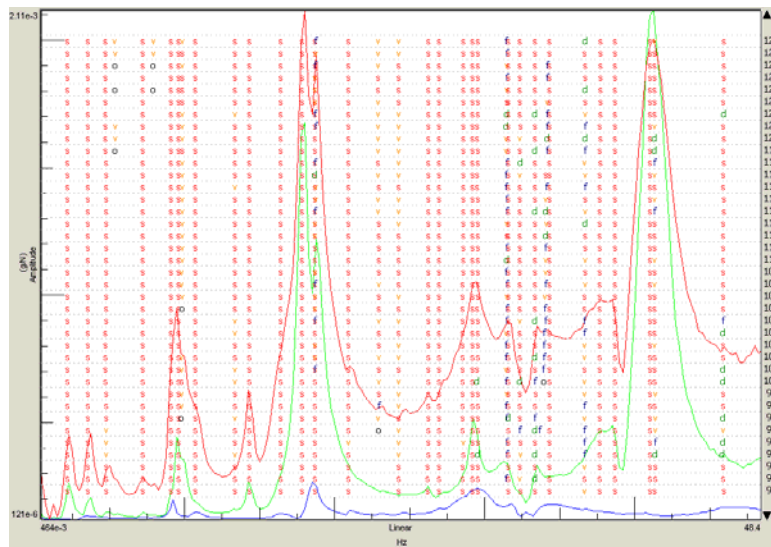


Figure B.2 Stabilization graph of the complete helicopter fuselage modal analysis

APPENDIX C

MODAL ANALYSIS WITH LMS TEST.LAB

Modal analysis with LMS Test.Lab is a straightforward procedure. First of all, Frequency Response Functions (FRF) are introduced to the software inside “Navigator” window as shown in Figure C.1.

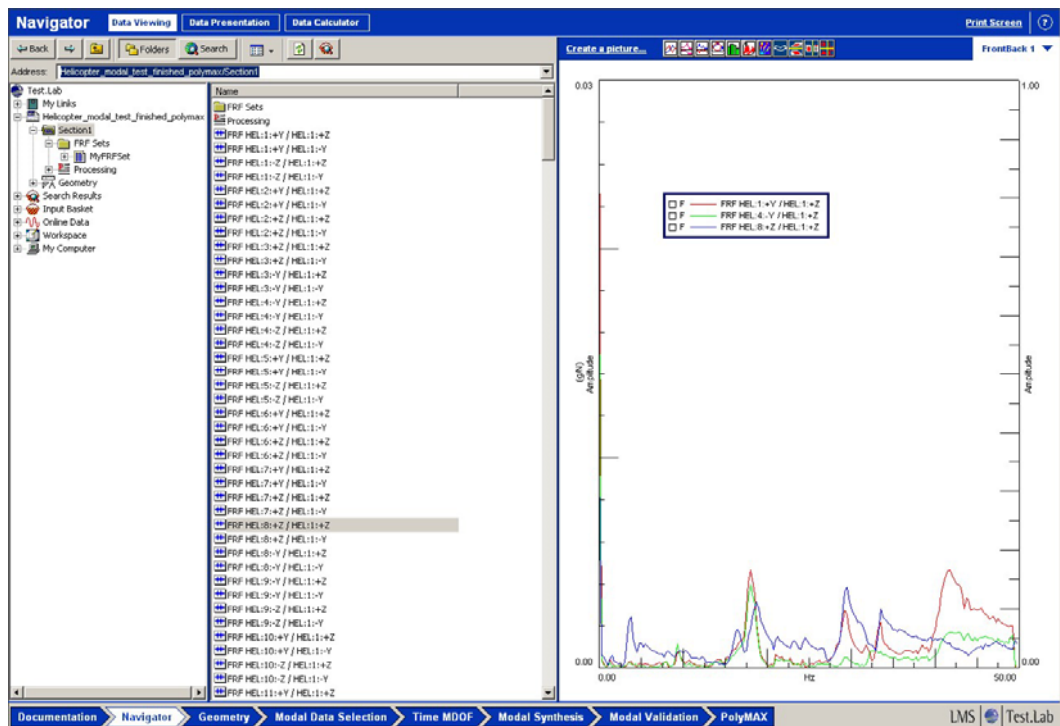


Figure C.1 Navigator window for navigation

After placement of all FRF, geometry of the modal tested structure is created in “Geometry” window. Only nodes, lines and surfaces can be used for this

operation. At first, accelerometer locations are entered inside “Nodes” tab as in Figure C.2.

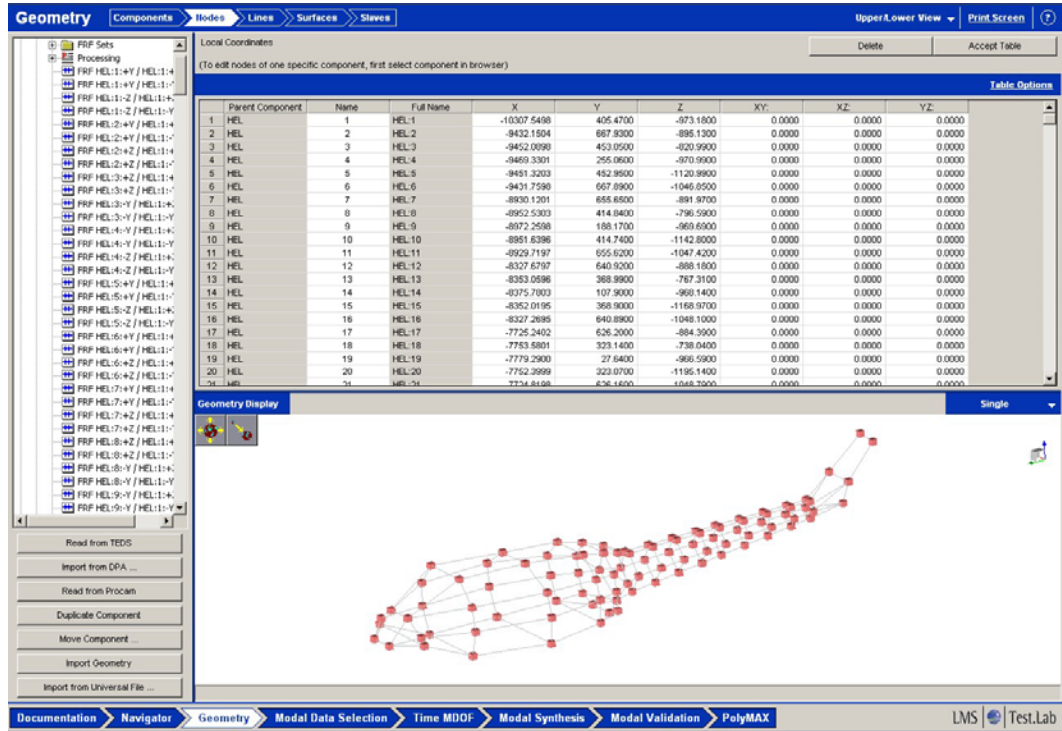


Figure C.2 Geometry window nodes tab

After insertion of nodes, they are used to form connecting lines. This operation is accomplished in “Lines” tab as in Figure C.3.

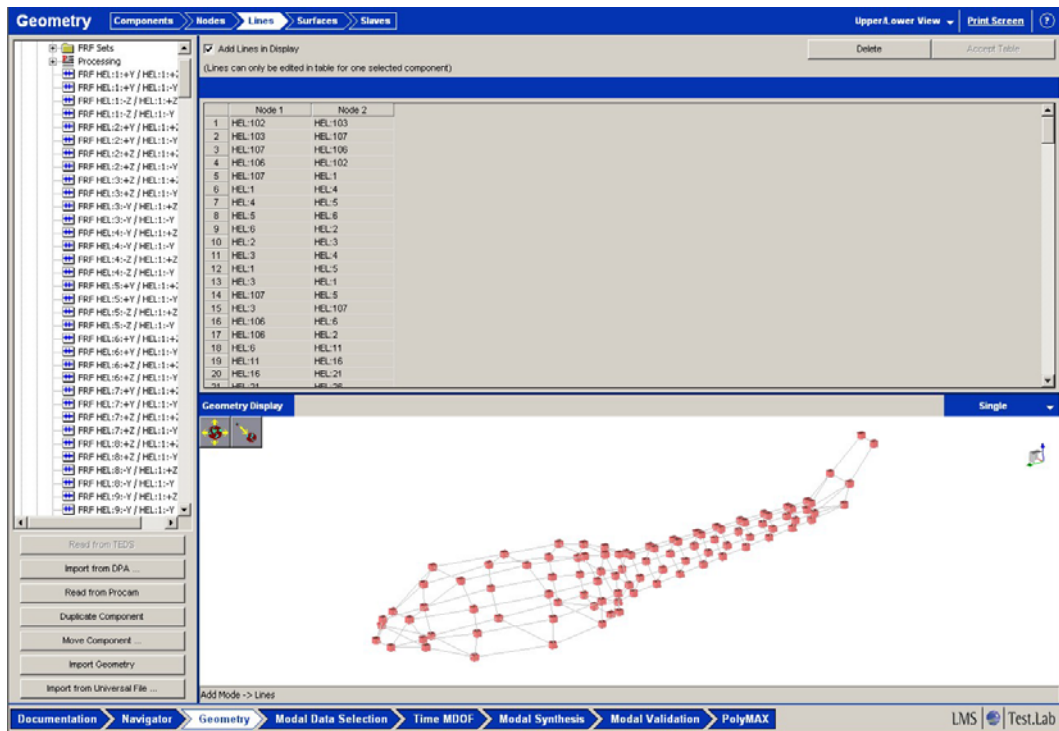


Figure C.3 Lines tab for node connections

Afterwards, necessary frequency response functions are selected inside “Modal Data Selection” window in order to indicate the scope of modal analysis. FRFs can be also plotted in this window as shown in Figure C.4.

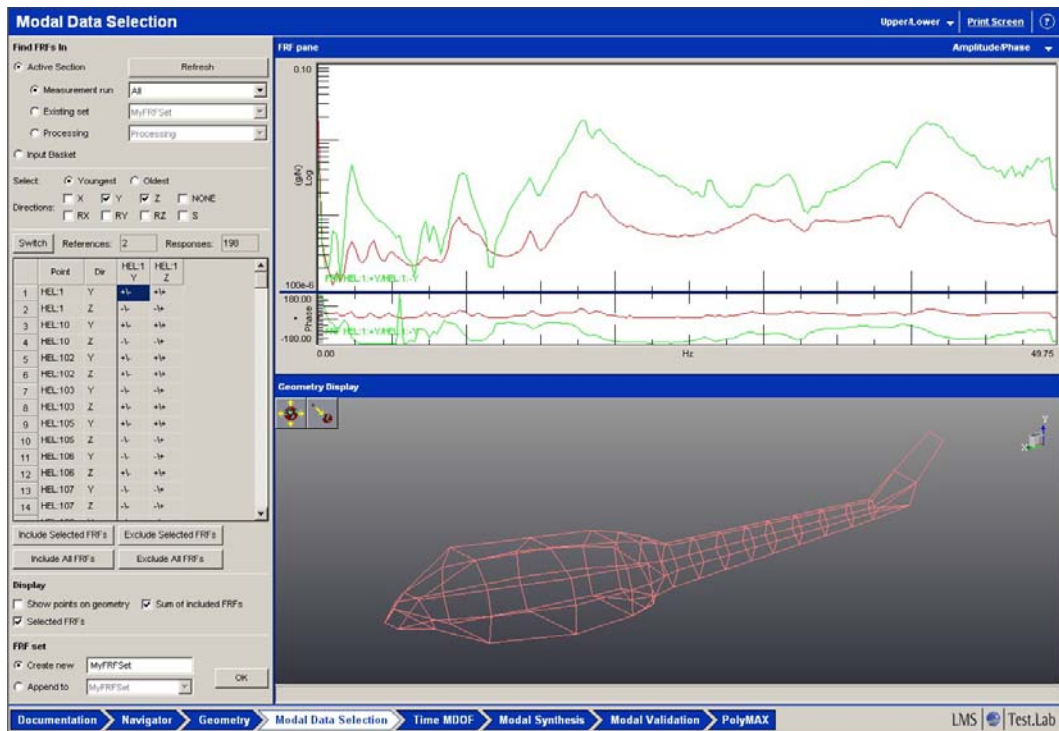


Figure C.4 Modal data selection window

When all these geometry creation and data selection operations are completed, modal analysis is performed automatically. There are two different modal analysis algorithms. The procedure of Polyreference is shown in this example. Inside “PolyMax” window as a first step, range of the frequency for modal analysis is selected as shown in Figure C.5.

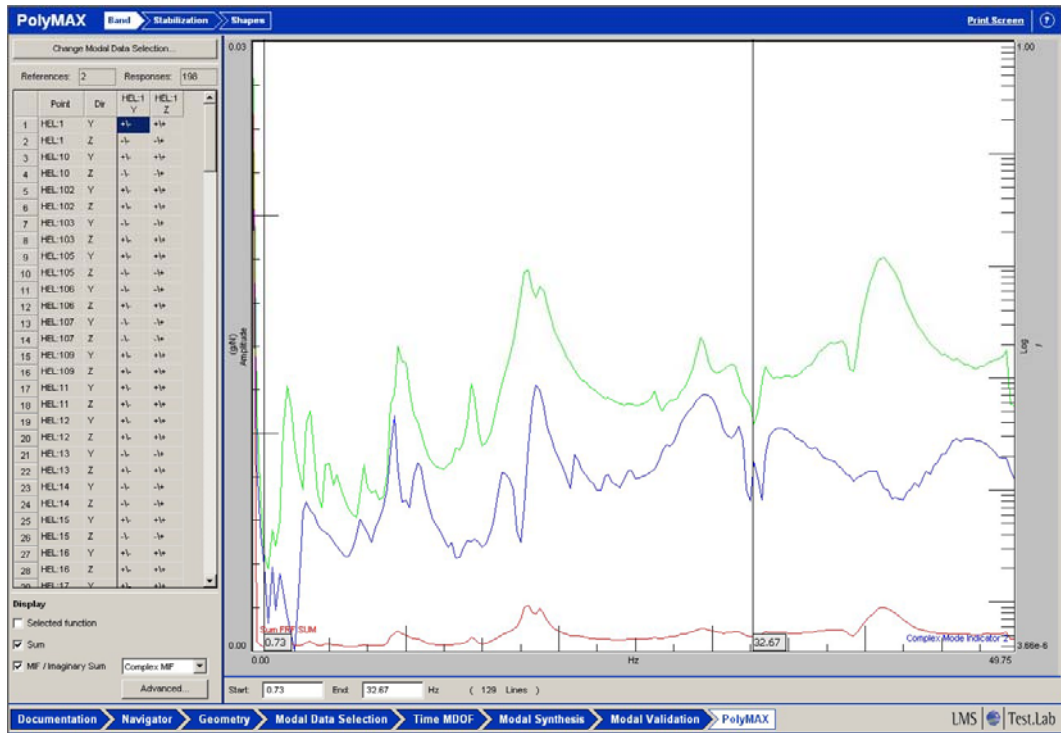


Figure C.5 PolyMax window frequency band selection tab

Then, inside “Stabilization” tab, algorithm calculates the modes by stabilizing on different frequencies as shown in Figure C.6.

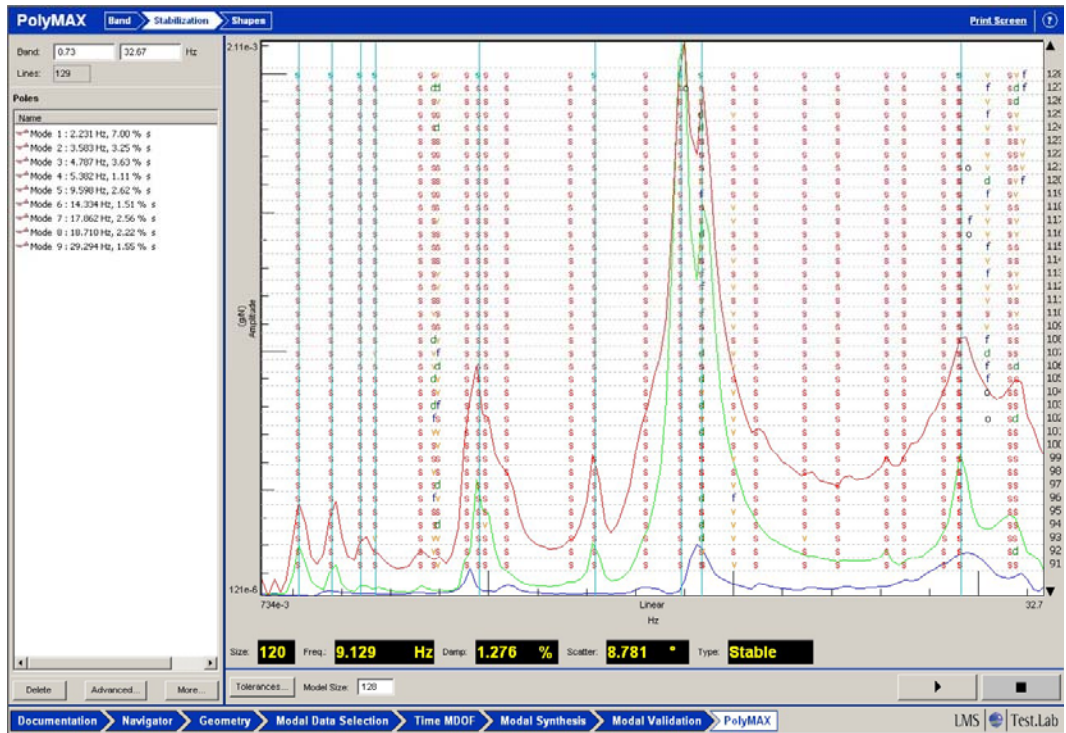


Figure C.6 PolyMax window stabilization and frequency selection tab

At this point, frequency points that are stabilized more (at least 4 s are required to consider that frequency as a candidate for natural frequency) are selected. After this selection process, mode shapes at these frequencies are animated for visual check inside “Shapes” tab as in Figure C.7.

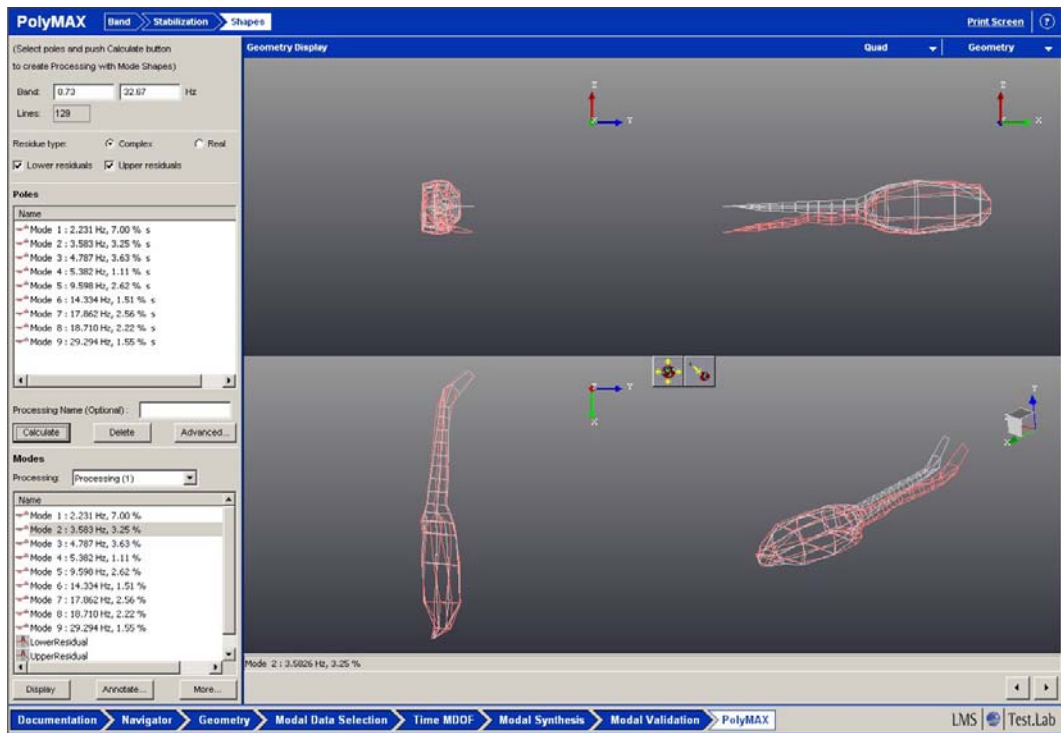


Figure C.7 PolyMax window mode shape animation tab

APPENDIX D

MODEL UPDATING WITH LMS VIRTUAL.LAB

The procedure of model updating with LMS Virtual.Lab software is described in this section. First of all, numerical (.op2 file) and experimental (.lms file) models are imported to the Virtual.Lab environment with the menu File>Import as shown in Figure D.1.

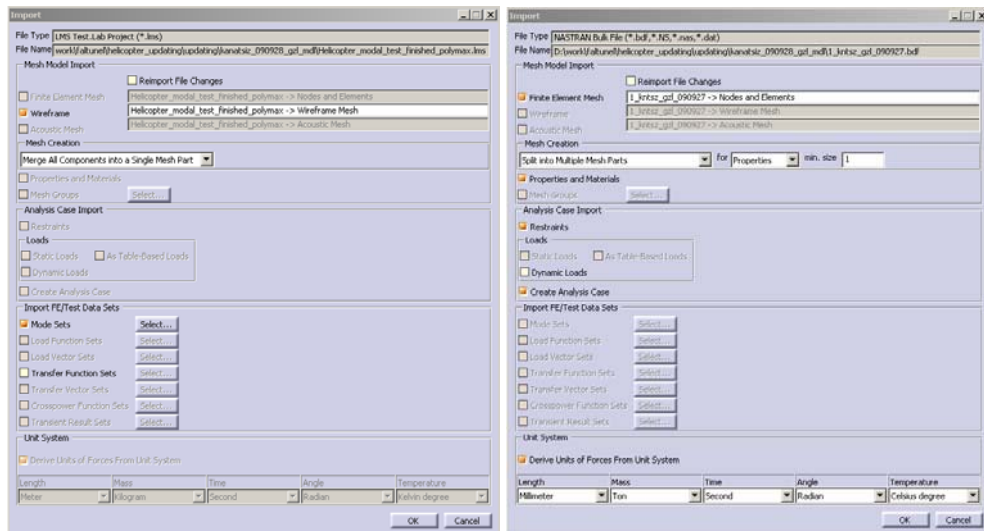


Figure D.1 LMS Virtual.Lab model import windows

Modal analysis and sensitivity analysis are performed by MSC.Nastran. Virtual.Lab creates and submits the input documents automatically to MSC.Nastran for necessary analyses. For modal analysis purpose, a new MSC.Nastran modal case is set up under “Insert>Nastran Analysis

Cases>Nastran Modal Solution Case” in order to compute finite element modes. The necessary selections are performed on the window shown in Figure D.2.

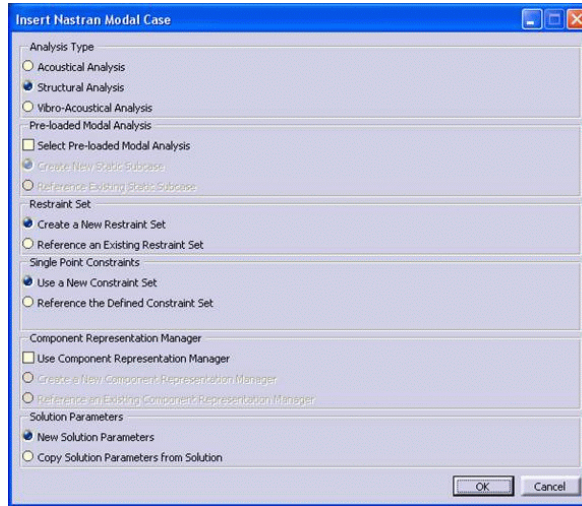


Figure D.2 LMS Virtual.Lab MSC.Nastran modal case selection window

Afterwards, numerical and experimental modes are activated or deactivated as shown in Figure D.3. The main purpose of this process is to select/deselect the modes that will be used for updating. For example, rigid body modes are deactivated in order not to include in the correlation analysis.

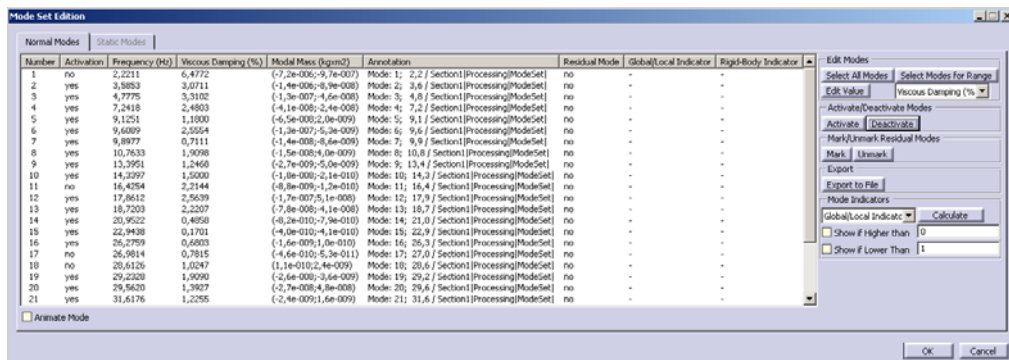


Figure D.3 LMS Virtual.Lab Mode activation/deactivation window

Then, in order to align the two models, geometrical correlation (mapping) of the models is performed. For this process, three paired nodes of the two models are selected by the user. After this assignment, the remaining coordinates are paired automatically by the software as shown in Figure D.4. According to this dialog, the coordinates that have a maximum distance of 5mm are paired.

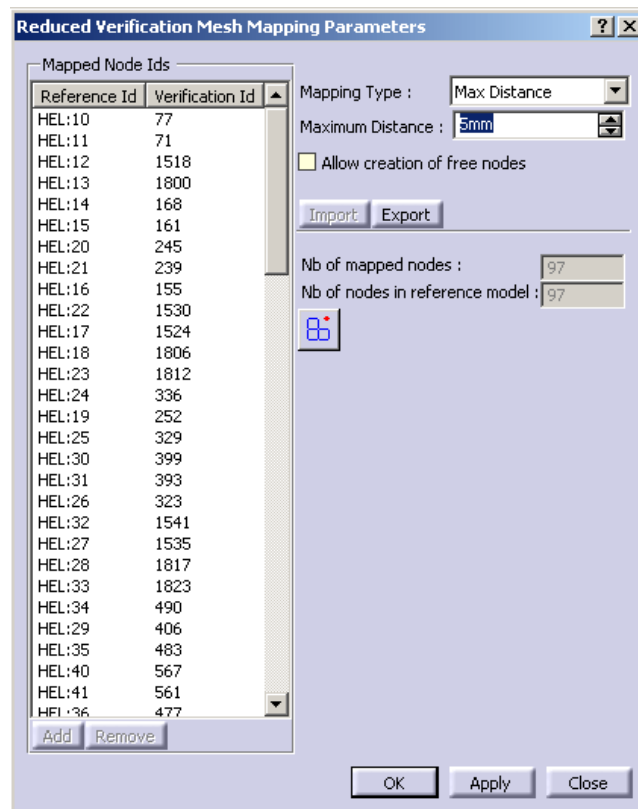


Figure D.4 LMS Virtual.Lab geometric correlation window

Software generates a transformation matrix for this pairing process. As a result, paired numerical and experimental models fit on each other as shown in Figure D.5.

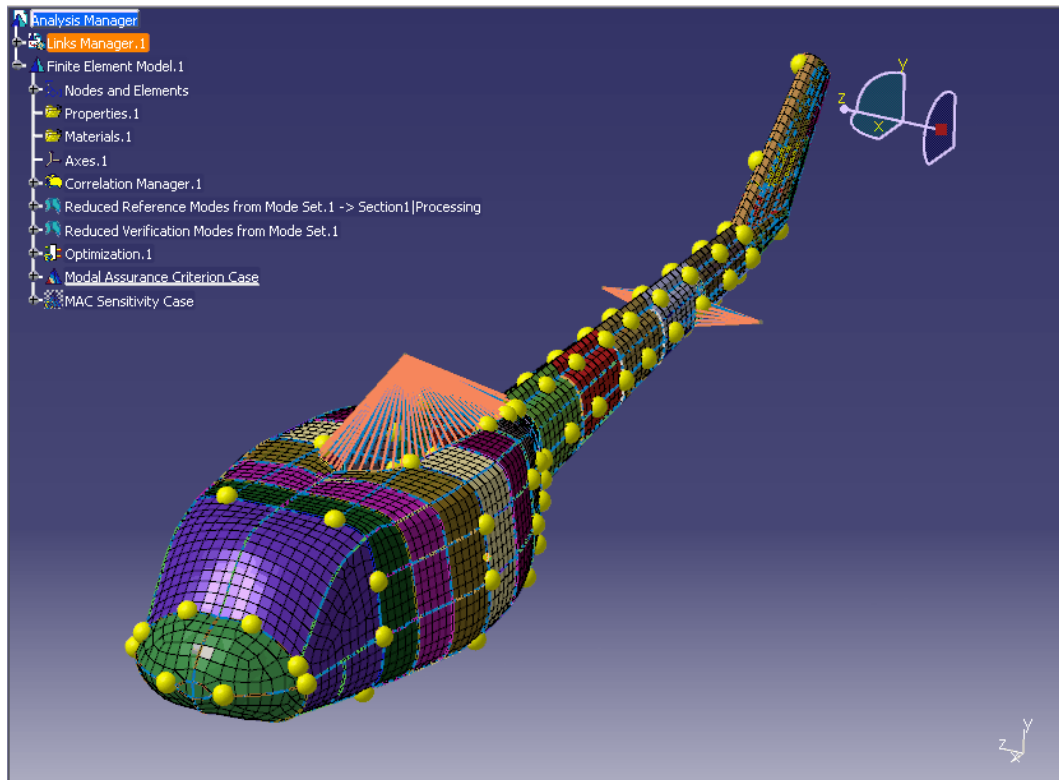


Figure D.5 The fitted reference and verification models

After geometric correlation, geometry of the verification model is reduced to the paired coordinates. Additionally, reduced modal vector data is generated by using the node pair table and transformation matrix under menu Transfer->Reference Mode Set or Transfer->Verification Mode Set.

The next step is to insert MSC.Nastran Sensitivity Case together with the design variable set. This case is inserted under Insert>Nastran Sensitivity Case menu. The necessary selections are performed on the window as shown in Figure D.6.

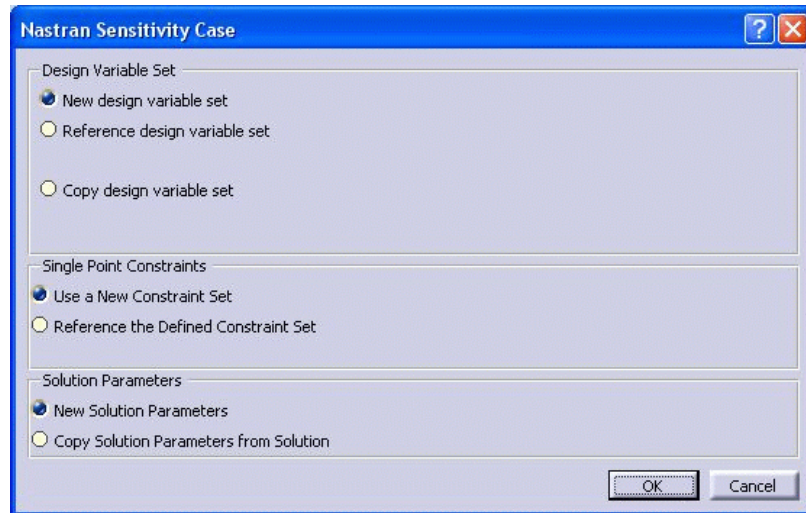


Figure D.6 LMS Virtual.Lab Nastran sensitivity case selection window

After that, design variables are introduced inside “Design Variable Set” dialog box as shown in Figure D.7. These variables will be used to modify the correlation between FE and test modes.

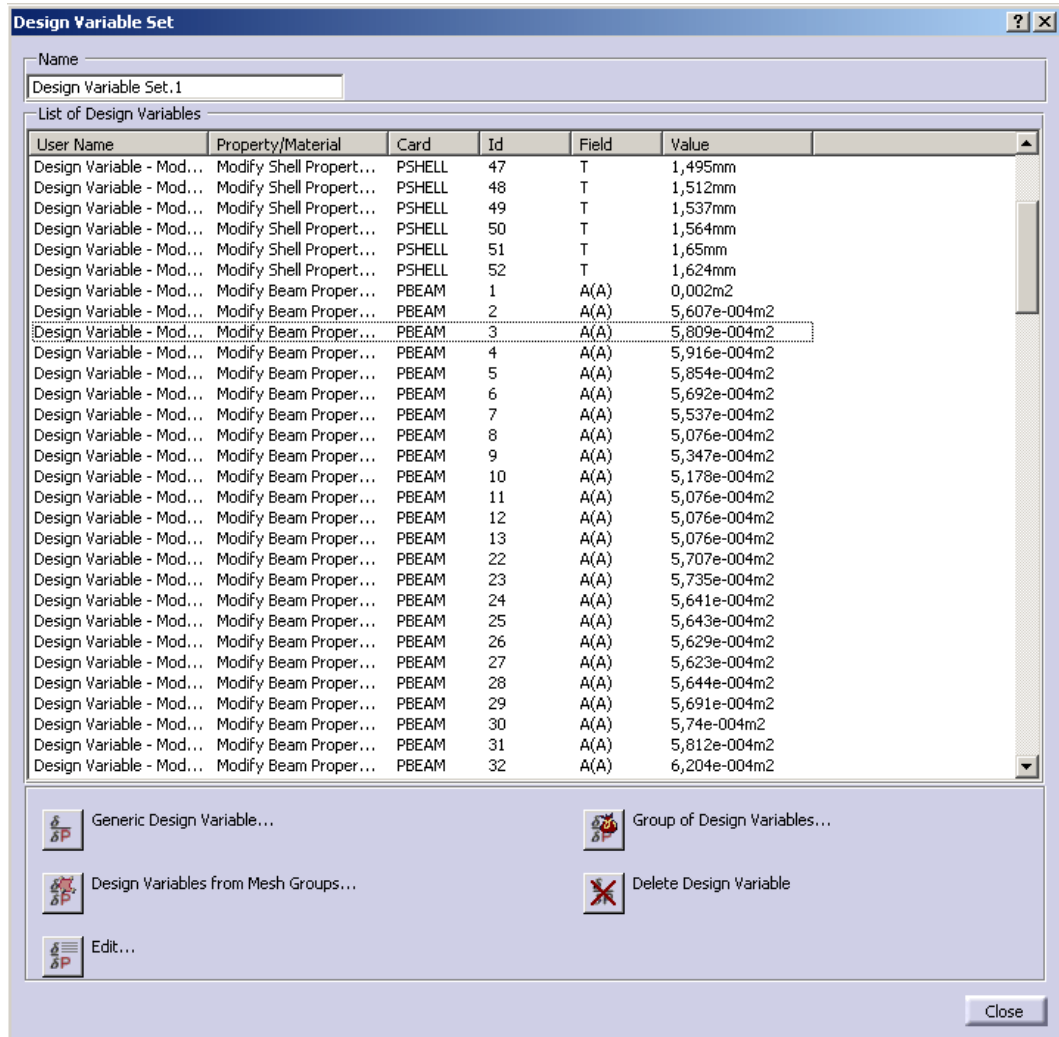


Figure D.7 LMS Virtual.Lab design variable generation window

After model preparations, MAC analysis is performed under Modal-based Correlation->Modal Assurance Criterion Case menu. Necessary information is selected inside the MAC case window as shown in Figure D.8.

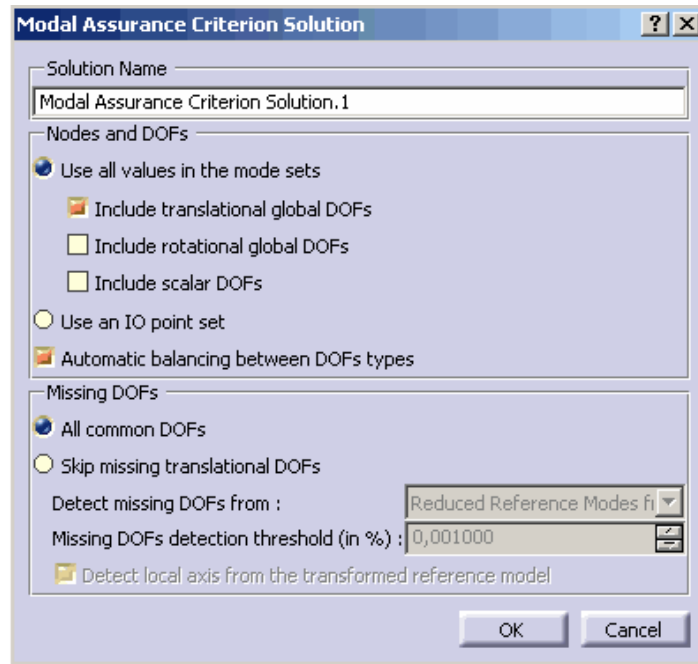


Figure D.8 LMS Virtual.Lab selection window for MAC Solution

When computation is over, MAC matrix figure can be plotted as shown in Figure D.9.

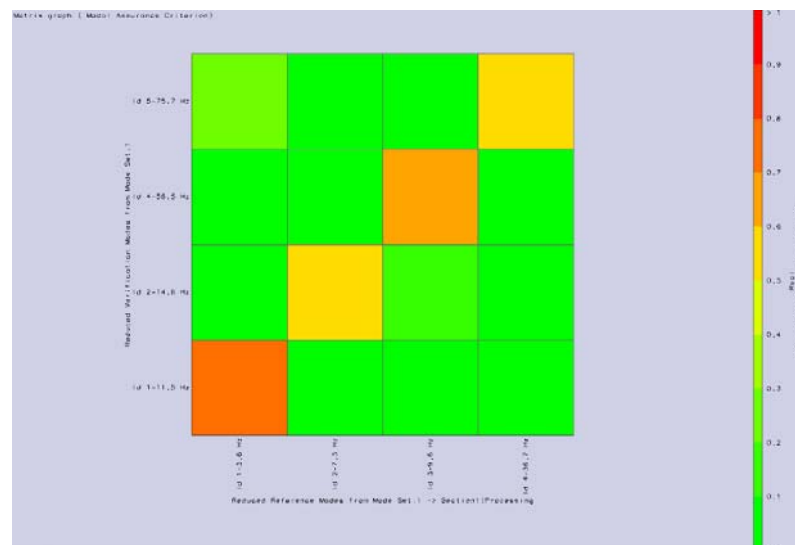


Figure D.9 LMS Virtual.Lab MAC matrix

After introduction of design variables and MAC solution, MAC sensitivity case is created under the menu Insert>Modal-based Correlation>MAC Sensitivity Case. This case computes the sensitivities of paired MAC values on previously defined design variables. After MAC sensitivity case solution, sensitivities of paired modes to desired design variables are calculated as shown in Figure D.10.

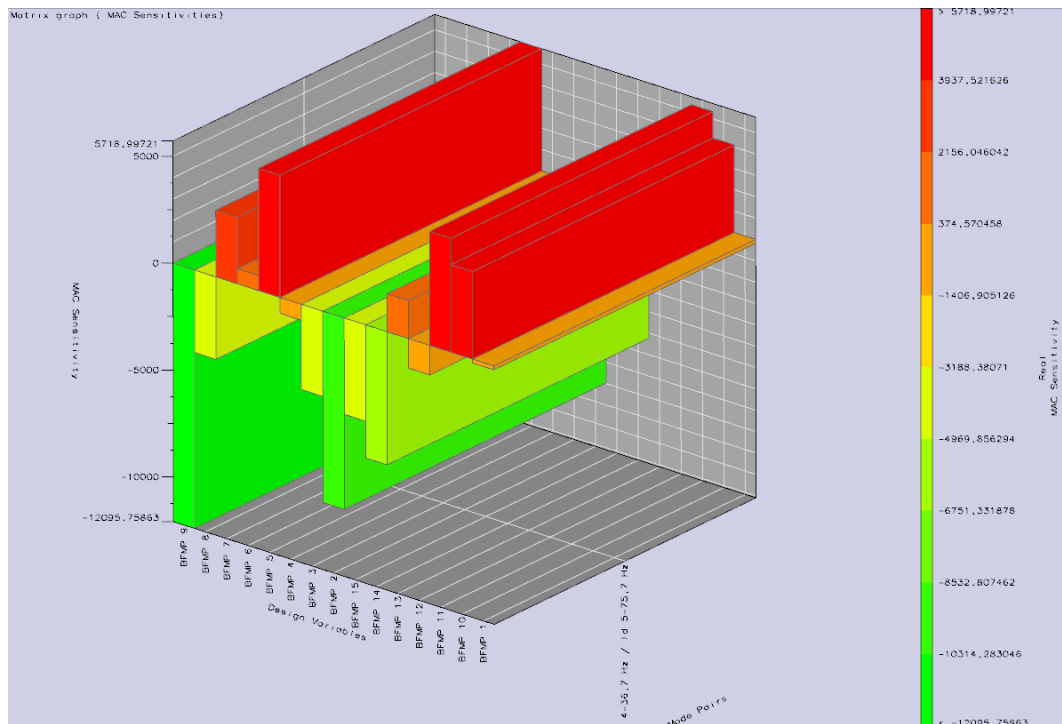


Figure D.10 Sensitivities of paired modes to selected design variables

After all these procedures, optimization is carried out to improve the MAC values. Optimization run is inserted from the menu Insert>Create a new optimization setup. Appropriate design variables and objective functions are assigned to the optimization problem. Additionally, lower-upper bounds of design variables, target values of objective functions are entered on input and output set as shown in Figure D.11.

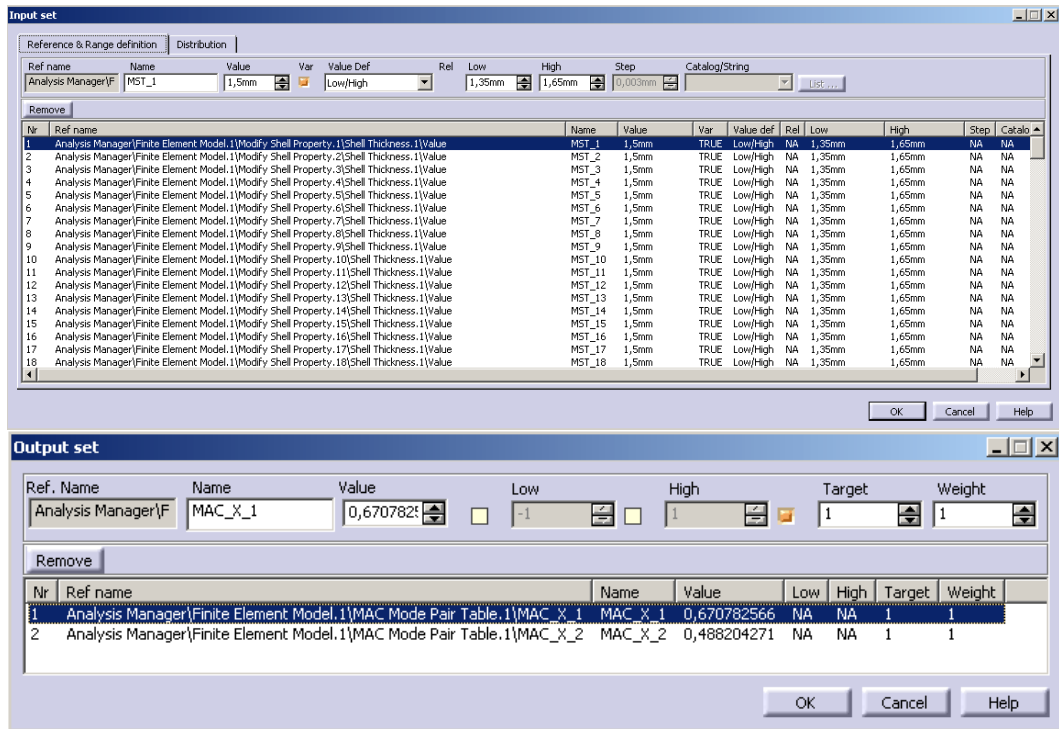


Figure D.11 LMS Virtual.Lab input and output windows for optimization

For the optimization process, objectives, design variables, optimization algorithm and iterations, etc. are selected as shown in Figure D.12.

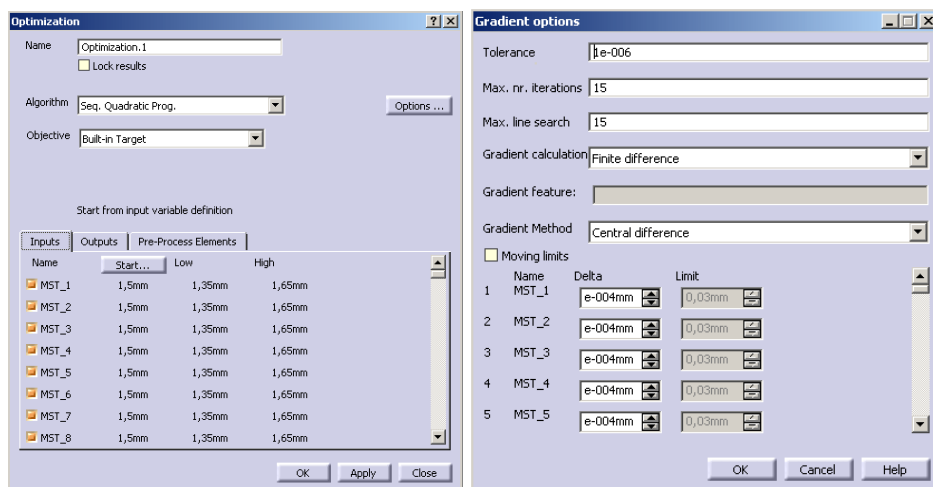


Figure D.12 LMS Virtual.Lab optimization details window

After that, optimization run is ready to be started. If it is started, optimization process gives a small change to each of the design variables to reach the target values of objectives functions. Process makes advances by frequently triggering the computation of the MSC.Nastran modal solution.

APPENDIX E

MODEL ANALYSIS WITH MSC.PATRAN AND MSC.NASTRAN

Modal analysis with MSC.Patran&Nastran is a very straight-forward procedure. MSC.Patran is used for pre and post processing. On the other hand, MSC.Nastran is the solver. The procedure is given in detail below.

First of all, geometric model is imported to the MSC.Patran environment by using the menu File>Import. Software has capabilities of importing many formats as shown in Figure E.1.

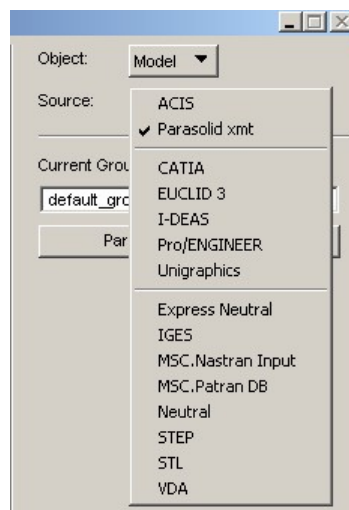


Figure E.1 MSC.Patran importing menu

Geometry can be drawn in MSC.Patran by using the Geometry module as shown in Figure E.2. However, it is recommended to draw the complex geometries in a CAD software. MSC.Patran geometry module is suggested to be used for editing and simplifying operations for the aim of preparing the geometrical model to meshing.



Figure E.2 MSC.Patran geometry module

After geometrical operations, meshing is performed using the “Elements” module as shown in Figure E.3.

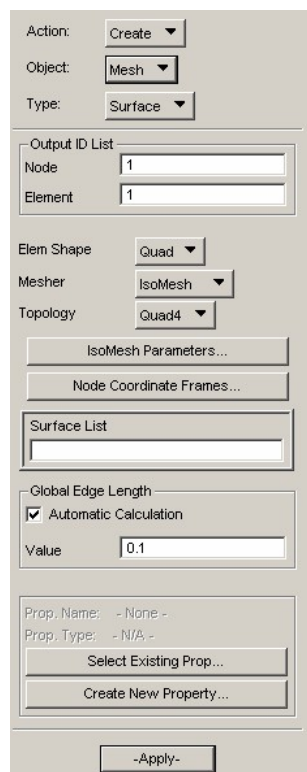


Figure E.3 Elements module

After meshing, boundary conditions are assigned in “Load/BCs” module as shown in Figure E.4.

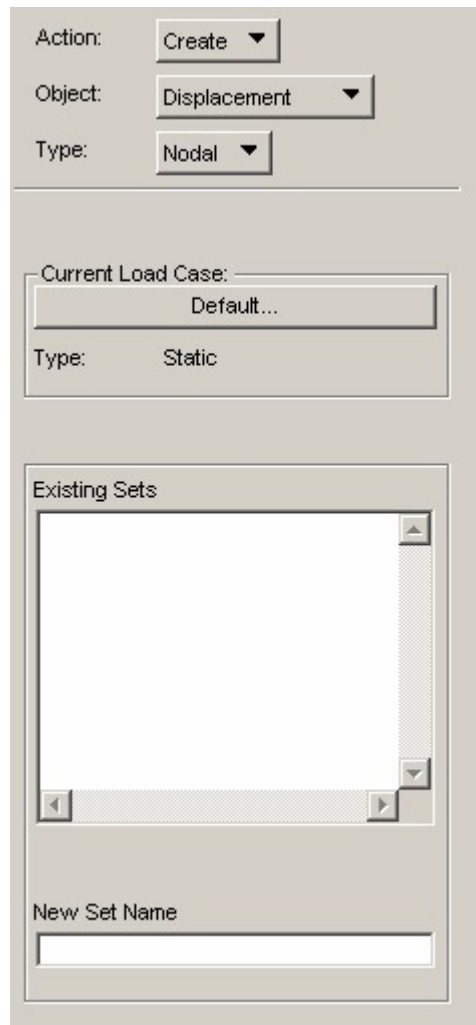


Figure E.4 Load and boundary conditions module

After assignment of boundary conditions, material properties are entered inside “Materials” module as shown in Figure E.5.

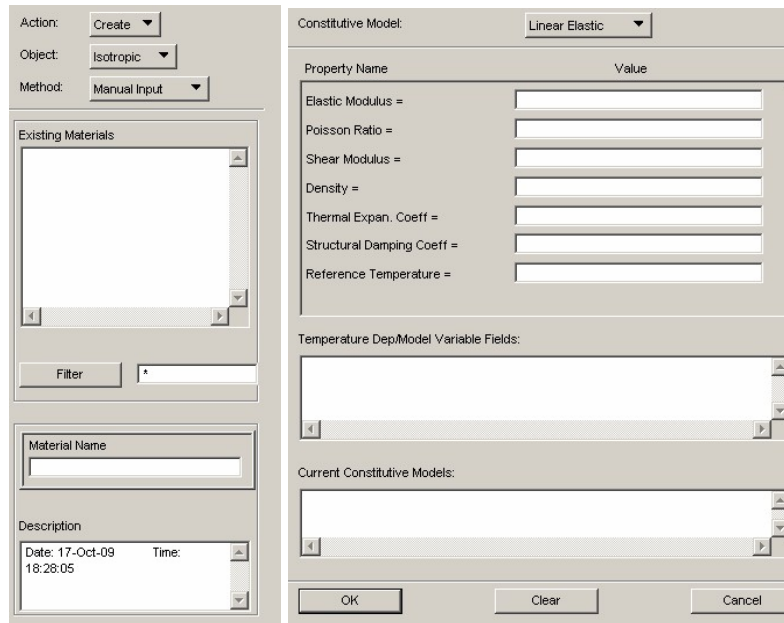


Figure E.5 Materials module

Assigned material properties and shell thicknesses are entered inside “Properties” module as shown in Figure E.6.

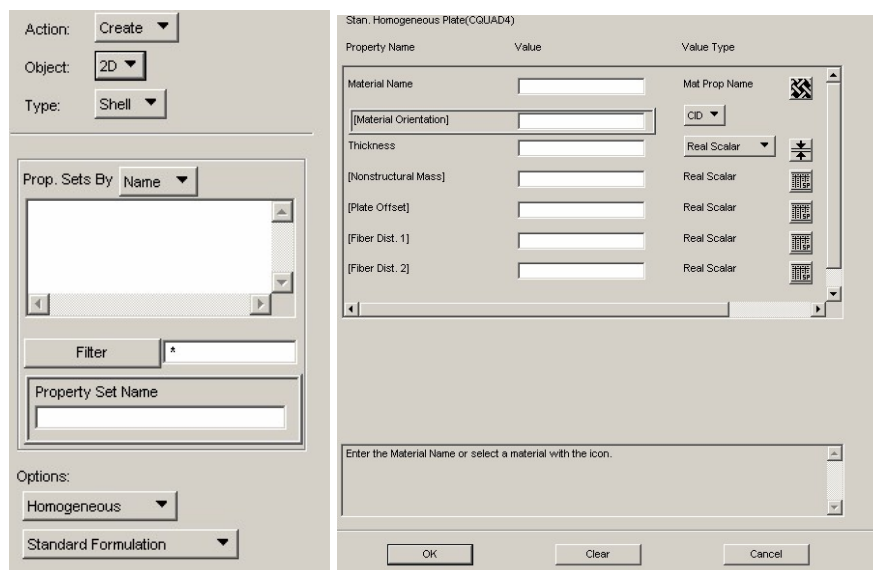


Figure E.6 Properties module

Finally, finite element model is transferred to the MSC.Nastran for problem solving in Analysis module as shown in Figure E.7.

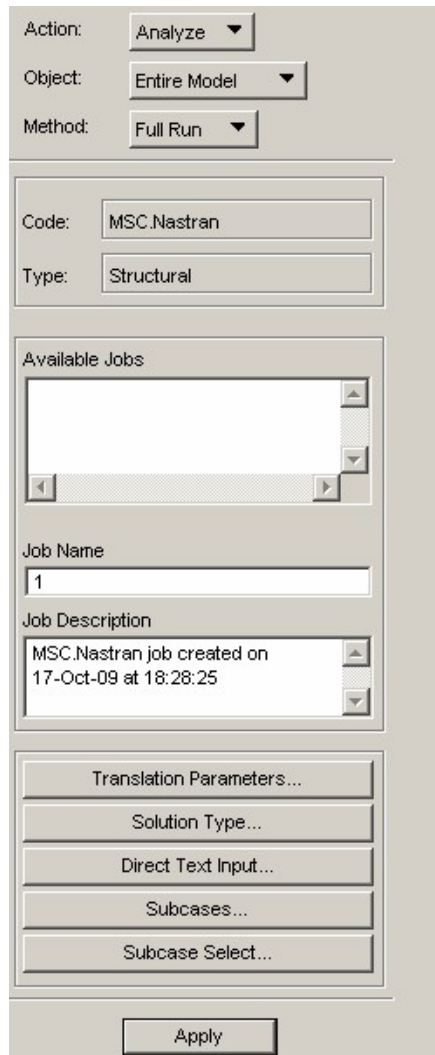


Figure E.7 Analysis module

When MSC.Nastran solves the problem, results are imported to the MSC.Patran environment inside “Analysis” module. Results are plotted and summarized inside “Results” menu.